

Flight simulator for training gynaecologists

Citation for published version (APA):

Hout-van der Jagt, van der, M. B. (2010). *Flight simulator for training gynaecologists: a mathematical model of the cardiotocogram for use in simulation training*. Technische Universiteit Eindhoven.

Document status and date:

Published: 01/01/2010

Document Version:

Publisher's PDF, also known as Version of Record (includes final page, issue and volume numbers)

Please check the document version of this publication:

- A submitted manuscript is the version of the article upon submission and before peer-review. There can be important differences between the submitted version and the official published version of record. People interested in the research are advised to contact the author for the final version of the publication, or visit the DOI to the publisher's website.
- The final author version and the galley proof are versions of the publication after peer review.
- The final published version features the final layout of the paper including the volume, issue and page numbers.

[Link to publication](#)

General rights

Copyright and moral rights for the publications made accessible in the public portal are retained by the authors and/or other copyright owners and it is a condition of accessing publications that users recognise and abide by the legal requirements associated with these rights.

- Users may download and print one copy of any publication from the public portal for the purpose of private study or research.
- You may not further distribute the material or use it for any profit-making activity or commercial gain
- You may freely distribute the URL identifying the publication in the public portal.

If the publication is distributed under the terms of Article 25fa of the Dutch Copyright Act, indicated by the "Taverne" license above, please follow below link for the End User Agreement:

www.tue.nl/taverne

Take down policy

If you believe that this document breaches copyright please contact us at:

openaccess@tue.nl

providing details and we will investigate your claim.

Flight simulator for training gynaecologists

A mathematical model of the cardiotocogram for use in simulation training

ir. M.B. van der Hout-van der Jagt
Máxima Medical Center, Veldhoven
Eindhoven University of Technology

February 2010

Abstract

Due to the high complexity and low incidences of emergencies during labor and delivery, gynaecologists often cannot rely on previous experiences during a crisis. Simulation training can provide both experience and skills in a safe environment, such that complications due to emergencies can be reduced as much as possible.

Several simulators are available that support a safe learning environment for obstetric emergency training. However, none provides a realistic and physiology-based (simulation of) the cardiotocogram (CTG), which is a continuous and synchronous registration of uterine contractions and fetal heart rate. However, at the labor and delivery ward, the CTG is widely used as main indicator for fetal welfare. The CTG provides information on the fetal stress reaction to uterine contractions, based on oxygen levels in the fetal blood. Since the CTG is widely available and the only non-invasive method for fetal monitoring, medical decisions are often based on deviations in the CTG. The CTG is therefore an essential part of the clinical environment in medical simulation training.

In a one-year clinical project as part of a qualified medical engineer training, a start is made with the development of a CTG simulator. The three main deviations in the CTG were studied: early, late and variable decelerations in fetal heart rate, caused by uterine contractions and complications in labor. The mechanism of these three deceleration types were studied, and each step was quantified for early and late decelerations. In this project, early decelerations were implemented in a mathematical model, based on the underlying physiological principles. In future, implementation of late and variable decelerations are planned within a PhD-project.

A validation study was performed for the modeled CTG, where a comparison was made between real and computer-generated CTG tracings from our model, based on experts' opinion. The first results show no significant differences between real and computer-generated CTG tracings. However, the number of clinical experts was low, and a larger study has to be performed to confirm these results.

Coupling of the modeled CTG to a simulator interface is planned in future. The model can be implemented in different types of simulators: in a screen-based simulator (individual in-depth training to improve insight into and interpretation of the CTG), as part of a full-body delivery simulator, and as part of a serious game (in these two cases the CTG is part of the clinical environment). Future plans include implementation in a screen-based simulator and a full-body delivery simulator.

Contents

1	Introduction	1
2	The cardiotocogram	3
2.1	Interpretation and classification of the cardiotocogram	4
2.2	Early decelerations	5
2.3	Late decelerations	6
2.4	Variable decelerations	7
3	Simulation of early decelerations with a mathematical model	10
3.1	Available mathematical model	10
3.2	Methods	12
3.2.1	Necessary model adaptations	12
3.2.2	Uterine contractions	12
3.2.3	Influence of uterine contractions on cerebral flow	13
3.2.4	Influence of diminished cerebral flow on cerebral oxygen pressure	13
3.2.5	Influence of reduced cerebral oxygen pressure on vagal nerve fire rate	14
3.2.6	Influence of vagal nerve fire rate on fetal heart rate	14
3.2.7	Implementation of variability in heart rate and contraction signal	15
3.3	Model overview after model adaptation	17
3.4	Clinical evaluation	18
3.4.1	Method	18
3.4.2	Results	19
3.5	Discussion & Conclusion	20
4	Model requirements for late decelerations	21
4.1	Fetal physiologic response to central hypoxia	21
4.2	Influence of decreased utero-placental flow on chemoreceptor activation	22
4.2.1	Relation between chemoreceptor activation and vasoconstriction leading to hypertension	23
4.2.2	Influence of hypertension on baroreceptor activation	23
4.2.3	Relation between baroreceptor activation and fetal heart rate deceleration	24
5	Discussion & Conclusion	25
A	Physiological cardiovascular processes and adaptation	26
A.1	Maternal circulation	26
A.1.1	Physiologic cardiovascular adaptation in pregnancy	26
A.1.2	Cardiovascular physiology during labor	28

A.2	Fetal circulation	30
A.2.1	Development of fetal circulation	30
A.2.2	Fetal hemodynamic data at term	31
B	Literature review of mathematical models	33
B.1	Cardiovascular models	33
B.1.1	Maternal cardiovascular models	33
B.1.2	Placental cardiovascular models	34
B.1.3	Fetal cardiovascular models	34
B.2	Oxygen models	34
B.3	Hemodynamic regulation: baroreceptor and chemoreceptor model	35
C	Mathematical model	36
C.1	Model summary	36
C.1.1	Maternal circulation	37
C.1.2	Fetal circulation	38
C.1.3	Placental circulation	38
C.2	Cardiovascular model	38
C.2.1	Navier-Stokes and continuity equations	38
C.2.2	Discretisation and assembling	41
C.2.3	Vessel segment	42
C.2.4	The heart: ventricle component	42
C.2.5	Model description	44
C.3	Cardiovascular regulation model	47
C.3.1	Model description	49
C.4	Oxygen model	52
C.4.1	Model description	52
C.5	Variability in heart rate and contraction signal	56
D	Model in Matlab	58
D.1	Initialization	59
D.2	DiSCo	59
D.3	Postprocessing	61
E	Analysis of CTG traces with early decelerations	64
F	Validation study	66

1 Introduction

Gynaecologists and pilots have in common that they have high responsibilities in their daily work. When an emergency occurs this responsibility is further stressed by rare and severe conditions. Since these conditions may be quite variable, both gynaecologists and pilots therefore cannot rely on previous experiences whenever such an emergency occurs. In aviation, simulation of emergency situations is used for several decades already. In order to reduce (complications of) errors, strict protocols are used for on the one hand flying an aircraft and technical operations, and on the other hand communication with colleagues. The latter has more to do with crew resource management (CRM) than with practical skills. Crew resource management was introduced for the first time in a training in 1979 developed by NASA. CRM focuses on human factors like leadership, interpersonal communication and decision making, since the major cause of errors is human error [39].

In health care, a great amount of effort has been put into practical skills teaching, but little or none into teaching CRM principles. However, this is changing more and more. In 2000, the Institute of Medicine estimated that medical errors are responsible for as many as 98,000 deaths in the United States annually [39]. In the Netherlands, an estimation in 2007 is in the range of 1735 deaths per year [20]. These figures triggered new initiatives for medical team training with the use of simulation. Both hospitals and medical simulation centers offer simulation training to teach CRM principles to health care providers. The Máxima Medical Center in Veldhoven (The Netherlands) trains the obstetric personnel every fortnight with the use of obstetric simulators. Recently, Medsim (medical education and simulation center) started CRM training for obstetric multidisciplinary teams of Dutch hospitals. These training sessions are primarily developed to teach and train CRM principles, but at the same time will address practice of skills if appropriate.

In the obstetric field, a number of simulators is available for different purposes. Devices for training of skills exist already for a couple of hundred years, and are getting more advanced. Some of these simulators for instance, give feedback on the amount of force used, show the (internal) position of applied instrumentation (e.g. in forceps- or vacuum-assisted delivery) or show the cardiotocogram (CTG: a synchronous registration of uterine contractions and fetal heart rate). The simulator may be as straightforward as a mechanical model of a pelvis with a fetus, or as comprehensive as a computer-driven full-body simulator. Scenarios are either (mechanically) created by the instructor (e.g. by hindering fetal birth) or preprogrammed in a computer-driven birthing simulator.

Since medical decisions are based on physiologic signs of mother and fetus, biofidelic generation of these vital parameters during a simulation is essential. However, none of the current simulators is equipped with a mathematical model that describes the relationships between the physiologic systems in the pregnant woman and her fetus: current simulators make use of so-called black box models. Black box models cannot provide insight in system coherence, but are useful in generating output. Ideally, simulators would make use of white box models to integrate the different physiologic systems in the human body in order to provide the physiologic coherence between different vital signs such as blood pressure, heart rate, uterine contractions, etc. However,

white box models require a complete insight in the system, which is often not the case in physiology. Therefore the term grey model is used for models that intend to capture the original system as much as possible in model equations. Often a grey model consists of "white" and "black" parts.

A grey model for a delivery simulator should link the cardiovascular parameters of mother and fetus, uterine contractions and fetal heart rate, such that it can provide all relevant parameters in their mutual relationship during delivery. Not only can such a model be used for skills and CRM training, it can also be used for teaching (patho)physiological principles and can thus provide more insight into (patho)physiology.

The development of a physiologic model of mother and fetus is planned within a PhD-project. As a part of that, in a one-year clinical project, a start is made with the modeling of the cardiotocogram. A cardiotocogram is the combined registration of uterine contractions and fetal heart rate in time, and is one of the main tools for fetal monitoring during labor and delivery. The one-year project consists of two parts: a full implementation of so-called "early decelerations", and the specification of additional model requirements for the implementation of so-called "late decelerations" in the available model [78]. Both early and late decelerations are deviations in the cardiotocogram related to uterine contractions during labor. The implementation of late decelerations is beyond the scope of the one-year project, but is planned within the PhD-project. This report presents a brief overview of the one-year clinical project, for more details on technical implementation the reader is referred to appendices. The result of the project is based on a combination of previous work [78] and new elements developed in this project.

The model aims to simulate (patho)physiologic changes during labor and delivery correctly. A special focus is put on the physiologic coherence of the subsystems, such that the model can provide insight into (patho)physiology. In future a link will be made between mechanic processes during labor and delivery, as simulated with a full-body delivery simulator, and the physiologic response of vital signs in the mathematical model. This allows for an easy setup of obstetric training, such that the instructor can fully focus on team aspects and is not occupied with a complicated simulation environment. It also secures the repeatability of training programs, which will facilitate research projects on team aspects.

This report first focuses on the cardiotocogram as monitoring tool and how it is used during labor and delivery (chapter 2). In this chapter, also a brief overview of deviations in the cardiotocogram will be described, together with the physiologic mechanisms that are responsible for the occurrence of these deviations. This includes the mechanism of early and late decelerations. In chapter 3 it is described how early decelerations are implemented in the mathematical model. The mechanism as described in chapter 2 is thereby used as a lead. Validation of implementation has been obtained via review of clinical experts. The chapter ends with a discussion and conclusion. Chapter 4 will describe the definition of model specifications for late decelerations. The specifications may serve as a starting point for extending the applicability of the current model. Finally in chapter 5 a reflection on the total clinical project will take place.

2 The cardiotocogram

During labor and delivery, the obstetric team bases medical decisions on fetal and maternal welfare. Ideally the oxygen state at different sites in the fetus would serve as the best parameter for fetal welfare. However, this information can currently not be obtained in normal clinical practice. Therefore parameters are used that are influenced by oxygen state, such as the fetal heart rate and peripheral blood oxygen content. The fetal heart rate can be obtained non-invasively, which means that no (internal) access is needed to the fetus and the mother. Continuous fetal heart rate monitoring is therefore widely used. Fetal heart rate is directly influenced by uterine contractions, and therefore mostly registered simultaneously with uterine pressure measurement. This combined registration is known as the cardiotocogram (CTG), with *cardio* referring to heart rate and *toco* referring to childbirth. In clinical practice however, the uterine pressure signal is often called the *toco signal*. The second important method for monitoring fetal welfare in labor and delivery is an analysis of (peripheral) blood sample from the fetal scalp. This invasive and non-continuous measurement can only be performed once the membranes are broken. Due to the invasive character, the scalp blood sample (micro blood examination) is only used in critical situations.

The fetal heart rate, given as beats per minute (bpm) can be measured externally or internally. External measurement is based on the ultrasound Doppler principle to detect fetal heart movements through the abdominal wall of the mother. Internal measurement can be obtained via a scalp electrode on the fetal head via the birth canal to measure the ECG (electrocardiogram): the corresponding heart rate can then be obtained from R-R-intervals. Both techniques are useful and accurate. However, if the membranes are still intact, internal measurement of the heart rate signal is not possible. Internal measurement is a minimal invasive technique: the scalp electrode is "screwed" into the skin, therefore external measurement is more widely used. However, in some situations it might not be possible to detect a clear fetal heart rate signal via the abdominal wall: in obese women it might be difficult to retrieve a clear Doppler signal, while in other cases there might be doubt about a maternal instead of fetal origin of the heart rate tracing. In the current study no distinction is made between the signal for internal and external registration, assuming that no signal loss occurs [8].

The toco signal - the uterine pressure signal used for contraction tracing - can be measured externally or internally with a pressure sensor. External measurement is inaccurate, since the pressure signal is highly dependent on the position of the sensor. Toco signals cannot be compared between different measurement sessions, even within one recording, since quantitative interpretation is difficult due to positional changes of the women, which influence the pressure signal. In obese women, toco signal recording might even be impossible. Internal measurement is far more accurate, but is only possible once the membranes are broken. The contraction strength is only reliable during internal measurement and differs from woman to woman. The toco signal is therefore mostly used qualitatively only, since variations in the fetal heart rate signal need to be linked mainly to the timing of the contraction. For detection of contraction length and interval external measurement precise is enough. A picture of a normal (reassuring) CTG-tracing is shown

in figure 2.1.

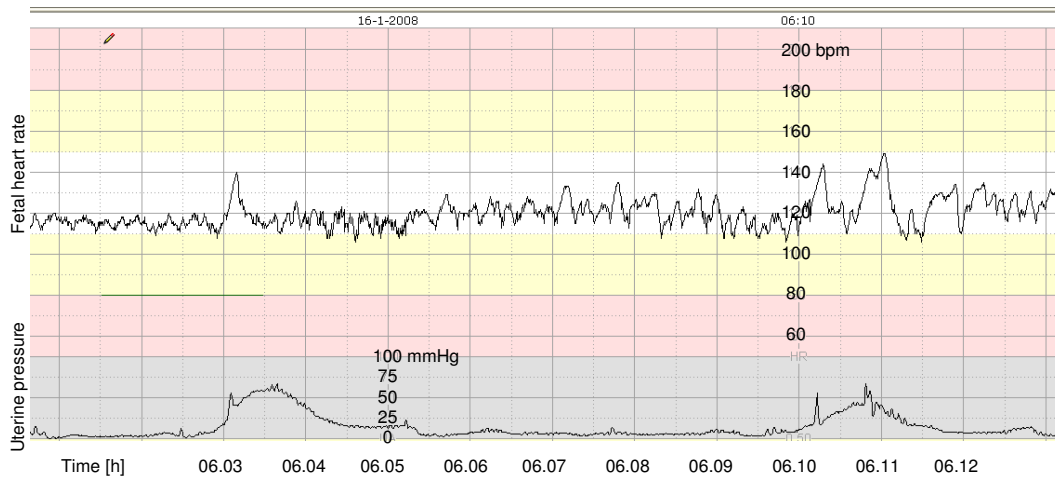


Figure 2.1: Reassuring CTG tracing. A reassuring CTG should show both short- and long-term variability. Baseline is in between 110-150 bpm and no decelerations are seen.

2.1 Interpretation and classification of the cardiotocogram

The toco signal is calibrated at the beginning of each registration by setting the measured pressure in between contractions at 20 mmHg. On top of this baseline, contractions will show up with a more or less bell-shaped form and a duration of 1-2 min. During labor, both contraction frequency and contraction strength will increase. At the end of labor, a typical flattened toco signal might be recorded during pushing effort of the women, since the combined pressure of uterine contraction and voluntary muscle contraction exceeds the maximum pressure detection level of the sensor.

The *baseline* of the fetal heart rate signal is the mean of the fetal heart rate in time. The baseline can be constant or slightly increasing or decreasing in time. Variations with respect to baseline can be divided into two groups: *short-term variability* and *long-term variability*. Short-term variability is also known as beat-to-beat variability and ranges normally between 20-30 μ s (corresponding to 2-3 bpm) in two subsequent heart beats [24]. Long-term variability is evaluated over periods of one minute and can be quantified via bandwidth (normally between 5-20 bpm) or the number of zero-crossings with respect to the baseline (normally 3-6 times per minute) [24]. Variability originates from the central nervous system (parasympathetic and sympathetic nerves) and is an important measure for fetal well-being. Minimal or absent variability might be a sign of a compromised fetus, while normal variability is reassuring [24].

Besides baseline variability, periodic changes might occur. *Accelerations* are deviations in baseline of at least +15 bpm for at least 15 s. Accelerations are associated with fetal movements and are reassuring. *Decelerations* are deviations in baseline of at least -15 bpm for at least 15 s, and can be divided into three categories: *early decelerations*, *late decelerations* and *variable decelerations*. They are related to uterine contractions: the nadir of an early deceleration appears at the peak of the contraction, they mirror the contraction shape; late decelerations mirror the contraction shape as well, but their nadir appears at least 30 s after the contraction top; variable

decelerations are variable in shape, appearance and depth, and are not necessarily related to the contraction timing. These three deceleration types originate from different mechanisms and will be described separately in sections 2.2, 2.3 and 2.4, where also a CTG tracing is shown of each type.

Classification of the CTG was recently unified by the International Federation of Obstetrics and Gynaecology as a result of the introduction of STAN registration for non-reassuring CTG's. STAN is a combined registration of CTG tracings and ST-events in the fetal ECG (computerized ST-waveform analysis). The introduction of STAN pointed out the necessity for unified CTG classification, whereafter new guidelines were developed that included both CTG classification and STAN-events classification [2]. A CTG can be classified as *normal*, *intermediary*, *abnormal* or *preterminal*, as can be seen in table 2.1, depending on baseline, variability and decelerations.

Table 2.1: Guidelines for CTG interpretation. [2]

CTG class	Baseline Heart Rate	Variability/Reactivity	Decelerations
Normal CTG	110-115 bpm	5-25 bpm Accelerations	Early uniform decelerations Uncomplicated variable decelerations with a duration of <60 s and loss of <60 beats
Intermediary CTG	100-110 bpm 150-170 bpm Short bradycardia episode (<100 bpm for ≤3 min)	>25 bpm (saltatory pattern) <5 bpm for >40 min with absence of accelerations	Uncomplicated variable decelerations with a duration of <60 s and loss of >60 beats
Abnormal CTG	150-170 bpm with reduced variability >170 bpm Persistent bradycardia episode (<100 bpm for >3 min)	<5 bpm for >60 min Sinusoidal pattern	Complicated variable decelerations with a duration of >60 s Repeated late uniform decelerations
Preterminal CTG	With or without bradycardia	<2 bpm	With or without decelerations

2.2 Early decelerations

A typical recording of early decelerations is shown in figure 2.2. Early decelerations are uniform in shape - they appear with a U-form - and are related to the descent or engagement of the fetal head in the birth canal. The pressure of the birth canal on the fetal head increases highly during contractions. Intracranial blood flow is hereby reduced, which results in a transient hypoxia of the nervus vagus, a parasympathetic nerve. The fire frequency of the nervus vagus increases due to this hypoxia and causes a reduction in heart rate (chemoreceptor-mediated response). Once blood flow is restored, vagal hypoxia is relieved and its fire frequency returns to baseline level. Heart rate

is thus mostly restored at the end of the contraction. Early decelerations are mostly seen in the transition of first to second stage of labor, i.e. from the transition of passive labor to the active phase with maternal bearing down effort. In a breech presentation, early decelerations might occur earlier in labor, due to head compression in the fundus of the uterus during contractions. In most cases, early deceleration depth does not exceed 20-30 bpm [24, 53, 56] and fetal heart rate rarely falls below 100-110 bpm [24]. The transient vagal hypoxia is fully restored in between contractions and is not associated with a compromised fetal outcome. Hence, once correctly recognized as early decelerations, they require no further attention and can be neglected.

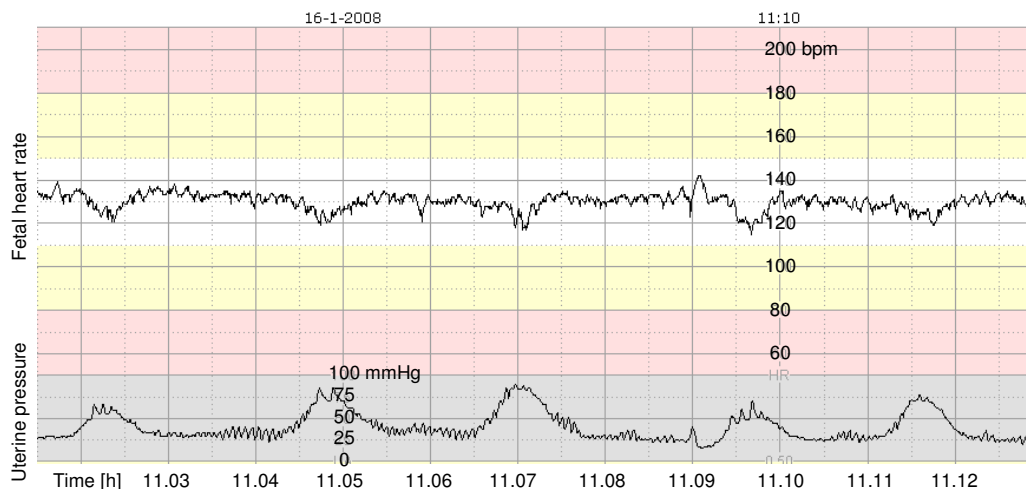


Figure 2.2: Early decelerations. Uniform U-shaped decelerations can be seen simultaneously at each contraction.

2.3 Late decelerations

Late decelerations (see figure 2.3 for a typical CTG recording) are a sign of pathologic hypoxia. They are associated with diminished oxygen transport to the fetus from the placenta, also known as utero-placental insufficiency. Late decelerations follow from the fact that uterine blood flow intermittently arrests during contractions [24]. The lack of oxygen delivery to the intervillous space together with the continued oxygen diffusion over the placental membrane towards the fetus, results in a lowering of oxygen concentration in the intervillous space. It takes some time before this affects fetal oxygen levels in the blood (hypoxemia), which explains the delay of these decelerations [3].

In acute form during labor, the carotid chemoreceptors detect the lowered oxygen content in the arterial blood (triggered by uterine contractions) and stimulate the sympathetic nerve system. Noradrenaline is then released and generates systemic vasoconstriction, resulting in fetal hypertension. This hypertension is sensed by the baroreceptors that respond with an increase in parasympathetic activity that generates a deceleration in fetal heart rate. When acidosis (i.e. low tissue pH) occurs, myocardial depression will result in brain damage. Late decelerations will often be accompanied with diminished variability and the lack of spontaneous accelerations.

Fetal outcome may be complicated with neonatal asphyxia (severe acidosis that affects organ functioning) or even intrapartum death [24]. Acidemia (low blood pH) can be confirmed or excluded via micro blood examination from a scalp blood sample. In severe cases, birth has to be accelerated, with - depending on fetal position - an assisted vaginal delivery (e.g. forceps or vacuum delivery) or a caesarian section.

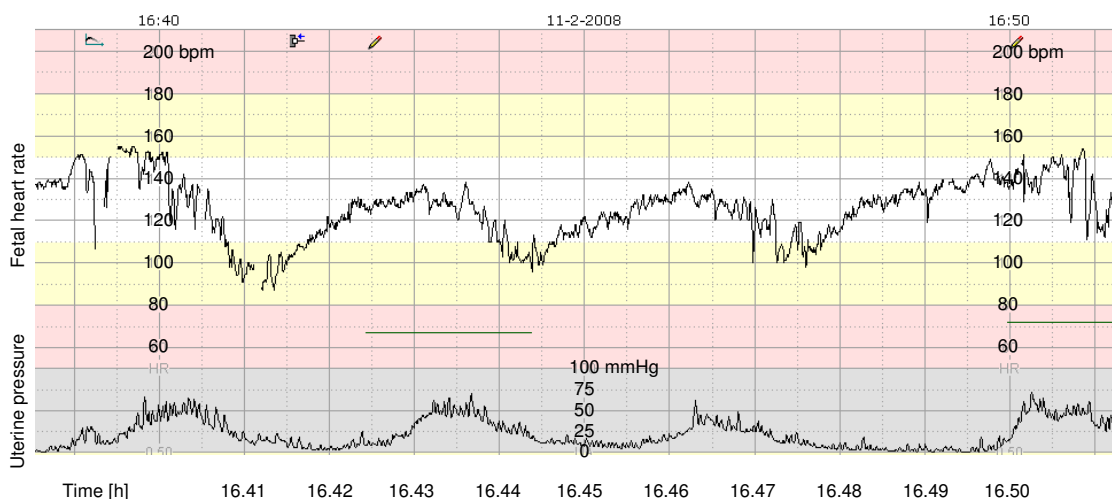


Figure 2.3: Late decelerations. Uniform U-shaped decelerations can be seen after each contraction: the delay exceeds 30 s.

2.4 Variable decelerations

Variable decelerations are all decelerations that do not match the definitions of early or late decelerations. A CTG tracing with variable decelerations is shown in figure 2.4. Variable decelerations are the most common type of decelerations and are mostly associated with umbilical cord compression. Cord compression can occur at any time in labor and can take place before, during or after a contraction. Cord compression can occur between a limb and the uterine wall, or due to a nuchal cord (i.e. a cord around the neck). Cord compression will first occlude the umbilical artery, thereby causing fetal systemic hypertension. The hypertension will be detected by the baroreceptors, thus introducing an increase in parasympathetic activity (nervus vagus stimulation). The umbilical artery occlusion will on the other hand also cause fetal hypoxemia, which is sensed by the chemoreceptors. The chemoreceptors will then further increase vagal activity, that will result in a deceleration. Pronounced fetal hypoxemia will depress the myocardium, thereby decelerating fetal heart rate even more [24].

Variable decelerations may have a U-, V-, or W-shape, see figure 2.4. Shouldering (small heart rate accelerations before and/or directly after the deceleration) can take place, this is a compensatory mechanism. With diminished variability or when the shouldering effect disappears, hypoxia is more likely than in cases with preserved variability. Variable decelerations are definitely pathologic when they last for at least 60 s and/or have a depth of >60 bpm and/or reach a minimum heart rate of <60 bpm [24].

Prolonged decelerations are a subcategory of variable decelerations, and last at least 2 min

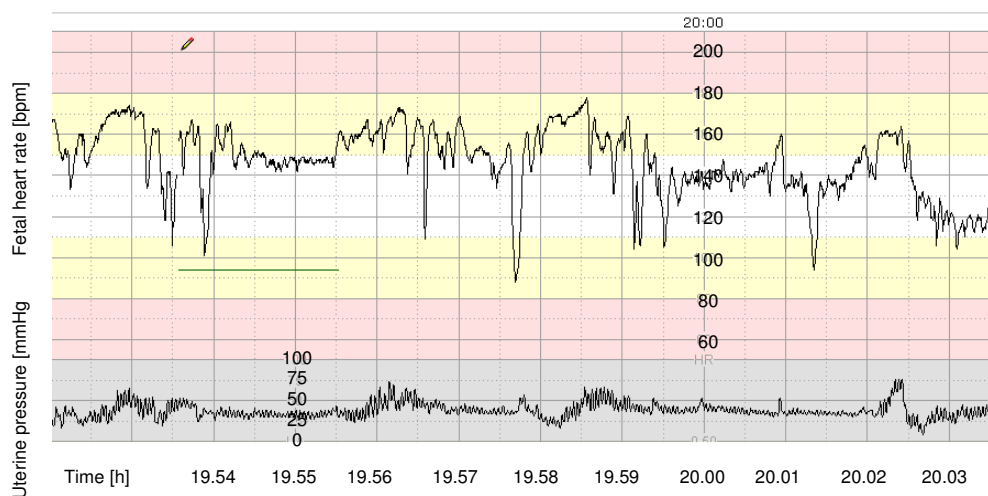


Figure 2.4: Variable decelerations. Variable decelerations can be seen before, during or after a contraction, and are variable in shape. U, V and W forms are common types of variable decelerations.

and reach a minimum heart rate of <100 bpm, as can be seen in figure 2.5. They can appear in a multitude of situations: repetitive variable decelerations might evolve into prolonged decelerations with increasing cord compression; they can be caused by profound utero-placental insufficiency and maternal hypotension; or occur suddenly in case of umbilical cord prolapse. Cord prolapse can occur when the presenting fetal part in the birth canal leaves space where the cord can slip beside. The cord will then be compressed severely with progression of fetal descent. Severe uterine contractions can also cause prolonged decelerations. Depending on the cause and the oxygenation state of the fetus prior to the prolonged deceleration, the fetus may completely be resuscitated by the placenta. On the other hand, a severe prolonged deceleration may immediately precede fetal death [24].

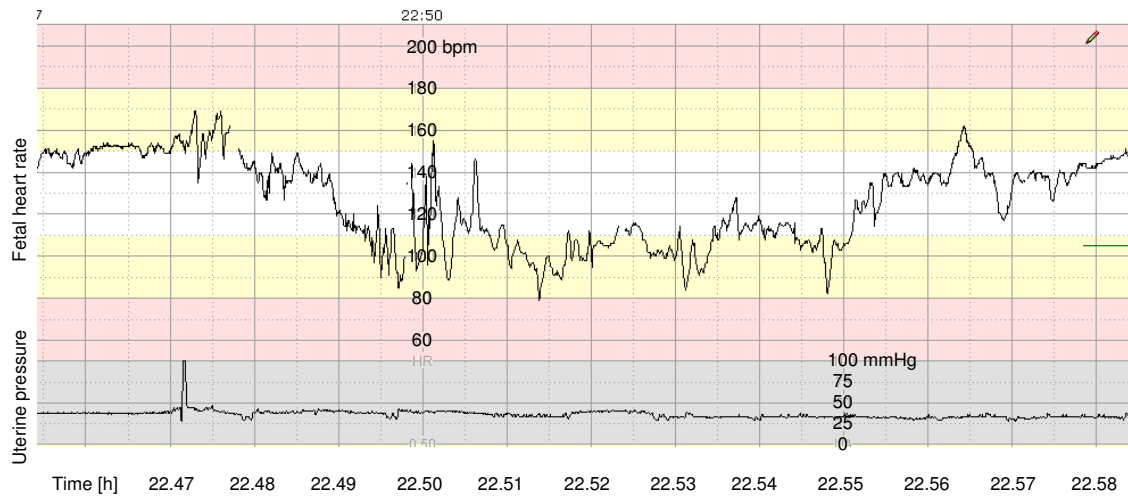


Figure 2.5: Prolonged deceleration. A prolonged deceleration lasts at least 2 min and has a minimum heart rate of <100 bpm.

3 Simulation of early decelerations with a mathematical model

The systems involved in the three different deceleration types are the chemoreceptor reflex and the baroreceptor reflex. The cascade leading to early decelerations is the simplest of the three mechanism schemes with only the chemoreceptor involved. Early decelerations are therefore chosen as the first scenario to be modeled. To be able to model early decelerations as extension in the existing mathematical model [78], an inventory need to be made of what is needed and what is already available in the model. This inventory is based on the early decelerations mechanism, as shown in figure 3.1 and described in paragraph 2.2. From the figure can be seen that uterine contractions reduce cerebral flow, which will reduce oxygen delivery to the fetal brain. In the brain, hypoxia will occur, including hypoxia of the vagal nerve. The vagal nerve reacts with an increase in fire rate (chemoreceptor-mediated response) that has a decelerating effect on fetal heart rate.

In order to capture this model in the existing mathematical model [78], first model parts that are missing will be designed with model parameters derived from literature. Finally the complete system will be implemented in Matlab.

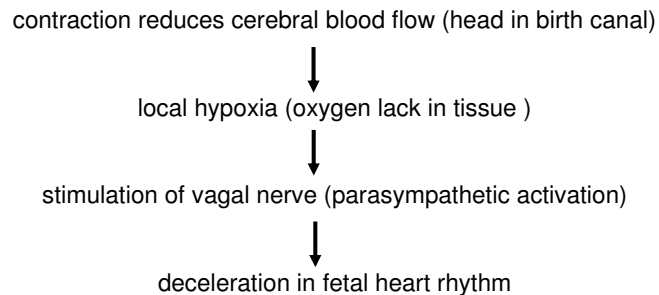


Figure 3.1: Mechanism of early decelerations. The contraction reduces cerebral flow, which results into local hypoxia, including the vagal nerve. The vagal nerve therefore increases fire rate, which has a direct effect on heart period length and causes thus an early deceleration. (After Freeman [24], modified with information of Caldeyro-Barcia [15].)

3.1 Available mathematical model

The existing model is developed in cooperation with Eindhoven University of Technology, department of Biomedical Engineering and the Máxima Medical Center in Veldhoven to model complications that might occur during labor and delivery. These complications can originate from fetal, maternal and/or placental causes. A full description of the model is available in appendix C. Figure 3.2 shows a schematic overview of the blood vessels and organs (e.g. tissue, heart)

modeled prior to adaptations for scenarios. Its basic functions will be explained shortly in this section.

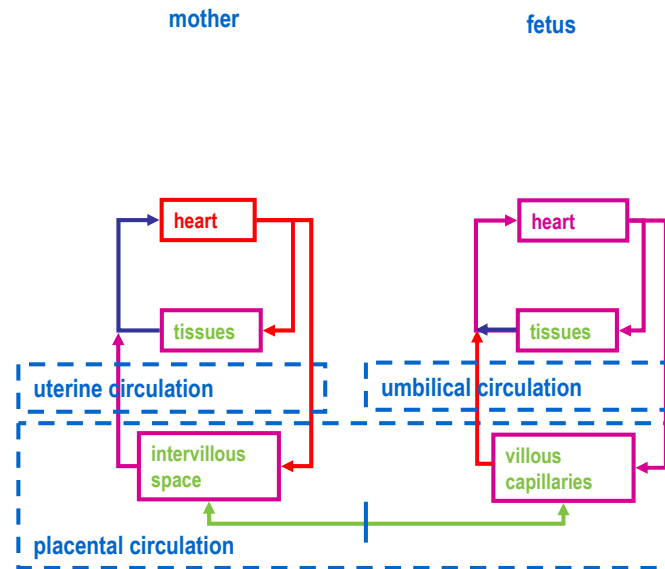


Figure 3.2: Block diagram of the available model. The maternal circulation is separated from the fetal circulation by the placental membrane (blue vertical line in the placenta). Oxygen is exchanged between mother and fetus (green arrow) over this membrane, blood is not exchanged between mother and fetus. Parallel to the main maternal circulation, the intervillous space is supplied with blood. Similarly the villous capillaries are parallel to the main fetal circulation, as is shown by arrows. The color of the arrows and the blocks give an indication of oxygenation level. Fetal circulation is split-up in a systemic circulation and umbilical/placental circulation.

The model includes the maternal circulation (heart and vessels) that are split-up into a systemic circulation with a separate uterine circulation, parallel to the systemic circulation. Lung circulation is not modeled explicitly: maternal blood is assumed to be fully oxygenated before entering the arterial system. Lung function is thus assumed constant and sufficient. Changes in maternal heart function or circulation system will affect the amount of oxygen delivered to the placenta, and thereby induce changes in the fetus.

The fetal circulation is modeled with a separate umbilical circulation parallel to the fetal systemic circulation. Fetal blood is oxygenated in the placenta, therefore fetal lung circulation is not explicitly needed and can be modeled within the systemic circulation. The modeled heart can be considered as the combined left and right ventricle, so the foramen ovale is included implicitly. The two umbilical veins are taken as one combined vein in the model, since no distinction between both vessels is necessary for the intended scenarios. If needed in future, any adaptation to anatomy can be executed easily.

The placental circulation is the combined uterine and umbilical circulation. One of the major (cardiovascular) functions of the placenta is the exchange of oxygen over the placental membrane. In the model this is described with diffusion laws that link placental flows to oxygen content on both sides of the placental membrane.

With the current model, only scenarios can be performed that can be covered by the subfunctions available. To be able to create any other scenario, new model functions have to be included, based on the steps in the underlying mechanism of the scenario. For early decelerations, several steps lead to the actual fetal heart rhythm decrease: uterine contractions diminish fetal cerebral circulation, thus lowering fetal cerebral pO_2 that increases vagal nerve fire rate and subsequently lowers fetal heart rate, see also figure 3.1. Thus, the feto-maternal model should be able to represent:

- uterine contractions (paragraph 3.2.2),
- the influence of contractions on cerebral flow (paragraph 3.2.3),
- the influence of diminished cerebral flow on cerebral oxygen pressure (paragraph 3.2.4),
- the influence of cerebral reduced oxygen pressure on vagal nerve fire rate (paragraph 3.2.5),
- the influence of vagal nerve fire rate on fetal heart rate (paragraph 3.2.6),
- heart rate variability (paragraph 3.2.7).

As can be seen from this list, uterine contractions are the input for early decelerations and all other model requirements originate from the contractions. However, heart rate variability is in fact part of a bigger system that is beyond the scope of this project. Heart rate variability plays an important role in the interpretation of the CTG and needs therefore to be included in the modeling of early decelerations as well. To achieve this within the time limit of the current project, heart rate variability is obtained from a black box model instead of being calculated within a physiologic model.

3.2 Methods

3.2.1 Necessary model adaptations

Currently, the model has no uterine contractions: external pressure on the blood vessels is zero. However, a pressure curve in time, representing uterine pressure, can easily be applied at all vessels involved. Also cerebral blood circulation is not modeled separately, but as a part of the total systemic circulation. The blood flow to the total systemic circulation has thus to be divided into two parts: one towards the brain and the remaining part to the other organs of the systemic circulation. Oxygen pressures can be calculated in the systemic circulation, but not yet in the to-be-developed brain circulation. Mathematical equations for oxygen pressures have therefore to be extended for the brain circulation. The vagal nerve has to be added in the model. This parasympathetic nerve is part of the autonomous nerve system that is also involved in other types of decelerations. Besides the vagal nerve, hence also the sympathetic nerve, chemoreceptors and baroreceptors are needed for the total regulatory mechanism. In the current project, the model of Ursino [76] will be implemented to fulfil this requirement.

3.2.2 Uterine contractions

As explained in chapter 2, the toco signal should be qualitatively recognizable as a baseline of 20 mmHg and additional contractions. Contractions have a more or less bell-shaped form and are modeled with a sine quadratic function. The contraction interval, strength and duration are chosen randomly from the normal distribution as determined from available CTG's with early decelerations, as can be found in appendix E.

The contraction pressure is modeled as an external pressure at all vessels that are present in the uterus, i.e. uterine artery, vein and intervillous space; and all fetal vessels. This does not

result in flow changes, since the external pressure is applied equally at all places and resistances are not changed. Figure 3.3 shows the toco signal as modeled.

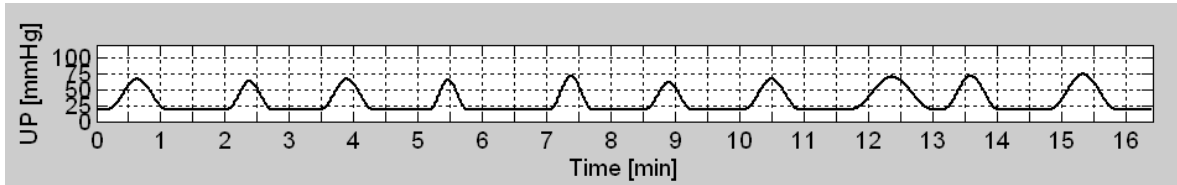


Figure 3.3: Contractions as generated with the model. Uterine contractions are visualized via a uterine pressure (UP) signal. Baseline is set at 20 mmHg as is common with external uterine pressure measurement.

3.2.3 Influence of uterine contractions on cerebral flow

Since the brain circulation was not modeled explicitly, firstly normal values for cerebral blood flow and volume for a term fetus had to be determined from literature. (See table A.2 in the appendix.) In the model, the amount of cerebral flow is subtracted from systemic blood flow and redirected in a new vessel that originates from the systemic artery and ends in the systemic vein, thus forming the cerebral circulation.

The compression of the cerebral vessels by the birth canal during contractions results in a smaller vessel diameter and a higher intravascular resistance. To model the influence of uterine contractions on cerebral flow, the vessel resistance of the cerebral arterial circulation is made linearly dependent on uterine pressure: the stronger the contraction, the higher the intravascular resistance and thus the lower the flow. (See appendix C for modeling details.)

It is known that cerebral pO_2 reduces up to maximal 20% [53]. It was assumed that this maximum reduction was accompanied with a maximal fetal heart rate reduction of 30 bpm (see paragraph 2.2). To achieve this pO_2 reduction, the cerebral resistance had to be increased by a factor 6.4 at the top of the contraction. The calculated dependency of cerebral flow on uterine contractions can be seen in figure 3.4.

3.2.4 Influence of diminished cerebral flow on cerebral oxygen pressure

The paper of Sà Couto et al.[62] describes the relationship between cardiovascular variables (e.g. blood flow, blood volume) and oxygen content at different sites in the fetomaternal circulation. This is done with a system of differential equations for oxygen content at four sites (intervillous space, villous capillaries, fetal arteries and fetal microcirculation). Partial oxygen pressures are calculated via oxygen saturation curves from oxygen content via oxygen saturation curves. Saturation curves differ for mother and fetus (see also appendix A.2.1) and form another four equations, for each compartment one. Since in Sà Couto's work [62] the cerebral compartment was not considered separately but as an integrated part in the fetal systemic circulation, the system of differential equations had to be rewritten for the current study. The system of eight differential equations is therefore extended with two new equations; furthermore the equation for arterial oxygen content (one of the existing eight equations) had to be reformulated, since it is also dependent on (the

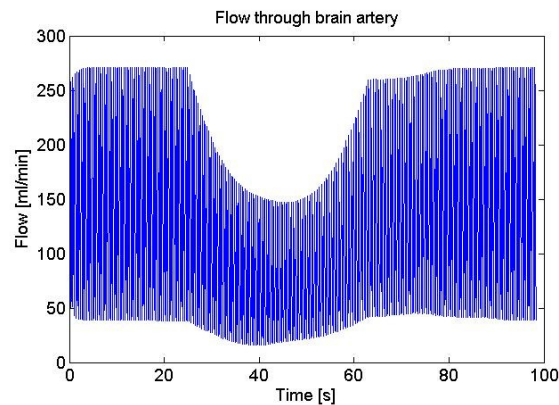


Figure 3.4: Cerebral flow reduces during a contraction. Due to caput compression during contractions, cerebral flow will reduce. Arterial blood flow oscillates due to blood pressure changes. Both mean cerebral flow and maximum and minimum flows are reduced.

now explicitly modeled) cerebral blood flow and volume. All equations can be found in appendix C.4.

Since both cerebral blood flow and volume reduce (and restore) during contractions, cerebral oxygen pressure follows the same trend (in accordance with the oxygen saturation curve). This can be seen in figure 3.5; note that partial oxygen pressures in other compartments (intervillous space, villous capillaries, fetal arteries, fetal microcirculation) are only slightly influenced by the oxygen changes in the brain. This is due to the fact that blood volume in the brain is just a small fraction in comparison with blood volume in these other compartments.

3.2.5 Influence of reduced cerebral oxygen pressure on vagal nerve fire rate

Cerebral oxygen pressure influences the nervus vagus. During vagal nerve hypoxia, vagal nerve fire rate increases. Sympathetic nerve fire rate is not influenced by head compression, therefore heart rate decrease during early decelerations is assumed to be fully caused by vagal fire rate increase. The additional vagal fire rate needed to achieve the maximum deceleration depth of 30 bpm was found to be 1.3 Hz at the maximum decrease of normal cerebral partial oxygen pressure of 20%.

Note that this additional fire rate is scaled with the oxygen pressure, such that the current deceleration depth is related to the oxygen reduction that is based on contraction strength. Total vagal nerve fire rate is the sum of additional fire rate and original fire rate (baseline fire rate) as calculated according to Ursino [76], see also appendix C.3. Figure 3.6 shows the original fire rate and the additional fire rate. Note that the relation between uterine contraction and the additional fire rate can still be easily recognized.

3.2.6 Influence of vagal nerve fire rate on fetal heart rate

The relation between vagal nerve fire rate and heart rate in the fetal model is based on the work of Ursino [76]. The complete model implementation is described in appendix C.3. Heart rate is the inverse of heart period, which is one of the output parameters of Ursino's model [76]. He modeled heart period as the sum of a baseline heart period and changes in heart period introduced by

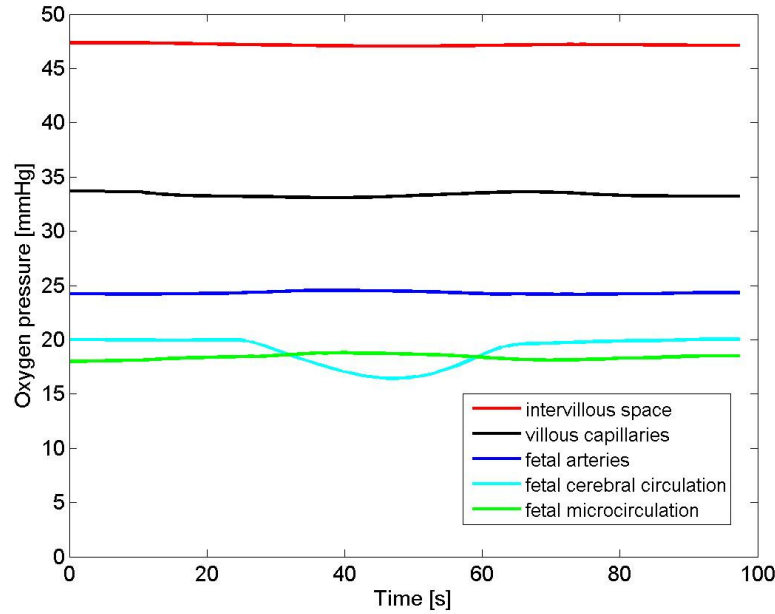


Figure 3.5: Partial oxygen pressures during early decelerations in the feto-placental circulation. The partial pressure in the fetal brain decreases during a contraction. Due to the diminished oxygen delivery to the brain, the partial pressures in the fetal arterial and microcirculation increases initially. After flow restoration in the brain, partial oxygen pressure in the brain is increased by increased flow and oxygen extraction from the other blood compartments. Since blood volume in the brain is small compared to the other compartments, pO_2 -change is much higher in the brain than in the other compartments.

sympathetic (ΔT_s) and parasympathetic nerves (ΔT_v). Since sympathetic nerves are not involved in early decelerations, ΔT_s is a constant. The relation between vagal nerve fire rate f_v and ΔT_v can be described via a first order differential equation [76], see appendix C.3. Figure 3.7 shows fetal heart rate as a function of time, in relation to uterine contractions.

3.2.7 Implementation of variability in heart rate and contraction signal

To obtain a realistic tracing of the fetal heart rate variability, a new variability signal is added to the smooth computer-generated heart rate signal. This new variability signal consists of two combined signals: a filter based on original tracings that is multiplied with a random (white noise) signal. For details see appendix C.5.

The filter, once determined, can be used to generate unlimited numbers of unique variability signals by filtering new white noise signals. By adding the variability signal (see figure 3.8 for an example) to the heart rate signal as determined from the model, a realistic tracing is obtained.

The same procedure can be repeated for the toco signal. In clinical practice it is very difficult to measure uterine activity without disturbances caused by maternal breathing and movements. These show up on the toco signal as "noise" and have no clinical relevance, in contrast to the variations in heart rate. Since validation of the computer-generated CTG tracings will be done via CTG interpretation and comments by experts, the toco variability is needed to mask the fact that the tracings are computer-generated. The variations in uterine activity can be easily generated with the same procedure as for heart rate variability. The filter is obtained from an original toco

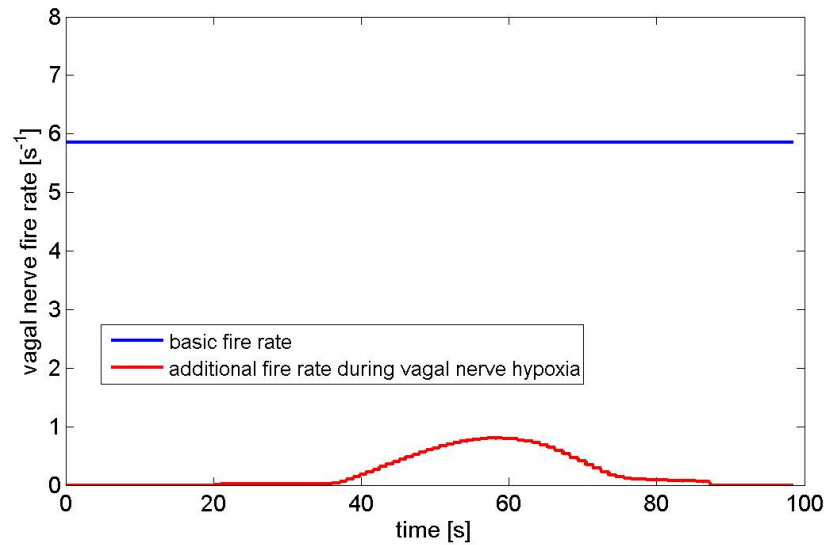


Figure 3.6: Contributions of baseline and hypoxia to vagal nerve fire rate. Without hypoxia, total vagal nerve fire rate is equal to baseline level (in blue). In case of vagal nerve hypoxia, an additional fire rate exist (in red), which together with baseline level, forms the total vagal nerve fire rate (not shown).

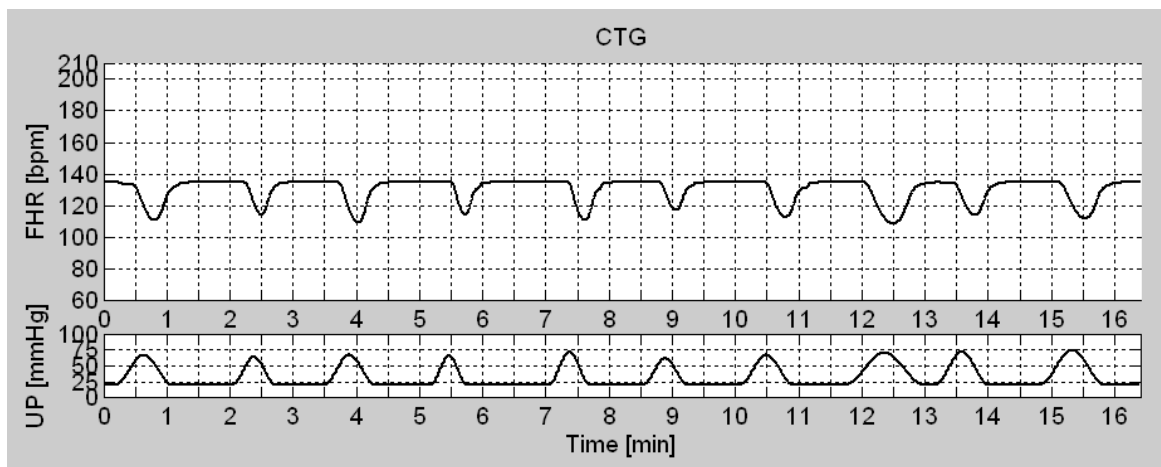


Figure 3.7: CTG signal as calculated with the model. The fetal heart rate (FHR) is shown as function of time in relation to the intrauterine pressure. Short term heart rate variability is not calculated by the model and therefore missing in this CTG tracing. The shape of the deceleration is directly related to the shape of the vagal nerve fire rate and thus vagal nerve hypoxia. This is not fully symmetric due to feedback mechanism of hypoxia on fetal heart rate which will effect the amount of hypoxia.

signal.

In figure 3.9 the modeled CTG with heart rate variability and pressure variation is shown.

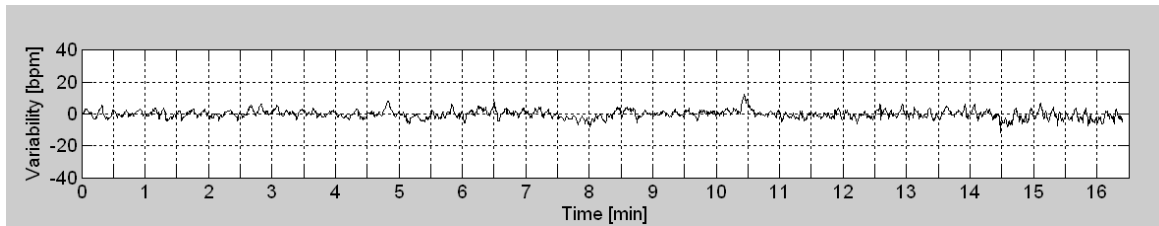


Figure 3.8: Variability signal based on real variability. The variability is located around a baseline of zero and can be added to the FHR-tracing as shown in figure 3.7.

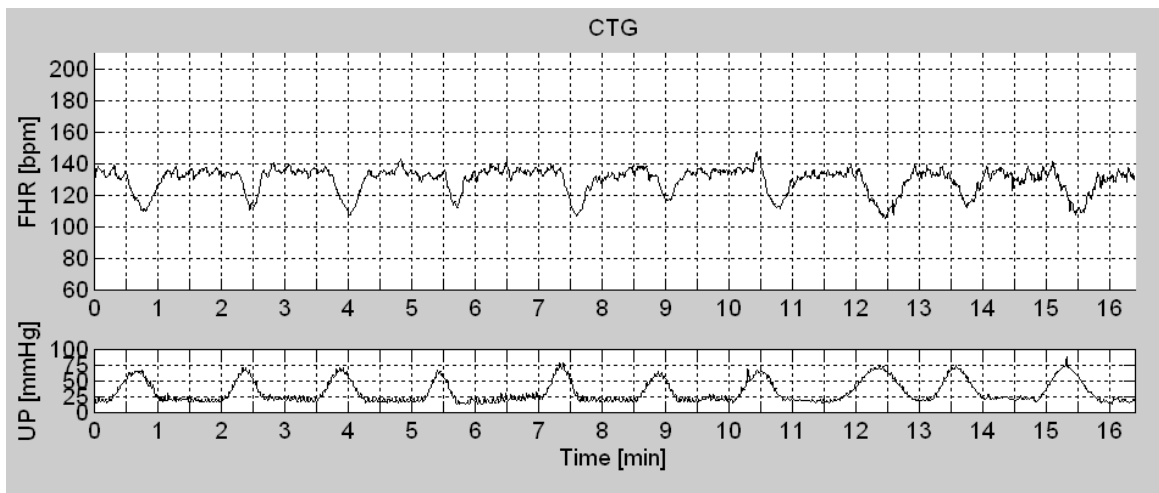


Figure 3.9: CTG signal from the model with added short term heart rate variability. Heart rate variability is added to the calculated heart rate signal from the model. Noise is also added to the toco signal to obtain a more realistic tracing.

3.3 Model overview after model adaptation

An overview of the mathematical model with extensions after implementation of early decelerations, is shown in figure 3.10. As can be seen, the fetal brain circulation is now modeled explicitly and the baro- and chemoreceptor (BRR and CRR respectively) are included in the fetal circulation. Although the fetal baroreceptor function is assumed constant during early decelerations, it is not in late decelerations, and the model used for implementation (Ursino's model [76]) has both, therefore they are included together. Uterine contractions (not shown) are applied at the placental and fetal circulation.

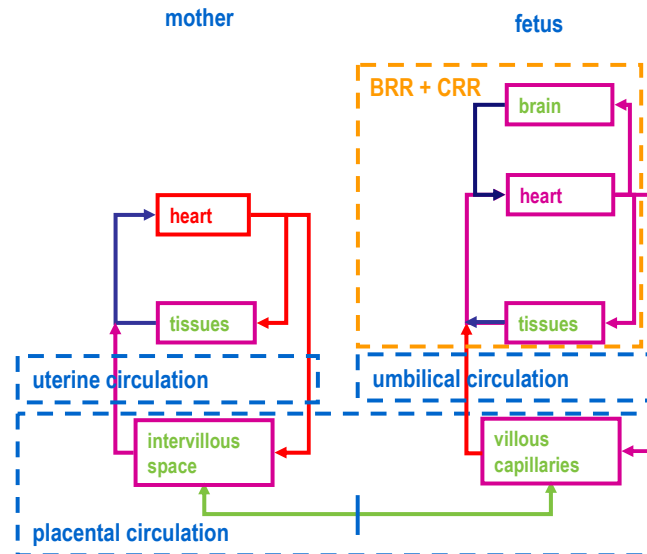


Figure 3.10: Block diagram of the model. The maternal circulation has not been adapted. Oxygen is exchanged between mother and fetus (green arrow) over the placental membrane, and due to different consumption rates and shunt flows, oxygen pressures differ at several sites in the fetus (included in the model: umbilical, arterial, cerebral oxygen pressure and oxygen pressure in the microcirculation). Cardiovascular regulation is only modeled in the fetus (BRR and CRR) since the maternal circulation is assumed to be in steady state.

3.4 Clinical evaluation

3.4.1 Method

For evaluation of the modeled CTG tracings, 5 gynaecologists-perinatologists (gynaecologist with a specialization in perinatology) were requested to evaluate (in Dutch) a series of 10 CTG tracings with early decelerations. From the 10 tracings, 5 were computer-generated by the model and 5 were obtained from CTG registrations from the hospital database (these tracings were two years old to prevent recognition). All 10 tracings can be found in appendix F. Gynaecologists were asked to rate realism of fetal heart rate, early decelerations and uterine rest tone and uterine contractions in the tracing for several aspects:

- fetal heart rate baseline and variability;
- early decelerations delay, duration, depth and morphology;
- uterine rest tone level and morphology
- uterine contractions amplitude, frequency, duration and morphology.

The rating levels for each of these items were: *realistic*, *fairly realistic* or *not realistic*. Per item remarks could be made on realism.

Finally, respondents had to classify the tracing as *real*, *computer-generated* or as *not distinguishable*. From the 5 gynaecologists, 3 responded. Two of them have 6-10 year, and one >10 years experience with interpretation of the CTG.

3.4.2 Results

All tracings were evaluated by all 3 raters. A total of 349 out of 360 items were evaluated (10 tracings times 12 items times 3 raters). Ratings per item varied mostly between *realistic* (204 of 349) and *fairly realistic* (140 of 349). In total 5 times out of 349 a *not realistic* rating was given:

- 2 gynaecologists identified in the same computer-generated tracing a non-realistic deceleration delay (delay was too late);
- for the same trace as under the first bullet, 1 gynaecologist commented twice on the variations in the toco signal (both baseline and contraction variations are too "trembling");
- 1 gynaecologist found the contraction morphology of a real tracing not realistic.

Per gynaecologist, the ratio between *realistic* and *fairly realistic* differed considerably: 33:87, 108:8 and 63:55. In total 30 tracings were classified (3 raters times 10 tracings): 12 correct (identified correctly as *real* or *computer-generated*), 10 could not be classified (*not distinguishable*), and 8 were incorrectly classified. For all results, see figure 3.11. From figure 3.11 becomes clear that about two-third of the tracings - either real or computer-generated tracings - was classified as *real* or *not distinguishable* and about one-third was identified as *computer-generated*.

	Real CTG tracings		Computer-generated CTG tracings		P-value
	N	[%]	N	[%]	
Rated items	N=173		N=176		
<i>Realistic</i>	103	[29.5]	101	[28.9]	* 0.50
<i>Fairly realistic</i>	69	[19.8]	71	[20.3]	* 0.51
<i>Not realistic</i>	1	[0.3]	4	[1.1]	0.15
Classification of CTG's	N=15		N=15		
<i>Real</i>	4	[13.3]	2	[6.7]	0.50
<i>Computer-generated</i>	6	[20.0]	5	[16.7]	0.58
<i>Not distinguishable</i>	5	[16.7]	8	[26.7]	0.43

Figure 3.11: Validation results. Three clinical experts rated 12 items on 5 real and 5 computer-generated CTG's on realism. They also had to distinguish real and computer-generated CTG's from each other. The number of raters is low and only the first two categories had enough statistical power (p-values marked with *).

From the results can be concluded that there was difficulty to distinguish real tracings from computer-generated tracings. Secondly, the items of computer-generated tracings that were correctly identified as *computer-generated*, were rated merely *realistic* and *fairly realistic*: only 4 of 176 rated items were considered *not realistic*. This implies that, although half of the computer-generated tracings could be identified as *computer-generated*, computer-generated tracings still have a high level of realism for simulating early decelerations. This also became clear from the remarks of the raters, who found it very difficult to classify a tracing as *real* or *computer-generated*. None of the categories differed significantly between real and computer-generated tracings. However, only the first two categories (*realistic* and *fairly realistic*) had enough statistical power to prove no difference.

3.5 Discussion & Conclusion

For the development of a delivery simulator, a mathematical model [78] was further extended with the implementation of early decelerations during labor. The current implementation aims to link physiologic insights as much as possible to heart rate changes. The mechanism of early decelerations was derived from literature. Although there are different hypotheses on the actual mechanism involved in early decelerations, it is clear that there is a chemoreceptor-mediated response of the vagal nerve (i.e. hypoxia-mediated) that results in an increase in vagal fire rate [11, 15, 24]. However, it is also suggested that the vagal nerve fire rate increases under influence of increased intracranial pressure, similarly as the oculocardiac reflex [15]. Since vagal nerve hypoxia was found the most common explanation with current research methods, this mechanism was adopted for the implementation of early decelerations. With progressing research methods, insights in early decelerations mechanism might improve. Thus in future, our implementation of early decelerations might need a review.

It was possible to link each physiologic step in the mechanism of early decelerations to a model extension, with parameter values adjusted either according to literature data - or when not available - obtained from estimations with the model. Hence the physiologic cascade from uterine contractions to influence on heart rate could be implemented. The model also allows for estimation of other parameters which currently not have been measured during early decelerations, such as cerebral blood vessel diameter reduction during head compression. This value can not be validated yet, since this requires intrapartal diameter measurement of cerebral vessels of the fetus, which is both aggravating during labor and difficult to achieve with current measurement techniques. Hopefully future technical developments will allow validation.

Validation of estimated parameter changes during early decelerations is also currently not possible. For instance, vagal nerve fire rate (increase) has not been measured in human fetuses during early decelerations. This implies that, should this data become available in future, model values have to be compared to real data and probably adapted. Currently, vagal fire rate increase is estimated to be about 22%. In future this has to be validated with measurements in human fetuses.

Input (uterine contractions) and output (fetal heart rate reduction: early decelerations) were therefore evaluated by clinical experts: gynaecologist with a specialization in perinatology. They were requested to evaluate the modeled CTG tracings with early decelerations on each item that is used in clinical practice for evaluation of real CTG tracings. This included a total of 12 items for 10 CTG tracings of which 5 were modeled early decelerations and 5 were real tracings with early decelerations. The overall judgement of the clinical experts showed that there was no significant difference between real tracings and computer-generated tracings with respect to realism for each of the evaluated items, although the statistical power was too low for most items. They also had difficulties to distinguish real tracings from computer-generated tracings.

This suggests that the modeled CTG with early decelerations can be used in simulated scenarios to represent real CTG tracings with early decelerations. However, the number of experts was small, and no comparison was made with other available CTG simulators. Therefore in near future a more comprehensive evaluation will take place with more experts. Then also CTG tracings from a commercially available delivery simulator will be evaluated, together with real tracings and computer-generated tracings from our model. In the current study this was not possible, since tracings could not be exported from two available (commercial) simulators. Contact with the manufacturer of one of the simulators resulted in a software update that allows for exportation of CTG data, such that they become available for expert evaluation.

4 Model requirements for late decelerations

In section 2.3 it was briefly described that late decelerations both have a chemo- and a baroreceptor component. A full overview of the mechanism is shown in figure 4.1. Late decelerations are caused by a diminished oxygen delivery to the fetus during uterine contractions. In most cases, there is a pre-existing diminished utero-placental flow, which worsens during contractions. The contractions are the trigger, but the pre-existing reduced utero-placental flow is the underlying cause, resulting in central hypoxia. This hypoxia evokes a chemoreceptor response that results in the reduction of blood vessel diameter (vasoconstriction) in the systemic blood circulation. This on its turn will generate a blood pressure increase that is sensed by the baroreceptors, that on their turn respond with parasympathetic stimulation of the vagal nerve that decreases heart rate. Late decelerations are not harmless, since hypoxia is generalized and oxygen demands exceed oxygen delivery. It is therefore essential that the obstetric team is able to respond adequately to late decelerations.

In this chapter, the scheme as presented in figure 4.1 is followed to quantify each step. This quantification is necessary for a physiologic implementation in the model. Yet first some physiological principals on oxygen consumption are explained, since this is necessary to understand how the fetus responds to low oxygen supply in order to survive.

4.1 Fetal physiologic response to central hypoxia

The oxygen data in this section is based on fetal sheep data from Wilkening et al.,[85] since human data are difficult or impossible to obtain in vivo. The sheep is a commonly used model for investigation of cardiovascular (patho)physiology in pregnancy, and sheep data is often scaled to obtain estimates for human parameters. However, scaling is more complicated for cerebral flow and oxygen consumption, since the sheep brain is much smaller (proportionally) than the human brain. All data used in this section is derived from sheep data, but not yet scaled to human proportions. All values expressed in mmol oxygen, as given in original papers, were converted to milliliters since the mathematical model of Sà Couto uses ml oxygen. This was done according to Huntington et al.,[35] using 22.4 ml/mmol oxygen. Furthermore, parameters were scaled for a 3 kg fetal sheep, which is the fetal weight taken in the simulations of our model for a term baby. Thus values in this section correspond to a 3 kg fetal sheep.

During labor, contraction pressures from 35-60 mmHg will proportionally reduce uterine blood flow and once the contraction exceeds 60 mmHg flow will fully cease [7, 86]. This will result in a net reduction of oxygen delivery to the placenta and fetus (product of oxygen concentration and uterine blood flow) and will affect uterine and fetal oxygenation levels, since they are determined by: placental and fetal flows; current oxygenation levels and oxygen consumption.

In a normally oxygenized fetus this reduction in delivery can be fully compensated since there is still enough available oxygen in the fetal blood. Normal *uterine* oxygen delivery rate is about 112 ml O₂/min, which after oxygen consumption by the placenta reduces to an *umbilical* oxygen delivery rate of about 100 ml O₂/min. The term 3 kg fetus extracts about 22 ml O₂/min; this

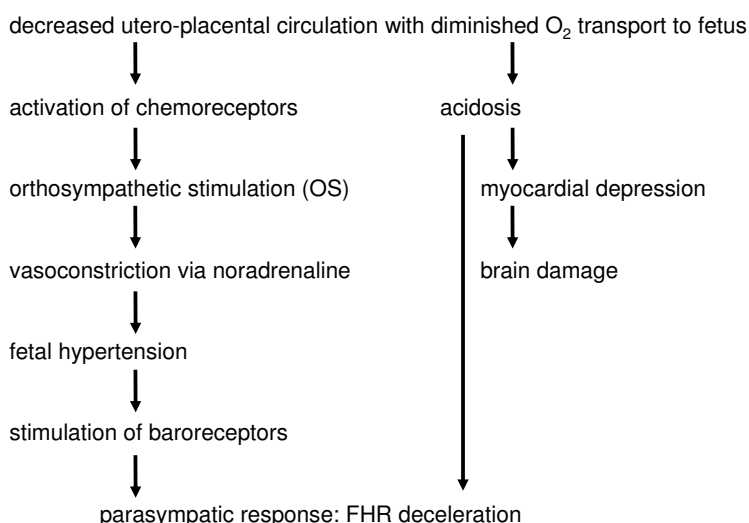


Figure 4.1: Mechanism of late decelerations. Contractions reduce utero-placental flow, and in case of pre-existing diminished placental flows (e.g. placental insufficiency), diminished oxygen transport to the fetus will lead to a cascade that results in late decelerations. Central hypoxia will activate the chemoreceptors that will react with vasoconstriction via noradrenaline. The so-induced hypertension will be sensed by the baroreceptors that react with a parasympathetic stimulation that results in a heart rate decrease. When acidosis occurs, a direct effect can be seen on the fetal heart rate, but via myocardial depression also brain damage can occur. (After Freeman.[24])

extraction rate can be secured with umbilical delivery rates exceeding 40 ml O₂/min [85]. This means that even with a reduction of 60% in oxygen delivery, the fetus can still answer its oxygen demands. However, below a 60% reduction, fetal systemic oxygen consumption is reduced to fulfil oxygen demands in the brain, an adaptation process which is called the brain-sparing mechanism.

4.2 Influence of decreased utero-placental flow on chemoreceptor activation

Hypoxemia, a low oxygenation level in the blood, is sensed by the chemoreceptors in the carotid arteries. The chemoreceptor response aims to minimize (long-term) negative effects of hypoxemia. The signal from the chemoreceptors to the brain increases sympathetic nerve fire rate, which results in the release of noradrenaline, causing vasoconstriction (blood vessel diameter reduction) in the systemic circulation. This increase in vascular resistance lowers systemic flow, thereby reducing oxygen delivery to the tissues. Thus oxygen delivery is peripherally reduced and helps maintaining oxygen delivery to critical areas such as the brain and the heart itself. Flow rates in these areas will increase (via vasodilatation) to fulfil oxygen demands. Below the critical threshold for oxygen delivery rates, oxygen extraction is linearly dependent on oxygen delivery (determined by flow). Thus by reducing flow in the systemic circulation, oxygen extraction is reduced there, and by increasing flow in the brain and myocardium, oxygen extraction can be maintained in these central areas. This linear dependency only holds for umbilical oxygen delivery rates below the critical threshold of 40 ml O₂/min, otherwise oxygen consumption is constant and independent

of supply [85].

Oxygen extraction in the critical tissues (heart, brain) cannot be preserved once oxygen delivery further reduces. Then glucose, the main energy source in the body, will not be metabolized with oxygen (aerobe metabolism), but anaerobically, since oxygen lacks. This has several consequences: glucose metabolism is much less efficient (the same amount of glucose will give only a fraction of the energy when compared with aerobic metabolism) and waste products from anaerobe glucose metabolism will decrease blood pH (acidosis). The depletion in energy production due to glucose deprivation in the brain will finally result in neuronal death. Acidemia (decreased pH of the blood) will also affect cardiac performance. Only a small buffer of glucose is stored as glycogen in the heart, so lack of glucose can result in changes in heart activity [36]. Decreased variability and fetal tachycardia (rising of heart rate baseline) are important signs of developing acidosis [24]. In case of hypoxia without acidosis is cardiac function often preserved [36].

Hence, model requirements for late decelerations are based on fetal response to hypoxemia and chemoreceptor response. During contractions, a decrease in the amount of oxygen delivered to the fetus. Until an umbilical delivery rate of 40 ml O_2 /min, no regulation takes place and oxygen consumption will remain equal. However, together with a decreased oxygen delivery rate this will lead to a further decrease in oxygenation levels. Bearing in mind that normal fetal arterial oxygen levels is about 22 mmHg, chemoreceptor activation takes place after reduction of arterial pO_2 to 17-19 mmHg [53]. In our fetal implementation of the (adult) model of Ursino et al. [76] it has to be determined whether this threshold works correctly or has to be rescaled. Chemoreceptor activation due to (carotid) arterial pO_2 change was not yet tested, and might need some adaptation to obtain the desired response.

4.2.1 Relation between chemoreceptor activation and vasoconstriction leading to hypertension

An increase in sympathetic activity will lead to an increase in peripheral vascular resistance as well. This reflex will reduce flow (to diminish peripheral oxygen delivery) and increase blood pressure. Vascular resistance regulation is described in adults by Ursino et al., [76] and probably needs some adaptation and/or scaling for use in the fetus. In the implementation phase it has to be determined whether original fire rate of the adult results in reasonable response in the fetus. For modeling purposes, it is desirable to minimize adaptations in parameter values that are not related to scalable properties such as body weight, blood pressure, etc. Therefore the original formulas as proposed by Ursino et al. [76] will be used and parameters will be rescaled only when necessary.

4.2.2 Influence of hypertension on baroreceptor activation

An increase in fetal arterial blood pressure will activate fetal arterial baroreceptors. The baroreceptor responds to changes in (mean) arterial blood pressure by sending a signal to the central nervous system. The response curve for this afferent activity (activity towards the central nervous system) is more steep around the physiologic working point than at the edges, it has a sigmoidal response. Since fetal blood pressure is normal prior to uterine contraction, a noticeable response will occur.

The central nervous system will respond to increased baroreceptor fire rate with increasing vagal and decreasing sympathetic fire rates. These signals will lead to both peripheral and central changes in the cardiovascular system in the adult: sympathetic effects are a decrease in peripheral vascular resistances, increased venous unstressed volumes in the systemic circulation (both effects

should lead to a decrease in hypertension) and a combined vagal and sympathetic enlarging of heart period, thus a decrease in heart frequency. These responses are available in the cardiovascular regulation model of Ursino et al. [76] However, these regulatory systems are known to exist in the human *adult*. In the human fetus, one often only refers to increased vagal activity, which leads to heart period enlarging and thus heart rate decrease. More detailed information on baro- and chemoreceptor function in the fetus has to be studied before the comprehensive regulation mechanism of the adult as stated above can be copied and scaled to describe processes in the fetus. Unfortunately it was not possible to include this in the current work due to the time frame.

4.2.3 Relation between baroreceptor activation and fetal heart rate deceleration

Martin et al. [47] was able to relate fetal heart rate deceleration to increase in systolic blood pressure: an increase of 1 mmHg in systolic blood pressure leads to a change in fetal heart rate of approximately -3 bpm. This relation was found to be linear for all cases in the absence of asphyxia. The relation between lowest pO_2 and maximal fetal heart rate reduction within a late deceleration has to be determined to connect all steps in the mechanism of late decelerations. This requires further literature research.

5 Discussion & Conclusion

The development of a simulator to train gynaecologists, requires a clear link between physiologic processes and simulator performance. During this project, feedback from simulation instructors using current CTG simulators confirmed that current simulators have their shortcomings, both in realism and labor-intensiveness. Instructors would like to focus on team aspects rather than running a simulator. Trainees also complained about the lack of realism of simulated CTG tracings from current CTG simulators. Both shortcomings were part of investigation in the current study, and will be in future studies.

The scenarios discussed in this report were therefore fully investigated to understand the mechanism of the cascade in both early and late decelerations. In most cases it was even possible to quantify the individual steps in the process. The scenario of early decelerations was implemented in accordance with literature data and validation results were satisfactory. For late decelerations, implementation and validation were beyond the scope of the project, but a first investigation showed that most steps in the process can be quantified.

The first validation results show that real and computer-generated tracings from our model not seem to differ from real tracings. A more thorough validation with a larger number of experts and the inclusion of computer-generated tracings from commercially available simulators, has to confirm the level of realism of our simulated tracings.

A next step towards an operational simulator is the coupling of the model to an "interface". This can be either a computer with a user interface, or a full-body simulator. The aim is to have both for the simulation of the CTG: a screen-based simulator for individual improvement of knowledge and insight and a full-body delivery simulator for use in a simulated clinical environment to improve CRM-principles within an obstetric team.

Within a ten year cooperation between Máxima Medical Center and Eindhoven University of Technology, the development of a delivery simulator is planned. The development of the cardiovascular model for mother and fetus (PhD project) is planned within this cooperation. The scenario development (early, late and also variable decelerations) are part of this PhD project. Coupling of the complete cardiovascular model will probably take place at the end or directly after the PhD project. Both coupling projects - to a screen-based simulator and to a full-body simulator - will be done by partners within the cooperation. This time frame is set to ensure the thorough development of the mathematical model with as much scenarios as possible.

The coupling to a screen-based interface will take place in future: after scenario implementation of late decelerations, a user interface can be developed for the mathematical model such that clinicians can explore the mechanism of early and late decelerations and their effect on physiologic parameters such as oxygen pressure, blood flow, etcetera.

Simulation has proved to reduce adverse neonatal outcome [21]. Hopefully the introduction of physiology-based CTG simulators will not only make it possible to reduce perinatal errors, but also help obstetricians to obtain insight in the physiologic processes that govern heart rate regulation.

A Physiological cardiovascular processes and adaptation

The continuous fetal growth process requires continuous maternal adaptation. In this section, firstly the maternal physiologic cardiovascular adaptation to pregnancy and childbirth is described, followed by quantitative literature data. Secondly the end stage of the fetal cardiovascular growth process is described and characterized also with quantitative literature data.

A.1 Maternal circulation

A.1.1 Physiologic cardiovascular adaptation in pregnancy

During pregnancy, the placenta plays a key role in the exchange of nutrients, oxygen, fetal metabolic waste products and carbon dioxide between fetal and maternal blood.[71] Figure A.1 shows the fetal and maternal blood vessels and compartments involved in placental circulation.

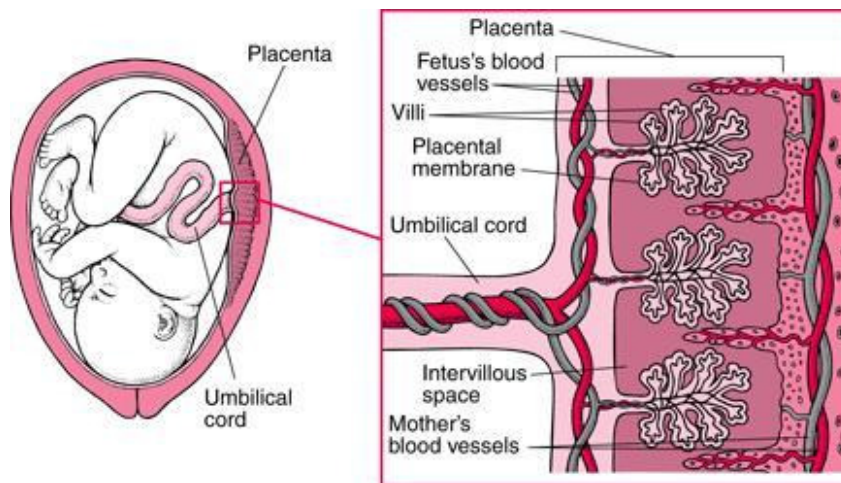


Figure A.1: Placental blood supply.[46] Maternal arterial blood supplies nutrients and oxygen towards the intervillous space, from where it can diffuse over the placental membrane into the villous capillaries. The umbilical vein directs the oxygen-rich blood towards the fetal circulation. Fetal waste products are transported in opposite direction via the umbilical arteries to the villous capillaries. Via diffusion over the placental membrane they enter the maternal blood in the intervillous space and are then transported towards the maternal venous circulation via the uterine vein.

The placenta can be considered as a "parallel circulation" to the uterine circulation. Inter-

action between fetal and maternal blood components takes place over the placental membrane: in between the (maternal) intervillous space and the (fetal) villous capillaries. Nutrients and oxygen-rich blood are supplied via the uterine arteries into the intervillous space. Diffusion takes place over the placental membrane towards the fetal villous capillaries that transport the blood to the umbilical vein. The umbilical vein supplies the fetal circulation with oxygen-rich blood. In opposite direction, carbon dioxide and waste products from fetal metabolism are transported via the umbilical arteries towards the villous capillaries. Via diffusion over the placental membrane, these compounds enter the intervillous space and are subsequently transported via the uterine veins where they enter the maternal venous circulation. Flow and diffusion principles govern the transport of oxygen and carbon dioxide. Partial pressures of O_2 and CO_2 differ in maternal arterial and venous circulation, intervillous space, umbilical vein and artery; as well in fetal arterial and venous circulation. Per "compartment" these partial pressures are influenced by the differences between supply and consumption. A schematic overview of the maternal circulation including the placental circulation, is given in figure A.2.

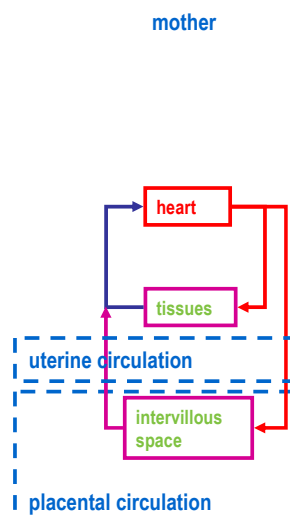


Figure A.2: Schematic model of the maternal circulation. The maternal heart pumps oxygen-rich blood to the maternal tissues. Parallel to these arteries, the uterine arteries transport oxygen-rich blood to the intervillous space. From the tissues and the intervillous space, oxygen-poor blood is transported back by the veins to the heart where it will be oxygenated by the lungs (not shown) and redirected into the arterial system via the heart.

To ensure perfusion, the maternal cardiovascular system adapts via a physiologic cardiovascular remodeling process. Changes are seen in peripheral vascular resistance, blood pressure, blood volume, blood composition, cardiac output and baroreceptor activity. Cardiac output is defined as the blood volume pumped by the heart per minute and can be calculated via the product of stroke volume and heart frequency. The baroreceptor reflex regulates the cardiovascular system to maintain a physiological blood pressure. Some of these adaptations occur already early in pregnancy.

Around eight weeks of pregnancy, a decrease can be seen in both mean arterial pressure

($p_{art,m}$) and peripheral vascular resistance ($R_{per,m}$) obtained by relaxation of the vascular tone. This introduces a relative hypovolemia which can cause a compensatory cardiac output (CO_m) rise of about 40%; this level is reached at 32 weeks of pregnancy.[71],[30] Identically, dilatation of the left ventricle[51] causes stroke volume ($V_{stroke,m}$) to increase significantly at eight weeks with a peak at 16-22 weeks.[71] Heart rate (HF_m) increases with about 20% at the end of pregnancy as a consequence of baroreceptor activation following blood pressure decrease.[51] Cardiac output slightly decreases after 32 weeks, but is still higher than before and after pregnancy.[55] Aortic compliance ($C_{art,m}$) increases throughout pregnancy.[31] Combined with the vascular tone relaxation, blood pressure elevation is thus prevented.

Maternal short-term heart rate variability decreases during pregnancy, probably caused by decreased vagal and increased sympathetic heart rate control from the baroreceptor. This variability decrease cannot be explained from pregnancy-induced respiration changes, neither from the heart rate increase.[22] Brooks et al.[14] conclude that due to a reduced baroreceptor gain in pregnancy, arterial blood pressure maintenance during blood volume loss is more difficult. During the entire pregnancy, the blood volume $V_{blood,m}$ increases, with a highest rate in the second trimester. The total plasma rise is about 30-50%.[71],[30] In the second trimester, the red blood cells amount increases with about 20%. As a result, the hematocrit (HT_m) and hemoglobin (HB_m) concentration first decline until about 30 weeks of gestation, but rise in the third trimester.[71] The total increase in blood volume may be 1-2 liters, which is about four times as much as the lost at parturition, assuring a reasonable buffer for the mother.[30]

Pregnancy also induces cardiac adaptations in both dimension and output parameters (e.g. cardiac output). Several studies investigated the effects of pregnancy on left ventricular function.[37],[25] Both end-diastolic dimensions and left ventricular wall mass increase during pregnancy, while ejection fraction (EF_m), percent of fractional shortening and mean normalized rate of internal diameter shortening do not significantly change.[37] Katz et al.[37] show that ejection fraction remains unchanged during and after pregnancy, from which they conclude that left ventricular function has not changed. The volume overload due to an increased stroke volume is thus fully compensated. Geva et al.[25] also conclude that in pregnancy normal pump function is preserved, without changing contractility, which is normally expected following increased filling pressure.

In table A.1 an overview of measured cardiovascular parameters is given, based on literature. As a reference non-pregnant or (12-)14 weeks postpartum values are given whenever possible. Unfortunately several of the parameters presented in table A.1 are not normalized, which means that variations caused by weight and/or age are not taken into account.

A.1.2 Cardiovascular physiology during labor

During labor, hemodynamics are influenced by both the uterine contractions and the bearing down effort of the mother, both introducing a higher intra-uterine pressure.[86] Intra-uterine pressure rises during contractions causing thus a higher transmural pressure at the intra-uterine blood vessels. Blood pressure in these vessels will rise due to this external pressure, while blood flow will be reduced due to a higher flow resistance following vessel compression.[7]

During each contraction 300-500 ml of blood from the uterus is additionally displaced into the central circulation, thereby placing an additional burden on the heart.[52] In between contractions, cardiac output rises with 12% of prelabor values, which is caused by an increased stroke volume; heart rate does not increase in between contractions. During contractions, stroke volume rises further and cardiac output progressively increases further during the first stage of labor, which

Table A.1: Maternal cardiovascular parameters

Variable	Symbol	Target value	Non-pregnant value	Unit	N	Reference
Heart frequency	$HF_m(t)$	92 ± 7	80 ± 7	bpm	50	[55]
		88 ± 2	69 ± 2		19	[37]
		78.9 ± 12	63.8 ± 8		34	[25]
		85.1 ± 12.5	71.1 ± 8.9		12	[61]
Systolic pressure	$p_{artsys,m}(t)$	95 ± 2	97 ± 2	mmHg	19	[37]
		103.8 ± 10	98.4 ± 8		34	[25]
		118.0 ± 8.3	110.0 ± 7.3		12	[61]
Diastolic pressure	$p_{artdias,m}(t)$	50 ± 2	57 ± 2	mmHg	19	[37]
		58.9 ± 11	54.6 ± 9		34	[25]
		118.0 ± 8.3	110.0 ± 7.3		12	[61]
Hemoglobin	$HB_m(t)$	11.6 ± 1.0	—	g/dl	101	[67]
		11.4 ± 0.95	—		1201	[68]
Hematocrit	$HT_m(t)$	34.3 ± 2.9	—	%	101	[67]
Ejection time	$t_{e,m}(t)$	0.281 ± 0.004	0.310 ± 0.005	s	19	[37]
		0.289 ± 0.024	0.315 ± 0.019		34	[25]
Left ventricular mass	$m_{lv,m}$	162 ± 8.3	143 ± 6.2	g	19	[37]
		161.2 ± 29	116.9 ± 19		34	[25]
Left ventricular length	$l_{lv,m}$	80.9 ± 5.1	75.9 ± 4.92	mm	34	[25]
Blood volume	$V_{blood,m}$	5752 ± 882	—	ml	20	[68]
Systemic resistance	$R_{sys,m}$	$(818.2 \pm 160) \cdot 10^5$	$(1118 \pm 217) \cdot 10^5$	s/m ³	34	[25]
		$899 \cdot 10^5$	—		NA	[82]
Aortic compliance	$C_{art,m}$	0.050	0.040	cm ² /m ² /mmHg	34	[25]
Cardiac output	$CO_m(t)$	6.37 ± 1.48	5.91 ± 1.34	l/min	50	[55]
		8.56 ± 0.51	5.40 ± 0.26		19	[37]
		7.35 ± 1.25	5.42 ± 0.99		34	[25]
		5.88 ± 1.96	3.93 ± 0.53		12	[61]
Stroke volume	$V_{stroke,m}(t)$	70 ± 14	75 ± 21	ml	50	[55]
		97 ± 5	79 ± 3		19	[37]
		96.6 ± 16.1	85.1 ± 13.3		34	[25]
		69.7 ± 8.4	56.0 ± 10.4		12	[61]
Enddiastolic volume	$V_{ed,m}(t)$	132 ± 6	109 ± 5	ml	19	[37]
		118 ± 21	109.5 ± 19		34	[25]
		94.0 ± 19.0	81.0 ± 2.6		12	[61]
Endsystolic volume	$V_{es,m}(t)$	24.3 ± 7.5	27.1 ± 3.9	ml	12	[61]
Ejection fraction	$EF_m(t)$	0.73 ± 0.01	0.73 ± 0.01	ml	19	[37]
		0.67 ± 0.06	0.66 ± 0.06		34	[25]
		0.74 ± 0.08	0.69 ± 0.05		12	[61]
Venous pressure	$p_{ven,m}(t)$	3 – 8	—	mmHg	NA	[65]
Uterine artery pressure	$p_{utart}(t)$	90	—	mmHg	NA	[32]
Uterine artery flow	$q_{utart}(t)$	500 – 700	—	ml/min	NA	[32]
		830 ± 284	—		18	[40]
Uterine artery pO_2	$pO_{2,utart}(t)$	93(90 – 95.6)	—	mmHg	9	[40]
		96.2 ± 13	—		41	[80]
Intervillous space pressure	$p_{ivs}(t)$	15	—	mmHg	NA	[32]
Intervillous space pO_2	$pO_{2,ivs}(t)$	29.2(28 – 33.9)	—	mmHg	9	[40]
		33.1 ± 5.35	—		30	[80]
		23.3(18 – 29)	—		4	[59]
		37.5(24.0 – 72.0)	—		NA	[58]

is then also caused by an increased heart rate.[60] This is a consequence of the autotransfusion of blood during contractions: since the preload volume of the heart will rise, myocardial fibers will extend more what results in a higher stroke volume (Frank Starling mechanism).[43] Mean arterial blood pressure increases progressively during the first stage of labor and rises further during contractions. Differences in hemodynamics are seen in lateral and supine position, both studied during epidural analgesia (which is accompanied with fluid bolus). For the lateral position no changes in stroke volume, cardiac output, mean arterial pressure and systemic vascular resistance are seen following both fluid bolus and epidural analgesia. For the supine position a significant lower stroke volume, cardiac output mean arterial pressure and systemic vascular resistance are measured after fluid bolus. Following epidural analgesia, mean arterial pressure decreases further, while systemic vascular resistance increases slowly. Heart rate is neither affected by fluid bolus nor by epidural analgesia.[19] In the current study only the supine maternal position will be assumed.

During the second stage of labor the arterial blood pressure rises slightly during the contraction, but increases rapidly when the mother is bearing down. In case that the intrauterine pressure rises above arterial pressure, effective uterine blood pressure will be zero.[86]

Immediately after delivery, intense uterine contraction and uterine involution suddenly relieve the inferior vena cava compression and increase cardiac output as much as 80% above prelabor values.[52]

A.2 Fetal circulation

A.2.1 Development of fetal circulation

In the nine months of intra-uterine life, a single cell develops into a full-functioning human being with a complete cardiovascular system, suitable for both intra-uterine life and - after some adaptations - for neonatal life. This requires quick adaptation of the circulation in the perinatal period. The fetal circulation therefore differs in several aspects from the neonatal circulation since oxygen and nutrients exchange takes place in the placenta before birth. Oxygenation is less efficient in the placenta than in the lungs. To compensate for this, some differences in the cardiovascular system can be seen, like a higher number of red blood cells, a higher hemoglobin concentration, a more active hemoglobin - necessary for the slightly more acid blood - and the use of some additional shunts.[71] Antenatally, the fetal lungs are not unfolded and lung circulation is therefore not yet fully developed. An overview of the fetal circulation is given in figure A.3, which also gives an impression of the oxygenation level of the blood.

There are three shunts redirecting the blood in the fetal circulation. The oxygenated blood enters the fetus via the umbilical vein. From there, the blood is mainly led through the liver. The ductus venosus acts as a shunt between the vena umbilicus and the vena cava inferior, so that about 20% of the blood flow is led away from the liver in the last pregnancy trimester. This shunt obliterates between 1 and 3 weeks after birth.[38] The vena cava collects blood from both the umbilical vein and the liver circulation, and directs it to the fetal heart. The oxygenated flow in the heart is led for a larger part directly towards the left atrium and ventricle via a gap in the cardiac septum, the so-called foramen ovale. The lungs are hence shortcutted by a second shunt.[38] The foramen ovale is a one-way valve, permitting only a right-to-left shunt. Closure is obtained after birth by the higher pressure in the left atrium after the first breaths.[71] A third shunt exists between the arteria pulmonalis and the aorta, whereby the lungs are shortcutted again. This ductus arteriosus leads 90% of the blood flow towards the aorta. The ductus arteriosus closes under influence of the oxygenated flow which is present from the onset of lung ventilation after birth.

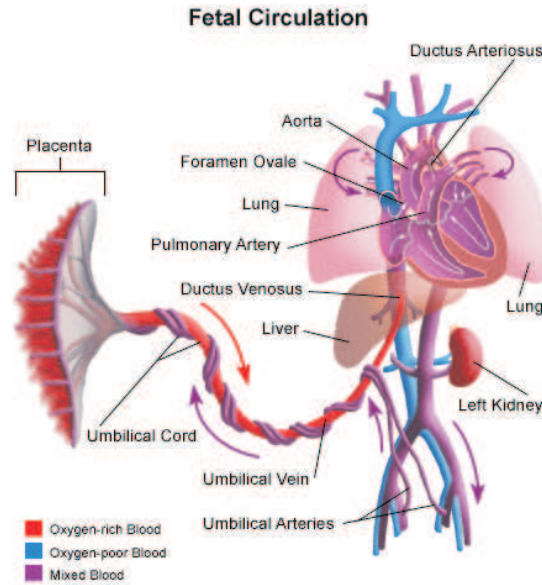


Figure A.3: Schematic model of the fetal circulation. The fetal heart pumps mixed oxygen-rich and oxygen-poor blood to the fetal tissues. Parallel to these arteries, the umbilical arteries transport this blood to the villous capillaries in the placenta. There it is oxygenated and redirected via the umbilical vein towards the systemic circulation and mixed with oxygen-poor blood from the tissues. The ductus venosus redirects blood from the umbilical vein toward the heart, thereby shortcutting the liver. The foramen ovale is a gap in the heart that redirects part of the flow in the right heart to the left heart, thus shortcutting the lungs. The ductus arteriosus does the same, since it forms a shunt between the arteria pulmonalis and the aorta.

Closure is normally obtained at 2-7 days postnatal.[38] Blood flow through the shunts is regulated with vasodilatation and offers the possibility of quick adaptation in for instance hypoxemic events or extreme flows.[38] About half of the cardiac output is directed to the placenta for reoxygenation and exchange of nutrients and metabolites.

A.2.2 Fetal hemodynamic data at term

Only fetal heart frequency and scalp blood pH are accessible during delivery. Other hemodynamic parameters are only available from patient studies and not measured in daily clinics. This data is presented in table A.2 and is given for full-term fetuses. If the exact number of term fetuses is not available, N is printed in italics and represents the total number of included fetuses (with varying age). Normalized data is also for the fetal parameters not always available. Due to relative large variations in fetal weight at term, fetal cardiac dimensions and especially flows may differ.

Table A.2: Fetal cardiovascular parameters

Variable	Symbol	Target value	Unit	N	Reference
Heart frequency	$HF_f(t)$	130.1 ± 6.9	bpm	155	[63]
pH (scalp)	$pH_{scalp,f}(t)$	7.31 ± 0.09	—	123	[17]
Ejection time	$t_{e,f}(t)$	0.184	s	155	[63]
Ejection fraction	$EF_f(t)$	0.66	—	50	[64]
Left ventricular mass	$m_{lv,f}$	8.1 ± 1.7	g	18	[42]
Combined stroke volume	$V_{stroke,f}(t)$	$5.5(95\%CI : 4.8 - 6.19)$	ml	100	[49]
Left enddiastolic volume	$V_{led,f}(t)$	7.80 $3.96(95\%CI : 3.41 - 4.51)$	ml	50 100	[64] [49]
Left endsystolic volume	$V_{les,f}(t)$	$1.56(95\%CI : 1.2 - 1.8)$	ml	100	[49]
Right enddiastolic volume	$V_{red,f}(t)$	7.39 $5.44(95\%CI : 4.69 - 6.18)$	ml	50 100	[64] [49]
Right endsystolic volume	$V_{res,f}(t)$	$2.29(95\%CI : 1.88 - 2.71)$		50	[64]
Blood volume	$V_{blood,f}$	70.3 ± 2.3 78.6 ± 6.5	ml/kg	12 15	[87] [44]
Systemic resistance	$R_{sys,f}$	2.2	mmHg · s/ml	21	[69]
Aortic compliance	$C_{art,f}$	0.08	ml/mmHg	21	[69]
Cardiac output	$CO_f(t)$	1385	ml/min	50	[64]
Umbilical artery flow	$q_{umart}(t)$	300	ml/min	252	[26]
Umbilical artery pO_2	$pO_{2,umart}(t)$	19.2 ± 4.8	mmHg	33	[45]
Umbilical vein pressure	$p_{umven}(t)$	6.5	mmHg	111	[81]
Umbilical vein flow	$q_{umven}(t)$	120 ± 44 154 ± 37	ml/min/kg	53 33	[9] [45]
Umbilical vein pO_2	$pO_{2,umven}(t)$	24.6 ± 6.5	mmHg	33	[45]

B Literature review of mathematical models

Different models have been made to investigate parts of the feto-maternal circulation. Both adult [6], [10],[84],[83], and fetal [29],[27],[34],[48],[54],[57] circulation models have been developed, as well as some models to study feto-placental flows. A specific maternal circulation model has not been developed yet, though an adaptation of the commercially available Human Patient Simulator (METI, Florida) has been proposed for simulation of pregnant women.[23] However, a combined model to investigate the influences of changes at one site of the feto-maternal circulation on another part of the circulation has not been reported in literature. In this section, subsequently available cardiovascular models, oxygen models and baroreceptor reflex models for cardiovascular control will be described. The cardiovascular models will be subdivided in adult, placental and fetal models.

B.1 Cardiovascular models

B.1.1 Maternal cardiovascular models

Numerical simulation of the adult cardiovascular system is an active research area. Various circulation models have been developed with different scopes of interest. These models provide local and/or global hemodynamics. A brief overview of published models is given by Korakianitis et al.[41]

Cardiovascular models consist of two types of modules: a heart module and a vessel module. The heart module generates a pressure pulse or a flow curve to represent the cardiac pumping function. Vessel modules can be connected together to form the vascular tree in a lumped-parameter model. Combined with one or two cardiac modules, the entire systemic and pulmonary circulation respectively, can be generated. In cardiac modeling the model of Suga et al.[70] is widely used to calculate left ventricular pressure phenomenologically. They introduced a time-varying elastance to simulate heart contractility. More recently, the group of Arts and Bovendeerd,[5],[13] introduced a one-fiber model for left ventricular pressure calculation which is based on myofiber mechanics. In this model left ventricular pressure calculation results from microstructural processes in the heart.

A vessel module represents vascular properties like resistance, compliance and inertance (windkessel function) which influence pressure and flow propagation through the system. Westerhof[84] determined vessel properties of the human arterial circulation which are used also by Huberts[33], who determined postoperative flow in an arteriovenous fistula. Similar lumped-parameter methods have been used by many others.[41] In our Cardiovascular Biomechanics group, Huberts[33] used the discrete computational system developed by Schreurs[66] which is based on elements connected to each other by nodes. Each element resembles a local vessel property - inertance, compliance and resistance - as calculated by Westerhof.[84] The model provides pressure at each node and flow through each element by solving the set of differential equations that govern pressure and

flow in the system.

B.1.2 Placental cardiovascular models

In a similar way as the systemic circulation, also the placental circulation can be modeled. The "separate" placental circulation is modeled by Mo et al.[50] to obtain more insight into uterine Doppler waveforms. They modeled a single artery as a transmission line and studied flow waveforms. This placental model was not coupled to the maternal or fetal circulation. Thompson et al.[72],[73] developed a separate placental model that is connected to the umbilical vein and artery. Fetal and maternal circulation were not modeled. They investigated mainly placental resistance indices. The group of Guiot and Todros[29],[74] modeled the fetal arterial site of the placental circulation with 15 generations of branching of the umbilical artery in the placenta. With the model pulsatility index, mean umbilical artery flow, velocity and volume can be calculated as function of number of branching.

B.1.3 Fetal cardiovascular models

One of the first published fetal circulation models is developed by Huikeshoven et al.[34] where the effect of fetal stress on hemodynamics was investigated. Guettouche et al.[27],[28] modeled the fetal arterial circulation in detail and included end-segments to mimic venous return. Pressure, flow and velocity are calculated per segment (in total 16 segments). The group of Pennati[57] developed a lumped parameter model of the fetal cardiovascular system, including fetal placental circulation. The heart is modeled with a time-varying elastance model according to Suga et al.[70] and the vessels are modeled with an RLC-network. Maternal placental circulation was also included.

Ménigault et al.[48] developed an arterial feto-placental circulation model that also includes the uterine arteries. They introduced a bifurcation and arterial segment to model the different parts of the circulation. The fetal side includes a heart with a variable elastance model (according to the model of Suga et al.[70]) and the peripheral parts of the circulation are represented by a windkessel element, as is done for the placenta. Based on the input pressure in the uterine arteries, the blood pressure and velocity for all (fetal) segments can be calculated.

Myers et al.[54],[16] proposed a transfer function-based model to solve the two-dimensional Navier-Stokes equation for the arterial part of the fetal-placental circulation. The model provides flow and pressure at all places in the circulation. The flow can be decomposed into its forward and backward components. Only the fetal side of the placenta is modeled; the uterine vessels and intervillous space are not taken into account.

B.2 Oxygen models

Several oxygen exchange models have been derived to describe oxygen exchange in the human or the placental circulation. A short-term adult model of oxygen and carbon dioxide regulation was developed by Andreassen et al.[4] which provides all parameters needed to calculate the pH-level at different sites of the circulation. Metabolic and respiratory perturbations can be simulated with the model. Placental and fetal circulation are not modeled.

An oxygen exchange model of the placenta was developed in 1992 by Costa et al.[18] The model is based on a maternal blood pool with a constant oxygen pressure for the whole exchange site: the placental membrane which divides the villous capillary from the intervillous space. Diffusion

of oxygen between fetal and maternal blood is hindered only by the placental membrane. Based on Fick's law and the oxygen dissociation curve for the fetus, the oxygenation of the blood can be calculated. The model can provide oxygen pressure at the end of the villous capillaries for different moments in pregnancy. This is achieved by increasing the number of capillaries, as happens during pregnancy. The model of Costa et al.[18] calculates oxygen pressure only at the distal side of the villous capillary.

In 2002 Sá Couto et al.[62] presented a mathematical model to simulate oxygen delivery to the fetus, based on a three-compartment model with blood pressures, volumes and flow rates, including a constant compartment resembling the maternal circulation. The oxygen concentration in the blood compartments is based on the oxygen consumption or exchange. It includes an intervillous space, villous capillaries and fetal peripheral circulation compartment. Oxygen consumption in the fetus - at the fetal peripheral site - is reduced linearly in case of fetal hypoxia. A steady blood flow and maternal arterial oxygen pressure is taken as input.

B.3 Hemodynamic regulation: baroreceptor and chemoreceptor model

Both adult and fetal baroreceptor reflex (BRR) models have been developed, which are included in circulation systems to regulate short-term cardiovascular adaptation to pressure changes. Although pregnancy influences on the BRR have been reported in literature, no maternal cardiovascular model is yet combined with a BRR adapted to pregnancy. Euliano et al.[23] however, report how they adapted adult BRR to simulate BRR in pregnancy on an existing "non-pregnant" cardiovascular model which is incorporated in a commercially available simulator. Van Roon et al.[79] have developed an extensive (adult) BRR model to investigate the influences of mental tasks on cardiovascular changes. In this model the heart rate, vascular resistance and arterial compliance are modeled as a function of arterial blood pressure and respiration. Chemoreceptors which model heart rate based on oxygen pressures were not included. Ursino[75] presented a model for short-term adaptation (1-2 minutes) in adults of systemic peripheral resistance, systemic venous unstressed volumes, heart rate and end-systolic cardiac elastances. In a later study, chemoreceptor regulation was modeled also.

C Mathematical model

The sections in this appendix provide model information for the complete model, i.e. the model that was available [78] and the adaptations as made during the one-year clinical project. The overall model description in this appendix is subdivided into sections on the cardiovascular model, the oxygen delivery model, the cardiovascular regulation model and the method used for the calculation of heart rate variability.

Since the mathematical model will be used in team training for intrapartal scenarios, it must be able to provide at least the clinically available parameters during delivery. The following maternal clinical parameters can be measured intrapartally:

- Heart frequency
- Systolic pressure
- Diastolic pressure
- Hemoglobin
- Hematocrit
- Uterine contractions

For the fetus these clinically available parameters are:

- Heart frequency
- Scalp blood pH

Since these parameters are needed for team training, they are the minimum the model should be able to provide. For educational or diagnostic purposes, the parameter set might be extended for more insight into physiologic processes.

These parameters are obtained from different submodels that interact with each other. In the first paragraph, a brief overview of the cardiovascular model is presented. This model is elaborated in the subsequent paragraphs by a mathematical description. The model is developed to provide the intrapartally available hemodynamic parameters. To simulate these output parameters, several model components are needed:

- Cardiovascular model including fetal, maternal and placental circulation for blood pressure and heart frequencies;
- Cardiovascular regulation models to regulate short term cardiovascular changes (baroreceptor and chemoreceptor function);
- Blood content model for hemoglobin, hematocrit and pH values;
- Uterine contraction model which also influences intrauterine blood pressures during labor.

The last two model components are not yet taken into account and therefore not described here.

C.1 Model summary

The model can be represented in a block diagram. The diagram shows that the placenta has both a maternal and a fetal side. Both circulations are separated by the placental membrane where oxygen diffusion takes place. Blood cannot pass the membrane. The fetal circulation is dependent

on maternal hemodynamics, since oxygen transport is flow-driven. In the next three subparagraphs a brief description of the model is given for its functional parts. Each block from figure C.1 will be elaborated in the following paragraphs. The level of detail of a model is determined by the aim of the model. Model parts that are needed but not varied, can be modeled more globally, while model parts of simulation interest require a higher level of modeling detail.

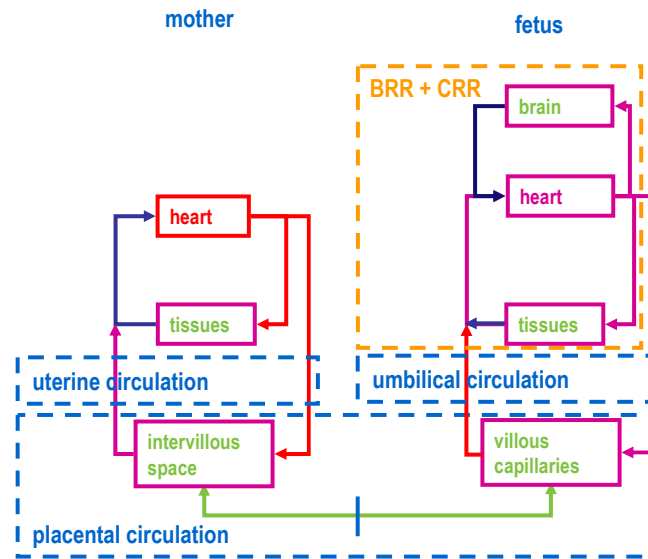


Figure C.1: Block diagram of the model. The maternal circulation is separated from the fetal circulation by the placental membrane (blue vertical line in the placenta). Oxygen is exchanged between mother and fetus (green arrow) over this membrane, blood is not exchanged between mother and fetus. Parallel to the main maternal circulation, the intervillous space is supplied with blood, similarly are the villous capillaries parallel to the main fetal circulation, as is shown by arrows. The color of the arrows and the blocks give an indication of oxygenation level. Fetal circulation is split-up in a cerebral compartment, systemic circulation and umbilical/placental circulation. Note that cardiovascular regulation is only modeled in the fetus (BRR and CRR) since the maternal circulation is assumed to be in steady state.

C.1.1 Maternal circulation

The maternal circulation is modeled briefly to obtain reasonable input data for the placental circulation. The maternal cardiovascular system is therefore reduced to a main artery, microcirculation and vein, that resemble blood flow through all organs, except the placenta. A steady maternal lung function is assumed, therefore systemic arterial blood is completely oxygenated when entering the placenta. Only the left ventricle is modeled, the left atrium is omitted since atrial contraction is neglected. The left ventricle is connected via the aortic valve to the main artery, representing the total maternal arterial system including the pulmonary artery. This artery ends in the microcirculation, which is represented again by only one vessel segment. The microcirculation is connected

via one vein to the left ventricle, separated by the mitralis valve. Maternal heart frequency and systemic vascular resistance are controlled by the baroreceptor reflex.

C.1.2 Fetal circulation

The fetal circulation differs significant from the postnatal circulation. Since left and right ventricle are connected via the foramen ovale, cardiac function is modeled by a combined left and right ventricle. Antenatally lung circulation plays a minor role since oxygenation does not take place in the lungs. Lung circulation is therefore modeled as part of the systemic circulation. The systemic circulation is modeled with one artery which originates in the right ventricle and ends in the fetal microcirculation. A central vein is connected between the microcirculation and the combined ventricle, to redirect the blood to the heart. The oxygen content is calculated for the arterial- and microcirculation, based on the oxygen exchange in the placenta and oxygen use in the fetal microcirculation. Cerebral circulation is modeled parallel to the systemic circulation to investigate the influence of intrapartum caput compression (also known as early decelerations). Fetal heart frequency and vascular resistances are controlled by the baroreceptor reflex.

C.1.3 Placental circulation

The placenta is connected to the systemic maternal circulation with a uterine artery and vein. The uterine artery is connected at the middle of the main artery, the uterine vein at the middle of the main vein. In between the uterine artery and vein, the intervillous space is modeled with one vessel segment. Oxygen content in the intervillous space is based on both maternal arterial oxygen content and diffusion towards the villous capillaries of the fetal placental circulation. The umbilical vein and arteries are connected similarly to the main fetal circulation as the uterine vein and artery to the maternal circulation. The villous capillaries are modeled by one segment in between the umbilical artery and vein. Together with the intervillous space the villous capillaries form one major cotyledon that represents the sum of all placental cotyledons. In the villous capillaries oxygenation of fetal blood takes place by diffusion of oxygen from the intervillous space blood. No blood exchange between mother and fetus takes place.

C.2 Cardiovascular model

This paragraph is based on the papers of van de Vosse et al.,[77] Bovendeerd[12] and Huberts.[33] One way to model the cardiovascular system is by means of an electrical equivalent. By subdividing the cardiovascular system into functional components, pressure and flow can be calculated per component.

C.2.1 Navier-Stokes and continuity equations

Pressure and flow relations in the model are based on the conservation of mass and momentum, the constitutive equations and initial and boundary conditions. By considering blood as an incompressible Newtonian fluid the Navier-Stokes equation and continuity equation are[77]:

$$\begin{cases} \rho \left(\frac{\partial \vec{v}}{\partial t} + \vec{v} \cdot \nabla \vec{v} \right) = \vec{f} - \nabla p + \eta \nabla^2 \vec{v} \\ \nabla \cdot \vec{v} = 0 \end{cases} \quad (\text{C.1})$$

with ρ the density, \vec{v} the velocity, t the time, \vec{f} body forces, p the pressure and η the viscosity. The Navier-Stokes equation represents the equilibrium between the unsteady inertial forces (first left term: acceleration as function of time-dependency), the convective forces (second left term: acceleration due to topological changes), body forces (first right term: gravity forces), pressure forces (second right term: pressure gradient in the system) and viscous forces (third right term: friction). Equation C.1 can be further simplified by considering the cardiovascular system as a

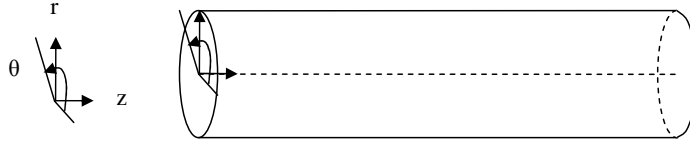


Figure C.2: Schematic representation of a blood vessel. The vessel can be characterized with cylindrical coordinates. Note that the vessel is axisymmetric and that only small tapering effects are taken into account.

system of straight axisymmetric vessels with circumferential coordinate θ , radial coordinate r , and axial coordinate z . For a schematic representation of a cylindrical vessel see figure C.2. By assuming the velocity in circumferential direction zero, v_θ and its derivatives can be omitted. The radial velocity component can be neglected by assuming only small tapering effects of the vessels. Now only an axial velocity component exists, dependent of r and z : [12]

$$\vec{v} = v(r, z)\vec{e}_z = v_z\vec{e}_z \quad (\text{C.2})$$

Assuming negligible gravity forces ($f = 0$), and a fully developed flow, ($\frac{\partial v_z}{\partial z} = 0$), equation C.1 reduces to: [77]

$$\frac{\partial v_z}{\partial t} = -\frac{1}{\rho} \frac{\partial p}{\partial z} + \frac{\nu}{r} \frac{\partial}{\partial r} \left(r \frac{\partial v_z}{\partial r} \right) \quad (\text{C.3})$$

Entrance effects due to geometry and secondary flow patterns due to branching are thus neglected. Equation C.3 represents the balance between inertial, pressure and viscous forces, which govern the hemodynamics in the system. In the next part, the individual contribution of each force will be determined.

Inertance

In vessels with a large diameter, inertial forces will play a more important role than viscous forces. If viscous forces can be neglected, (C.3) reduces to:

$$\frac{\partial v_z}{\partial t} = -\frac{1}{\rho} \frac{\partial p}{\partial z} \quad (\text{C.4})$$

After rewriting $v_z = q/A$ [m/s] with q [m³/s] the flow and A [m²] the - constant assumed - cross sectional area of the vessel, equation C.4 can be rewritten to:[12]

$$\frac{1}{A} \frac{\partial q}{\partial t} = -\frac{1}{\rho} \frac{\partial p}{\partial z} \quad (\text{C.5})$$

For a vessel segment with a certain length l , (C.5) results in:

$$\Delta p = \frac{\rho l}{A} \frac{\partial q}{\partial t} = \frac{\rho l}{\pi a^2} \frac{\partial q}{\partial t} = L \frac{\partial q}{\partial t} \quad (\text{C.6})$$

Quantity L [Pa·s²/m³] is the vessel inertance and represents the pressure drop per vessel segment with length l [m] due to inertial forces, a [m] is the vessel radius.

Resistance

In vessels with a small diameter, flow is dominated by viscous forces and equation C.3 can then be represented by:

$$0 = -\frac{1}{\rho} \frac{\partial p}{\partial z} + \frac{\nu}{r} \frac{\partial}{\partial r} \left(r \frac{\partial v_z}{\partial r} \right) \quad (\text{C.7})$$

The solution of v_z for equation C.7 results in the Poiseuille velocity profile:[12]

$$v_z = -\frac{1}{4\eta} (a^2 - r^2) \frac{\partial p}{\partial z} \quad (\text{C.8})$$

Integration of the velocity profile over the cross sectional area results in the flow, which is linearly related to the pressure gradient:[12]

$$\frac{\partial p}{\partial z} = -\frac{8\eta}{\pi a^4} q \quad (\text{C.9})$$

For a vessel segment with a certain length l , (C.9) results in:

$$\Delta p = \frac{8\eta l}{\pi a^4} q = Rq \quad (\text{C.10})$$

Here R [Pa·s/m³] represents the vessel resistance for a segment with length l [m]. From (C.10) and (C.7) it can easily be seen that viscous forces are especially important in small vessels and inertial forces play an important role in larger vessels.

Compliance

As a consequence of the distensibility of the vessel, the lumen expands under the pressure and thus a volume of blood can be stored and released. This property is referred to as the vessel compliance C [m³/Pa]. The mass balance for an infinitesimal vessel segment is given as

$$[A(z, t + \Delta t) - A(z, t)] \Delta z = [q(z, t) - q(z + \Delta z, t)] \Delta t \quad (\text{C.11})$$

which can be rewritten into:

$$\lim_{\Delta t \rightarrow 0} \left(\frac{A(z, t + \Delta t) - A(z, t)}{\Delta t} \right) = \lim_{\Delta z \rightarrow 0} \left(\frac{q(z, t) - q(z + \Delta z, t)}{\Delta z} \right) \quad (\text{C.12})$$

resulting in:

$$\frac{\partial A}{\partial t} = - \frac{\partial q}{\partial z} \quad (\text{C.13})$$

Since the left term depends on the pressure change, the relation between compliance, pressure and flow becomes clear:

$$- \frac{\partial q}{\partial z} = \frac{\partial A}{\partial p} \frac{\partial p}{\partial t} \Rightarrow \Delta q = \frac{\partial A}{\partial p} l \frac{\partial p}{\partial t} = C \frac{\partial p}{\partial t} \quad (\text{C.14})$$

C.2.2 Discretisation and assembling

Concluding from paragraph C.2.1, the mass and momentum equations for the simplified system hold:

$$\begin{aligned} \Delta p &= Rq \\ \Delta p &= L \frac{\partial q}{\partial t} \\ \Delta q &= C \frac{\partial p}{\partial t} \end{aligned} \quad (\text{C.15})$$

In our model, the continuous change of pressure and flow throughout the cardiovascular system is approximated by a limited number of pressure and flow values at discrete points (nodes). These nodes connect the line elements, which resemble either one of the three relations between pressure and flow as described in the previous paragraph, thus representing a resistance, inertance or compliance. For element E being an inertance, integration of equation C.15 leads to:

$$\frac{\partial q}{\partial t} = \frac{1}{L} \Delta p \rightarrow q(t + \Delta t) = q(t) + \frac{1}{L} \int_t^{t+\Delta t} (p_1 - p_2) dt \quad (\text{C.16})$$

In addition, because of conservation of mass, it holds that $q_1 = q_2$. Therefore equation C.16 can be written as:

$$\begin{bmatrix} q_1 \\ q_2 \end{bmatrix} = \frac{1}{L} \begin{bmatrix} 1 & -1 \\ -1 & 1 \end{bmatrix} \int \begin{bmatrix} p_1 \\ p_2 \end{bmatrix} dt \quad (\text{C.17})$$

Likewise, the relation between pressures p_1 and p_2 and flows q_1 and q_2 for a resistance can be derived from (C.15) and conservation of mass:

$$\begin{bmatrix} q_1 \\ q_2 \end{bmatrix} = \frac{1}{R} \begin{bmatrix} 1 & -1 \\ -1 & 1 \end{bmatrix} \begin{bmatrix} p_1 \\ p_2 \end{bmatrix} \quad (\text{C.18})$$

For the compliance, equation C.15 can be rewritten into: $-\Delta q = C \frac{\partial p}{\partial t} = C \frac{\partial(p_1 - p_2)}{\partial t}$, hence:

$$\begin{bmatrix} q_1 \\ q_2 \end{bmatrix} = C \begin{bmatrix} 1 & -1 \\ -1 & 1 \end{bmatrix} \begin{bmatrix} \dot{p}_1 \\ \dot{p}_2 \end{bmatrix} \quad (\text{C.19})$$

Combining these vessel segments in series or in parallel, enables the development of a whole arterial system as a transmission line model.[33],[84] Nodes of two subsequent elements need to have the same point variable: the pressure in node 2 of the first element has to be equal to the pressure in node 1 of the second element. The system behavior can then be described by combining equations C.16, C.17 and C.18 into:

$$\tilde{q} = \underline{C}\dot{\tilde{p}} + \underline{R}\tilde{p} + \underline{L} \int \tilde{p} dt \quad (\text{C.20})$$

The nodal point values for pressure and flow are stored in the columns \tilde{p} and \tilde{q} ; \underline{C} , \underline{R} and \underline{L} are the system matrices containing the values of the capacitance, reciprocal resistance and reciprocal inductance respectively.

C.2.3 Vessel segment

Now a vessel segment can be modeled by a combination of inertance L , resistance R , and compliance C . To reduce errors introduced by lumping, a symmetrical network is used.[84] Therefore the segment compliance is divided into two equal parts to obtain a symmetrical network.[33] Each compliance is grounded if no external pressure forces are taken into account. External pressures such as uterine contractions can be applied as pressures at these nodes. Distinction between arterial, venous and microcirculation components is made by parameter values for the inertance, compliance and resistance.

C.2.4 The heart: ventricle component

The heart generates a pressure gradient in both the pulmonary and systemic circulation. In fact the heart consists of two separated pumps that collect blood from the venous circulation and return it to the arterial circulation. Each pump consists of two serially coupled chambers that are separated by a one-way valve. The second of these chambers is the ventricle, which has the main pumping function. The ventricle is connected distally via a second one-way valve to the arterial circulation.

To model the heart, the functional parts are separated as follows. The atrium - the first chamber - can be modeled as part of the venous circulation, since it has a negligible pumping function. The heart valves can be seen as diodes: they are opened during a positive pressure and flow gradient. In the model the valve is closed by instantaneously increasing its resistance value by a factor 10^6 , to prevent retrograde flow. Since the pulmonary circulation is not modeled explicitly, only one ventricle is included: the left ventricle for the mother; for the fetus a combined left and right ventricle is taken.

The one-fiber model, used in this cardiovascular system for left ventricular pressure calculation, is based on the assumption that fiber stress and strain in the hart is distributed homogeneously.[13] Ergo, one representative fiber can be used to model fiber stress and strain in the cardiac cycle.

Left ventricular pressure is then related to fiber stress σ_f [Pa], and left ventricular wall and cavity volume V_w [m³] and V_{lv} [m³] respectively:[13]

$$p_{lv}(t) = \frac{\sigma_f(t)}{3} \ln \left(1 + \frac{V_w}{V_{lv}(t)} \right) \quad (C.21)$$

In the physiological range, this expression is approximately:[13]

$$\frac{\sigma_f(t)}{p_{lv}(t)} = \left(1 + 3 \frac{V_{lv}(t)}{V_w} \right) \quad (C.22)$$

Note that V_w is assumed to be constant during the simulation. Ventricular volume V_{lv} is a function of sarcomere length l_s [m] and related to the mechanical work W [J] of the ventricle:[13]

$$dW = p_{lv}(t)dV_{lv}(t) = V_w \sigma_f(t) de_f(t) \quad (C.23)$$

Fiber strain e_f [-] is defined as function of sarcomere length and reference sarcomere length $l_{s,ref}$ [m]:[13]

$$e_f(t) = \ln \left(\frac{l_s(t)}{l_{s,ref}} \right) \quad (C.24)$$

Combining (C.20)-(C.23) leads to the following expression for stretch ratio:[13]

$$\frac{l_s(t)}{l_{s,ref}} = \left(\frac{1 + 3 \frac{V_{lv}}{V_w}}{1 + 3 \frac{V_{lv,0}}{V_w}} \right)^{\frac{1}{3}} \quad (C.25)$$

For an incompressible tissue, uniaxial fiber stress σ_f is related to the stretch ratio according to:

$$\sigma_f = (T_a(t) + T_p(t)) \frac{l_s(t)}{l_{s,ref}} \quad (C.26)$$

Note that active and passive stress T_a [Pa] and T_p [Pa] together form the Piola Kirchhoff stress. Active stress originates from the stress generated by the sarcomeres. It can be modeled as function of l_s , t_a and v_s , representing respectively sarcomere length, time elapsed since activation and sarcomere shortening velocity. Length dependence, time dependence and velocity shortening dependence can be described separately:

$$T_a(l_s, t_a, v_s) = f(l_s)g(t_a)h(v_s) \quad (C.27)$$

This formula will be explained subsequently. Length dependency is modeled as:

$$f(l_s) = \begin{cases} 0 & l_s(t) \leq l_{sa0} \\ T_{a0} \tanh^2(c_a(l_s(t) - l_{sa0})) & l_s(t) > l_{sa0} \end{cases} \quad (C.28)$$

In this formula, T_{a0} [Pa] is a scaling parameter for active stress, c_a [–] a curvature parameter for active stress-length relation and l_{sa0} [m] the sarcomere length at zero active stress. The time dependency in (C.27) is given by:

$$\begin{aligned}
 g(t_a, l_s) &= \begin{cases} 0 & t_a < 0 \\ \sin^2\left(\frac{\pi t_a}{2\tau_r(t)}\right) & 0 \leq t_a < \tau_r(t) \\ 1 - \sin^2\left(\frac{\pi(t_a - \tau_d(t))}{2\tau_d}\right) & \tau_r(t) \leq t_a < \tau_r(t) + \tau_d(t) \\ 0 & t_a \leq \tau_r(t) + \tau_d(t) \end{cases} \\
 \tau_r(t) &= \tau_{r1} + a_r(l_s(t) - l_{s,ref}) \\
 \tau_d(t) &= \tau_{d1} + a_d(l_s(t) - l_{s,ref})
 \end{aligned} \tag{C.29}$$

Note that the increase in sarcomere activation takes place in time interval τ_r [s] and depends on sarcomere length. The decay in sarcomere activation takes place during time interval τ_d [s], and starts directly after τ_r . The reference τ_r and τ_d are respectively τ_{r1} and τ_{d1} , based on a reference sarcomere length $l_{s,ref}$. The length dependencies of τ_r and τ_d are described with the constants a_r [s/m] and a_d [s/m] respectively.

The shortening velocity $v_s(t)$ is defined as:

$$v_s(t) = -\frac{dl_s(t)}{dt} \tag{C.30}$$

The dependency of T_a on v_s is:

$$h(v_s) = \frac{1 - \left(\frac{v_s(t)}{v_{s0}}\right)}{1 + c_v \left(\frac{v_s(t)}{v_{s0}}\right)} \tag{C.31}$$

The shortening velocity at zero stress is represented by v_{s0} , the hyperbolic function $h(v_s)$ is scaled with curvature parameter c_v [–].

The passive muscle also contributes to total myofiber stress with a passive stress T_p . The time dependency of T_p is given by:

$$T_p(t) = \begin{cases} 0 & l_s(t) \leq l_{sp0} \\ T_{p0}(e^{c_p(l_s(t) - l_{sp0})} - 1) & l_s(t) > l_{sp0} \end{cases} \tag{C.32}$$

T_{p0} [Pa] represents the scaling parameter for passive stress, c_p [–] the curvature parameter for passive stress-length relation and l_{sp0} [m] the sarcomere length at zero passive stress.

C.2.5 Model description

The cardiovascular model can now be built from the components: a matrix is built from all elements and contains the first and second node and the value of its element. The nodal numbers generate the coupling between the different elements. The model consists of 2 ventricle and 19 vessel segments divided over the 7 compartments in figure C.1:

- 1 maternal left ventricle;

Table C.1: Model segments with abbreviations

	Maternal	Fetal
Ventricle	lv_m	rlv_f
First arterial	$art_{1,m}$	$art_{1,f}$
Second arterial	$art_{2,m}$	$art_{2,f}$
Microcirculation	mc_m	mc_f
First venous	$ven_{1,m}$	$ven_{1,f}$
Second venous	$ven_{2,m}$	$ven_{2,f}$
Uterine arterial	$utart_m$	-
Intervillous space	ivs_m	-
Uterine venous	$utven_m$	-
Umbilical arterial	-	$umart_f$
Villous capillaries	-	vc_f
Umbilical venous	-	$umven_f$
Cerebral arterial	-	$brart_f$
Cerebral capillaries	-	$brmc_f$
Cerebral venous	-	$brven_f$

- 5 systemic maternal segments (2 arterial, 1 microcirculation, 2 venous segments);
- 3 maternal placental segments (1 uterine arterial, 1 intervillous space, 1 uterine venous segment);
- 1 combined fetal left and right ventricle;
- 5 systemic fetal segments (2 arterial, 1 microcirculation, 2 venous segments);
- 3 fetal placental segments (1 umbilical arterial, 1 villous microcirculation, 1 umbilical venous segment);
- 3 fetal cerebral segments (1 cerebral arterial, 1 cerebral microcirculation, 1 cerebral venous segment).

The segment indices used in the equations are explained in table C.1.

The maternal and fetal heart pump the blood in their main circulation independently of each other. The flow and pressure values per segment in time are calculated at several increments per cardiac cycle: the time discretization of the system. The number of increments (ic) per cycle is based on the (constant) time step ts and the cycle length as determined by the regulatory systems (see paragraph C.3).

The initial conditions for the total system are based on estimates for the compartmental volumes as are given in the appendix. The initial values of pressure are taken from system mean values in dynamic steady state and pressure time derivatives are thus chosen zero. Initial external pressure p_e is applied at the system at several locations to represent respectively intrauterine pressure, ventricle pressure and arterial and venous blood pressure.

$$\begin{aligned}
 \tilde{p}(t_{ic=0}) &= p_e \\
 \dot{\tilde{p}}(t_{ic=0}) &= 0 \\
 \ddot{\tilde{p}}(t_{ic=0}) &= 0
 \end{aligned}$$

Incremental computation is based on several steps. Firstly from the nodal pressures, segmental flows are calculated based on the segment resistance:

$$q_{seg}(t_{ic+1}) = \frac{p_1(t_{ic+1}) - p_2(t_{ic+1})}{R_{seg}} \quad (C.33)$$

with p_1 and p_2 the pressures in the node before and after the segmental resistance, as defined in section C.2.2. Subsequently the segmental volumes are calculated with the law of conservation of mass. The previous volume of the segment $V_{seg}(t_{ic-1})$ is updated with the volume change based on segmental in- and outflow $q_{in}(t_{ic-1})$ and $q_{out}(t_{ic-1})$ during the last time step. All volumes are updated in this way:

$$V_{seg}(t_{ic}) = V_{seg}(t_{ic-1}) + \frac{dV_{seg}}{dt} \Delta t = V_{seg}(t_{ic-1}) + (q_{in}(t_{ic-1}) - q_{out}(t_{ic-1})) \Delta t \quad (C.34)$$

The volume in the second venous segment is calculated as the total blood volume minus the calculated volumes of the other segments to prevent rounding errors. The volume of the ventricle is used as input for the incremental ventricular pressure calculation, as derived in section C.2.4. This pressure $p_{lv}(t_{ic})$ is applied as external load $p_{e,lv}(t_{ic})$. System dynamics follow from this ventricle pressure only, and are together with the system properties (resistance, inertance and compliance) responsible for pressures in the rest of the system. However, currently arterial $p_{e,art1}(t_{ic})$ and venous pressure is also needed as external pressure $p_{e,ven2}(t_{ic})$, although yet not completely is understood why this is the case. This will be further investigated. These pressures are therefore currently calculated with:

$$p_{seg}(t_{ic}) = \frac{V_{seg}(t_{ic}) - V_{seg,0}}{C_{seg}} \quad (C.35)$$

The external pressure array $\tilde{p}_e(t_{ic})$ contains per node the external pressure (normally zero) and is eventually completed with pressures working on vessel compliances, like compliance nodes in the uterus which are exposed to uterine contraction pressures. During an incremental solution procedure, the first-order system of equation C.20 is solved to retrieve the unknown $\tilde{p}(t_{ic} + ts) = \tilde{p}(t_{ic+1})$. This is done in Matlab with the first order implicit method (trapezium rule), modeled in DiSCo.[66] The discrete system computation is based on the nodal pressure computation for the transmission line of the cardiovascular system (existing of compliances, resistances and inertances). In each node the internal flow variables of the separate elements have to be added (Kirchhoff's law). There are three types of elements that may contribute to the nodal internal flow:

$$q_i(t_{ic}) = q_{i,C}(t_{ic}) + q_{i,R}(t_{ic}) + q_{i,L}(t_{ic}) \quad (C.36)$$

The individual contributions are zero for nodes that are not connected to the corresponding element type. The contribution of each internal element flow follows from the discretization of equation C.20 and will be elaborated per element type. Equation C.20 can be rewritten into:

$$\tilde{q}_i(t_{ic+1}) = \underline{C} \dot{\tilde{p}}(t_{ic+1}) + \underline{R} p(t_{ic+1}) + \underline{L} \int_{\tau=0}^{\tau=t_{ic+1}} \tilde{p} d\tau \quad (C.37)$$

According to the trapezium rule it holds that $\frac{1}{2}(\dot{\tilde{p}}(t_{ic+1}) + \dot{\tilde{p}}(t_{ic})) = \frac{1}{\Delta t}(\tilde{p}(t_{ic+1}) - \tilde{p}(t_{ic}))$. Therefore the internal flow contribution of the compliance is:

$$\tilde{q}_{i,C}(t_{ic+1}) = \underline{C}\dot{\tilde{p}}(t_{ic+1}) = \frac{2}{\Delta t}(\tilde{p}(t_{ic+1}) - \tilde{p}(t_{ic})) - \dot{\tilde{p}}(t_{ic}) \quad (\text{C.38})$$

For the resistance, internal flow contribution is given by:

$$\tilde{q}_{i,R}(t_{ic+1}) = \underline{R}\tilde{p}(t_{ic+1}) \quad (\text{C.39})$$

By assuming a linear change in pressure between time $\tau = t$ and $\tau = t + \Delta t$, it follows that:

$$\underline{L} \int_{\tau=0}^{\tau=t_{ic+1}} \tilde{p} d\tau = \underline{L} \int_{\tau=0}^{\tau=t_{ic}} \tilde{p} d\tau + \frac{ts}{2} \underline{L}(\tilde{p}(t_{ic}) + \tilde{p}(t_{ic+1})) \quad (\text{C.40})$$

Therefore the discretized flow contribution of the inertance holds:

$$\tilde{q}_{i,L}(t_{ic+1}) = \underline{L} \sum_{\tau=0}^{\tau=t_{ic}} \frac{\tilde{p}(\tau) + \tilde{p}(\tau - \Delta t)}{2} + \frac{\Delta t}{2} \underline{L}(\tilde{p}(t_{ic}) + \tilde{p}(t_{ic+1})) \quad (\text{C.41})$$

The nodal pressures at t_{ic+1} can now be derived by substitution of C.38-C.41 into C.37, which results into:

$$\left(\frac{2}{\Delta t} \underline{C} + \underline{R} + \frac{\Delta t}{2} \underline{L} \right) \tilde{p}(t_{ic+1}) = \tilde{q}_i(t_{ic+1}) + \frac{2}{\Delta t} \underline{C}\tilde{p}(t_{ic}) + \underline{C}\dot{\tilde{p}}(t_{ic}) - \underline{L} \int_{\tau=0}^{\tau=t_{ic}} \tilde{p} d\tau + \frac{\Delta t}{2} \underline{L}\tilde{p}(t_{ic}) \quad (\text{C.42})$$

The external pressures \tilde{p}_e are applied at the corresponding nodes in the row vector $\tilde{p}(t_{ic+1})$ and are applied respectively at the left ventricle (calculated with the 1-fiber model), at the compliances (zero, since the extravascular pressure is assumed atmospheric) and non-zero at the intra-uterine compliances during uterine contractions. The external applied flows $\tilde{q}_e(t_{ic+1})$ are zero for all nodes, since no flow is prescribed in the system. The system of equation C.42 is solved for the nodes that do not have an applied pressure. This is done by multiplying the right hand system with the inverse of the bracketed term of the left hand side. The incremental calculation is now finished, t_{ic+1} becomes t_{ic} and the procedure is repeated for a new increment at the next time step Δt .

C.3 Cardiovascular regulation model

The cardiovascular regulation model of Ursino and Magosso[76] describes short-term regulatory mechanisms of the pulsating cardiovascular system, including chemo-, baro- and lungstretch receptors in human adults. This model is used in our cardiovascular model to regulate the fetal cardiovascular circulation, with a first focus on regulation during early decelerations. A maternal implementation has not been made yet, since the maternal cardiovascular circulation is in steady state which will not change during the scenario of early decelerations.

A few adaptations are made to fulfil fetal requirements. Since oxygenation of the fetal blood does not take place in the fetal lungs, but in the placenta, lungstretch receptors are not taken into account in our model. However, they are remained as a steady baseline to avoid the necessity for large model adaptations. Initially, baroreceptor function is included in steady state performance, thus no feedback is yet applied on changes in p_{art} . This is convenient for the first scenario that will be implemented (early decelerations) that does not deal with pressure changes. It permits to study the influences of the chemoreceptor regulation during early decelerations separately. However, once other scenarios are investigated that deal with pressure changes (e.g. late decelerations), this has to be adjusted. The model of Ursino also includes central nervous system (CNS) hypoxic response. Its input parameter is pO_2 as measured in the systemic arterial circulation, which will almost not change during early decelerations, and is therefore currently omitted. Since early decelerations induce vagal nerve hypoxia with corresponding increase of vagal nerve fire rate, [15] this had to be added to the model.

For an overview of model components as used in the cardiovascular control system, see figure C.3. It can now be easily seen that for early decelerations, only vagal nerve hypoxia plays a role in heart period change. Currently, the subsystems of the baroreceptor, lung stretch receptors and CNS hypoxic response. Note that, although not shown, effectors (resistances, unstressed volumes, contractility and heart period) influence input parameters (p_{art} , $p_{art}O_2$ and $p_{br}O_2$) and form thus a closed loop model.

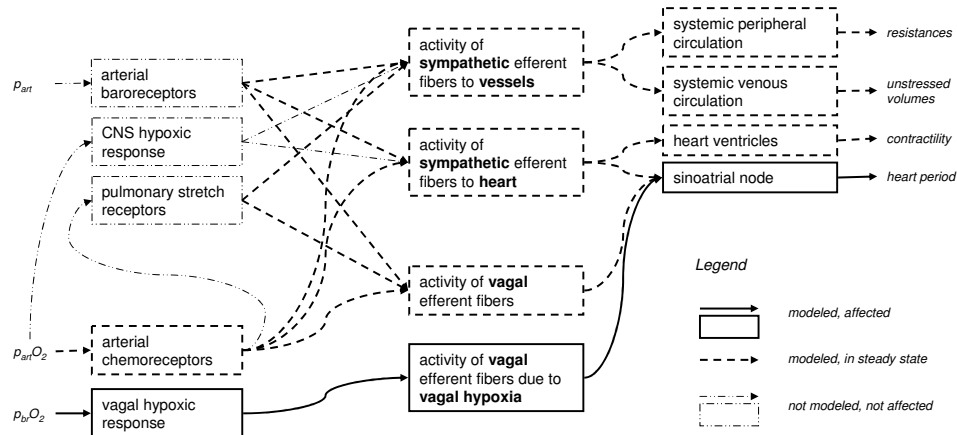


Figure C.3: Block diagram of the cardiovascular regulatory model. Arterial partial oxygen pressure ($p_{art}O_2$) is sensed by the arterial chemoreceptors that give a signal to sympathetic and parasympathetic fibers in the central nervous system (CNS). These signals are modified and forwarded to cardiovascular effectors (resistances, unstressed volumes, ventricle contractility, heart period) to minimize the effects of hypoxia on target organs. Vagal hypoxia response is included to react to local pO_2 changes ($p_{br}O_2$) which have an effect on vagal fire rate that controls heart period. Note that in the scenario of early decelerations changes $p_{art}O_2$ are too small to induce effector changes. These signals are therefore constant, which is graphically shown with dotted arrows (- -). In spite of the fact that input for the baroreceptor and pulmonary stretch receptors are available in the model (p_{art} and chemoreceptor fire rate respectively), these sensors are not modeled explicitly since their input does not change. (See body text, paragraph C.3.) They are therefore shown with thin dotted-striped arrows and blocks (- . -). Their outputs (steady state fire rates) are modeled as constants and used in other parts of the model as shown.

C.3.1 Model description

This paragraph is based on the work of Ursino and Magosso[76]. Only processes that were modeled (as shown also in figure C.3) are considered here. For more details with regard to the complete model is referred to the original paper of Ursino et al.[76]. Their cardiovascular model equations were not used in our work.

The model consists of afferent neural pathways, that bring information to the central nervous system (CNS) from the different sensory systems. In the CNS, these signals are modified and forwarded via efferent neural pathways toward the effectors.

Afferent neural pathways

In the baroreceptor, arterial blood pressure induces a fire rate signal ($f_{ab} [s^{-1}]$) that is send to three subsystems in the CNS: the sympathetic nerves that innervate the vascular system, the sympathetic nerves that innervate the heart, and the parasympathetic nerves (vagal nerve) that innervate the heart. Since this system is considered to be in steady state during early decelerations ($\tilde{P} = P_n$ which assumes that arterial pressure is constant at the physiological working point), its fire rate is calculated for steady state and applied during the whole simulation. Thus:

$$f_{ab}(t_{ic}) = \frac{f_{ab,min} + f_{ab,max} \cdot e^{\left(\frac{\tilde{P}(t_{ic}) - P_n}{k_{ab}}\right)}}{1 + e^{\left(\frac{\tilde{P}(t_{ic}) - P_n}{k_{ab}}\right)}} = \frac{f_{ab,min} + f_{ab,max}}{2} = 25.15 [s^{-1}] \quad (C.43)$$

Activity f_{ab} is therefore the mean of maximum and minimum fire rates ($f_{ab,min}$ and $f_{ab,max}$ respectively). For more information with regard to the other parameters (that are not used in this work) is referred to the work of Ursino et al.[76].

Afferent activity ($f_{ap} [s^{-1}]$) of the pulmonary stretch receptors is calculated from steady state according to:

$$\frac{df_{ap}}{dt} = \frac{1}{\tau_p} \cdot (-f_{ap}(t_{ic}) + \phi_{ap}(t_{ic})) \Rightarrow f_{ap}(t_{ic}) = \phi_{ap}(t_{ic}) = 13.58 [s^{-1}] \quad (C.44)$$

With ϕ_{ap} the product of a constant gain factor G_{ap} and tidal volume V_T . This steady state value is for adults, and currently also applied for the fetus, although fetal lungs cannot contribute in fetal oxygenation.

Chemoreceptor afferent activity is based on the following differential equation:

$$\frac{df_{ac}}{dt} = \frac{1}{\tau_c} \cdot (-f_{ac}(t_{ic}) + \phi_{ac}(t_{ic})) \quad (C.45)$$

Now ϕ_{ac} is the sigmoidal response of the chemoreceptor to arterial oxygen pressure $p_{art}O_2$, with again a minimum and maximum fire rate ($f_{ac,min}$ and $f_{ac,max}$ respectively). The slope in the working point $p_{art}O_{2,n}$ of this sigmoidal function is determined by parameter $k_{ac} [mmHg]$. Together this results into:

$$\phi_{ac}(t_{ic}) = \frac{f_{ac,min} + f_{ac,max} \cdot e^{\left(\frac{p_{art}O_2(t_{ic}) - p_{art}O_{2,n}}{k_{ac}}\right)}}{1 + e^{\left(\frac{p_{art}O_2(t_{ic}) - p_{art}O_{2,n}}{k_{ac}}\right)}} \quad (C.46)$$

In the current work, also vagal hypoxia afferent activity is modeled. Current $p_{br}O_2(t_{ic})$ is compared with normal $p_{br}O_{2,n}$. At the nadir of a maximal early deceleration, which is set at -30 bpm, $p_{br}O_2(t_{ic})$ is lowered with 20%. Hypoxia afferent activity is therefore normalized with respect to this value:

$$f_{av}(t_{ic}) = \frac{p_{br}O_{2,n} - p_{br}O_2(t_{ic})}{0.2 \cdot p_{br}O_{2,n}} \quad (C.47)$$

Efferent neural pathways

These four afferent activities (f_{ab} , f_{ap} , f_{ac} and f_{av}) are input for the CNS. Since only f_{ac} and f_{av} are considered as function of time, they are referred to as $f_{ac}(t_{ic})$ and $f_{av}(t_{ic})$ respectively; fire rates f_{ab} , f_{ap} are considered as constants. The CNS modifies these signals and responds to the cardiovascular effectors via the sympathetic and vagal nerve.

Sympathetic fire rate towards the (peripheral) vessels (f_{sp}) is governed by the afferent signals f_{ab} , f_{ap} and $f_{ac}(t_{ic})$:

$$f_{sp} = \begin{cases} f_{es,\infty} + (f_{es,0} - f_{es,\infty}) \cdot e^{(k_{es} \cdot (-W_{b,sp} \cdot f_{ab} - W_{p,sp} \cdot f_{ap} + W_{c,sp} \cdot f_{ac}(t_{ic}) - \theta_{sp}))} & f_{sp}(t_{ic}) < f_{es,max} \\ f_{es,max} & f_{sp}(t_{ic}) \geq f_{es,max} \end{cases} \quad (C.48)$$

In this equation, different (constant) weights are used for the different input signals ($W_{b,sp}$, $W_{p,sp}$ and $W_{c,sp}$ for f_{ab} , f_{ap} and $f_{ac}(t_{ic})$ respectively). An extra offset term (related to CNS hypoxia measured via $p_{art}O_2$) is introduced via θ_{sp} , which is considered as constant in the case of early decelerations since deviations in $p_{art}O_2$ are very small. Secondly, its value is near the upper saturation of the sigmoidal curve and will therefore have minor effect on changes in CNS hypoxia response. Therefore its value is calculated for steady state, which results into:

$$\theta_{sp} = \chi_{sp} = \frac{\chi_{min,sp} + \chi_{max,sp} \cdot e^{\left(\frac{p_{art}O_2(t_{ic}) - p_{art}O_{2,n,sp}}{k_{isc,sp}}\right)}}{1 + e^{\left(\frac{p_{art}O_2(t_{ic}) - p_{art}O_{2,n,sp}}{k_{isc,sp}}\right)}} = 13.32 [s^{-1}] \quad (C.49)$$

Note that CNS hypoxia threshold is scaled from adult to fetal partial oxygen pressure via the normal oxygen pressures of 92 versus 23 mmHg. Other parameters are unchanged.

Sympathetic fire rate for innervation of the heart (f_{sh}) is dependent on f_{ab} and $f_{ac}(t_{ic})$ in a similar way as for innervation of the vessels:

$$f_{sp} = \begin{cases} f_{es,\infty} + (f_{es,0} - f_{es,\infty}) \cdot e^{(k_{es} \cdot (-W_{b,sh} \cdot f_{ab} + W_{c,sh} \cdot f_{ac}(t_{ic}) - \theta_{sh}))} & f_{sh}(t_{ic}) < f_{es,max} \\ f_{es,max} & f_{sh}(t_{ic}) \geq f_{es,max} \end{cases} \quad (C.50)$$

Again, θ_{sh} is related to CNS hypoxia in a similar way as described in C.49. Its constant value is calculated as $\theta_{sh} = -2.9596 [s^{-1}]$.

Vagal fire rate is composed of two signals: vagal fire rate based on input from baro-, chemo- and pulmonary stretchsensors; and fire rate based on vagal hypoxia. The latter is an imposed signal on the basal fire rate of the sensors, and is not modeled in the original model of Ursino et al.[76]. Basal fire rate ($f_{v,b}$) is modeled according to:

$$f_{v,b}(t_{ic}) = \frac{f_{ev,0} + f_{ev,\infty} \cdot e^{\left(\frac{f_{ab}(t_{ic}) - f_{ab,0}}{k_{ev}}\right)}}{1 + e^{\left(\frac{f_{ab}(t_{ic}) - f_{ab,0}}{k_{ev}}\right)}} + W_{c,v} \cdot f_{ac} - W_{p,v} \cdot f_{ap} - \theta_v \quad (C.51)$$

Note that vagal activity increases by increasing baroreceptor activity via a sigmoidal function around working fire rate $f_{ab,0}$. Its slope is determined by parameter k_{ev} and maximum and minimum fire rates are set via $f_{ev,0}$ and $f_{ev,\infty}$. These fire rates will never be reached in practice, since input f_{ab} will be between $f_{ab,min}$ and $f_{ab,max}$. Chemoreceptor and pulmonary stretch receptor activation lead to a linearly increase and decrease with a certain weight factor ($W_{c,v} \cdot f_{ac}$ and $-W_{p,v} \cdot f_{ap}$ respectively). Parameter θ_v is a constant offset.

Vagal activity can be influenced by vagal hypoxia, as will happen during early decelerations. The relation between partial oxygen pressure in the brain and vagal additional fire rate is modeled according to:

$$f_{v,h}(t_{ic}) = W_{v,h} \cdot W_{con}(t_{ic}) \cdot f_{av}(t_{ic}) \quad (C.52)$$

Two weight factors are introduced: $W_{v,h}$ which is a constant describing the dept of deceleration to meet the requirement of -30 bpm at $p_{br}O_2$ reduction of 20%; and W_{con} , which resembles the power of the current contraction and thus is updated for every new contraction. Effective vagal fire rate f_v is the sum of $f_{v,b}$ and $f_{v,h}$ in time.

Effector response

Although several effectors are modeled, only heart period is influenced. Currently therefore in the mathematical model no feedback is applied to these effectors, except for heart period. Heart period is the inverse of heart frequency, and is modeled as the sum of the changes induced by sympathetic and vagal innervation (ΔT_s and ΔT_v respectively) and the basal heart period T_0 :

$$T(t_{ic}) = \Delta T_s(t_{ic}) + \Delta T_v(t_{ic}) + T_0 \quad (C.53)$$

Heart period is updated after each beat by averaging $T(t_{ic})$ over the last heart cycle. Both ΔT_s and ΔT_v are governed by differential equations:

$$\frac{d\Delta T_s}{dt} = \frac{1}{\tau_{T,s}} \cdot (-\Delta T_s(t_{ic}) + \sigma_{T,s}(t_{ic})) \quad (C.54)$$

$$\frac{d\Delta T_v}{dt} = \frac{1}{\tau_{T,v}} \cdot (-\Delta T_v(t_{ic}) + \sigma_{T,v}(t_{ic})) \quad (C.55)$$

Time constants of these systems are respectively $\tau_{T,s}$ and $\tau_{T,v}$; $\sigma_{T,s}$ and $\sigma_{T,v}$ are functions of sympathetic and vagal fire rate:

$$\sigma_{T,s}(t_{ic}) = \begin{cases} G_{T,s} \cdot \ln(f_{sh}(t_{ic} - D_{T,s}) - f_{es,min} + 1) & f_{sh}(t_{ic}) \leq f_{es,min} \\ 0 & f_{sh}(t_{ic}) < f_{es,min} \end{cases} \quad (C.56)$$

$$\sigma_{T,v}(t_{ic}) = G_{T,v} \cdot f_v(t_{ic} - D_{T,v}) \quad (C.57)$$

Ursino et al.,[76] also modeled local dilation effects, which were not taken into account in this study since cerebral resistance is governed by external (contraction) pressures and not by local vasodilatation effects. Oxygen consumption was modeled according to Sá Couto et al.[62] who modeled a complete model of placental oxygen exchange. (See also section C.4.)

C.4 Oxygen model

The three compartment model of Sá Couto et al.[62] is taken, which uses the output values from the hemodynamical system described in the previous paragraph. Since oxygen contents are only different in arterial, venous and placental compartments, the oxygen model has not been extended to a 21-segment model, but calculates oxygen pressures in all necessary model segments. However, cerebral circulation was not included in the original paper, and model equations as used in this section are adapted to a fulfil a four compartment model where the fourth compartment is the brain.

The maternal ventilation provides a constant assumed oxygen concentration in the maternal arterial circulation, which is transported to the placenta. In the intervillous space oxygen from the maternal blood diffuses to the villous capillaries of the fetus. The oxygen concentration of the maternal blood in the intervillous space is redirected to the central circulation and re-oxygenated in the lungs. The oxygen extracted from the maternal blood in the intervillous space oxygenates the fetal blood in the villous capillaries. This blood is transported by the venous system towards the central circulation. The fetal peripheral circulation (both in systemic capillaries as in the cerebral circulation) extracts oxygen from the central circulation. The oxygen-low blood is re-transported to the villous capillaries in the placenta to be re-oxygenated.

C.4.1 Model description

This paragraph is based on the paper of Sá Couto et al.[62] The original model provides concentrations in the intervillous space, the villous capillaries and the fetal peripheral circulation. The central oxygen concentration from the mother is constant assumed and the central oxygen concentration from the fetus can be calculated from the other concentrations. The oxygen concentration in the blood is easily converted to oxygen pressures. The gas concentration in a single homogeneous compartment can be represented by the general equation:

$$\frac{d(C(t)V(t))}{dt} = q(t)(C_{in} - C(t)) - \dot{C}(t) \quad (C.58)$$

Here the oxygen concentration is given as $C(t)$ [$\text{m}^3 \text{O}_2/\text{m}^3\text{blood}$], the blood volume of the compartment as $V(t)$ [m^3], the flow through the compartment as $q(t)$ [m^3/s] and the oxygen

consumption as $\dot{C}_0(t)$ [$\text{m}^3\text{gas/s}$]. For each of the three compartments, equation C.58 can be worked out. For the intervillous space this results in:

$$\frac{d(C_{ivs}(t)V_{ivs}(t))}{dt} = q_{ivs}(t)(C_{art,m} - C_{ivs}(t)) - D(pO_{ivs}(t) - pO_{ummc}(t)) \quad (\text{C.59})$$

Note that the oxygen metabolism in the intervillous space is only given as the extracted oxygen in the intervillous space as a consequence of diffusion, due to a oxygen gradient over the placental membrane. Here D [ml/min/mmHg] represents the placental diffusion capacity. The partial oxygen pressures in the intervillous space and in the villous capillaries are given by respectively $pO_{ivs}(t)$ and $pO_{ummc}(t)$ [mmHg]. Since not all blood enters the gas exchange compartments in the placenta, a certain shunt fractions SF_m and SF_f are taken in account. These represent the fraction of blood at respectively maternal and fetal sides which do not take part in the oxygen exchange in the placenta. For the umbilical capillaries - the villous capillaries - equation C.58 can be written as:

$$\frac{d(C_{ummc}(t)V_{ummc}(t))}{dt} = q_{ummc}(t)(C_{art,f} - C_{ummc}(t)) + D(pO_{ivs}(t) - pO_{ummc}(t)) \quad (\text{C.60})$$

The blood of the villous capillaries is oxygenated by the diffused oxygen from the intervillous space over the placental membrane. The oxygen metabolism is thus positively signed. Note that no oxygen is consumed by the villous capillaries themselves. The fetal arterial oxygen content is given by $C_{art,f}$ [$\text{m}^3 \text{O}_2/\text{m}^3 \text{blood}$]. The third compartment, the fetal capillaries, has an oxygen state according to:

$$\frac{d(C_{mc,f}(t)V_{mc,f}(t))}{dt} = q_{mc,f}(t)(C_{art,f} - C_{mc,f}(t)) - \dot{C}_f(t) \quad (\text{C.61})$$

Oxygen state in the fourth compartment, the fetal brain, is based on oxygen delivery by the fetal arteries and consumption in the brain:

$$\frac{d(C_{br,f}(t)V_{br,f}(t))}{dt} = q_{br,f}(t)(C_{art,f} - C_{br,f}(t)) - \dot{C}_{br,f}(t) \quad (\text{C.62})$$

Solving equations C.59-C.62, will result in the oxygen contents for each volume. Additional relationships are needed for the parameters presented in the formulas, these are given below. The fetal oxygen consumption is given by $\dot{C}_f(t)$ [$\text{m}^3 \text{O}_2/\text{s}$]. The oxygen consumption is reduced linearly via K_f [$\text{m}^3 \text{blood/s}$] in case of hypoxia:

$$\dot{C}_f(t) = \begin{cases} \dot{C}_f(t) & C_f(t) \leq C_{th} \\ \dot{C}_f(t) + K_f(C_{art,f} - C_{th}) & \text{else} \end{cases} \quad (\text{C.63})$$

And, similar in the brain:

$$\dot{C}_{br,f}(t) = \begin{cases} \dot{C}_{br,f}(t) & C_{br,f}(t) \leq C_{br,th} \\ \dot{C}_{br,f}(t) + K_f(C_{art,f} - C_{br,th}) & \text{else} \end{cases} \quad (\text{C.64})$$

As a consequence of the shunted blood in the villous capillaries, the oxygen content in the umbilical vein is not similar to the oxygen content in the villous capillaries:

$$C_{uv}(t) = SF_f C_{art,f}(t) + (1 - SF_f)(C_{ummc}(t)) \quad (C.65)$$

The overall fetal arterial oxygen content is represented by $C_{art,f}(t)$ [$\text{m}^3 \text{O}_2/\text{m}^3 \text{blood}$], and is a linear combination of the oxygen content in the umbilical vein, in the fetal capillaries and the fetal brain:

$$C_f(t) = \frac{C_{mc,f}(t)q_{mc,f}(t) + C_{br,f}(t)q_{br,f}(t) + C_{uv}(t)q_{ummc}(t)}{q_{mc,f}(t) + q_{br,f}(t) + q_{ummc}(t)} \quad (C.66)$$

The assumption is made that the flow through the umbilical vein is equal to the flow through the umbilical capillaries.¹ By combining equation C.65 and C.66, $C_f(t)$ can be written as:

$$C_f(t) = \frac{C_{mc,f}(t)q_{mc,f}(t) + C_{br,f}(t)q_{br,f}(t) + (1 - SF_f)C_{ummc}(t)q_{ummc}(t)}{q_{mc,f}(t) + q_{br,f}(t) + (1 - SF_f)q_{ummc}(t)} \quad (C.67)$$

Steady state: initialization

To solve the oxygen states for the different compartments in steady state, additional relationships are needed. In equations C.59 and C.60, the partial oxygen pressure is introduced. The relation between total oxygen content in the blood C and partial pressure pO is based on the two forms oxygen is found in blood:

- oxygen is bound to hemoglobin with a certain saturation;
- a small fraction of oxygen is dissolved in the blood;

both as a function of partial pressure. This results in the following equation to calculate oxygen content from partial pressure, with distinct parameters for mother and fetus since they differ in oxygen binding and hemoglobin concentration. The subscript *mat* and *fet* can be replaced by respectively every maternal or fetal compartmental subscript.

$$C_{mat}(t) = \frac{\alpha Hb_{mat} S_{mat}(pO_{mat})}{100} + \beta pO_{mat} \quad (C.68)$$

$$C_{fet}(t) = \frac{\alpha Hb_{fet} S_{mat}(pO_{fet})}{100} + \beta pO_{fet} \quad (C.69)$$

Here α [$\text{m}^3 \text{gas}/\text{gHb}$] represents the maximum binding capacity of hemoglobin, Hb [$\text{g Hb}/\text{m}^3$] the hemoglobin concentration and β [$\text{m}^3 \text{O}_2/\text{m}^3 \text{blood}/\text{mmHg}$] the content of dissolved oxygen

¹In the original model of Sá Couto et al.,[62] only two flows were used, $F_{mc,f}(t)$ and $F_{ummc}(t)$, hereby assuming that the flow through the umbilical vein equals the flow through the villous capillaries. The circulation model used in the current study provides both $F_{ummc}(t)$ and $F_{uv}(t)$; but since these calculated flows are almost similar, $F_{ummc}(t)$ was taken as flow through the umbilical vein, instead of a separate $F_{uv}(t)$.

as function of partial pressure. $S(pO)$ [%] represents the saturation as function of partial pressure, and is given as:[62]

$$S_{mat}(pO_{mat}) = \frac{100}{1 + \frac{c_{m1}}{pO_{mat}^3 + c_{m2} \cdot pO_{mat}}} \quad (C.70)$$

$$S_{fet}(pO_{fet}) = \frac{100}{1 + \frac{c_{f1}}{pO_{fet}^3 + c_{f2} \cdot pO_{fet}}} \quad (C.71)$$

The constants c_{m1} and c_{f1} are expressed in mmHg³, and c_{m2} and c_{f2} in mmHg². Now the steady state values for each compartmental oxygen content $C(t=0)$ and corresponding partial pressure $pO(t=0)$ can be calculated. In steady state the time derivatives are zero, and therefore the left terms of the main equations C.59-C.61 are zero. The oxygen contents $C(t)$ in these equations can now be written as a function of partial pressure $pO(t)$. For the first equation this is achieved by inserting C.70 in C.68, and this new equation in C.59. A similar procedure can be followed for the equations concerning the oxygen contents in the villous capillaries C.60 and the fetal microcirculation C.61. Therefore first equation C.71 needs to be substituted in equation C.69 to achieve partial pressure, and then inserted both in equations C.60 and C.61. These substitutions were performed in Matlab and result in quite large equations that are therefore not printed in this paper.

With known constant flow values - calculated from steady state mean flows in the circulation model - and known constants $C_m(t)$, SF_m and SF_f , D and $\dot{C}_f(t)$, these three equations contain four unknowns. Together with equation C.67, four equations and four unknowns remain, which can be solved in Matlab to retrieve the initial values for the states.

Oxygen as function of variable flow and volume values

In the circulation model, variable flow and volume values are calculated per increment as a consequence of the pumping function of the left ventricle. Therefore the left term in general equation C.58 is not zero. Application of the product rule[1] to this term leads to:

$$\frac{d(C(t)V(t))}{dt} = C \frac{dV}{dt} + V \frac{dC}{dt} \quad (C.72)$$

Now the discrete version of the compartmental blood volume change $\frac{dV}{dt}$ can be written as:

$$\frac{dV}{dt} = \frac{V(t_{ic,ox}) - V(t_{ic-1,ox})}{\Delta t_{ox}} \quad (C.73)$$

The discrete version of the compartmental oxygen content $\frac{dC}{dt}$ can be calculated according to:

$$\frac{dC}{dt} = \frac{C(t_{ic,ox}) - C(t_{ic-1,ox})}{\Delta t_{ox}} \quad (C.74)$$

The time step was adjusted for the oxygen model and noted as Δ_{ox} [s], which was set at 0.4320 seconds, which is about the length of a fetal cardiac cycle. Consequently incremental time was

noted as $t_{ic,ox}$ since the time step was adjusted. Volume and flow rates were averaged over the time step. Equation C.74 is only substituted in equation C.61, since the time derivatives of $C(t)$ from equation C.59 and C.60 can be rewritten in terms of partial pressure, which hold respectively:[62]

$$\frac{dC_{ivs}(t)}{dt} = \left[\frac{\alpha H b_m}{100} \frac{\partial S_{ivs}}{\partial pO_{ivs}} \Big|_{pO_{ivs}(t)} + \beta \right] \frac{dpO_{ivs}(t)}{dt} \quad (C.75)$$

$$\frac{dC_{ummc}(t)}{dt} = \left[\frac{\alpha H b_f}{100} \frac{\partial S_{ummc}}{\partial pO_{ummc}} \Big|_{pO_{ummc}(t)} + \beta \right] \frac{dpO_{ummc}(t)}{dt} \quad (C.76)$$

Together with the known variable flow values from the circulation model and equation C.67, the unknown partial pressures from equations C.59-C.61 can be stepwise solved per compartment.

Remark

Parer[56] noted that for human fetuses a total oxygen content of 55 ml is estimated. However, assuming a fetal blood volume of 300 ml - including the fetal blood in the placenta - results in an average fetal pO_2 of about 33 mmHg. This level is only reached in the villous capillaries, in all other blood compartments this level is much lower, see also table A.2 Fetal arterial pO_2 is normally around 24 mmHg. The total amount of oxygen in the fetus as calculated in the current study is 34.5 ml, which seems more in accordance with values for partial oxygen pressures and blood volume estimates for the different compartments.

C.5 Variability in heart rate and contraction signal

Variability is calculated according to the scheme in figure C.4 on the next page. To obtain a new variability signal, a random unique signal is modified via a (constant) filter to obtain a (unique) variability signal that is based on original variability signals. To achieve this, for the random standard signal so-called white noise is used. This is a certain random signal that contains all frequency components, thus besides the frequency components of the original heart rate also all other frequencies. By using a filter with only the frequencies of interest, i.e. the frequencies in an original heart rate signal, only these frequencies remain. The new signal is unique - although having the characteristics of the original variability signal - since the white noise signal is a unique signal every time. The filter is a constant.

The filter is obtained by calculating the frequency components of an original variability signal via a fast fourier transformation (upper left and right pane in figure C.4). The filter hence contains all frequency components of the original trace. By multiplying the filter with the fast fourier transform of a white noise signal (which is a standard function in mathematical software packages such as Matlab), the fourier transform of a new variability signal is generated. Via a fourier back-transform the new variability signal can be obtained. The filter, once determined, can be used to generate unlimited numbers of unique variability signals by filtering new white noise signals. Because of variations in amplitude of the original signal and the new heart rate variability, a factor c is used to calculate the correct amplitude.

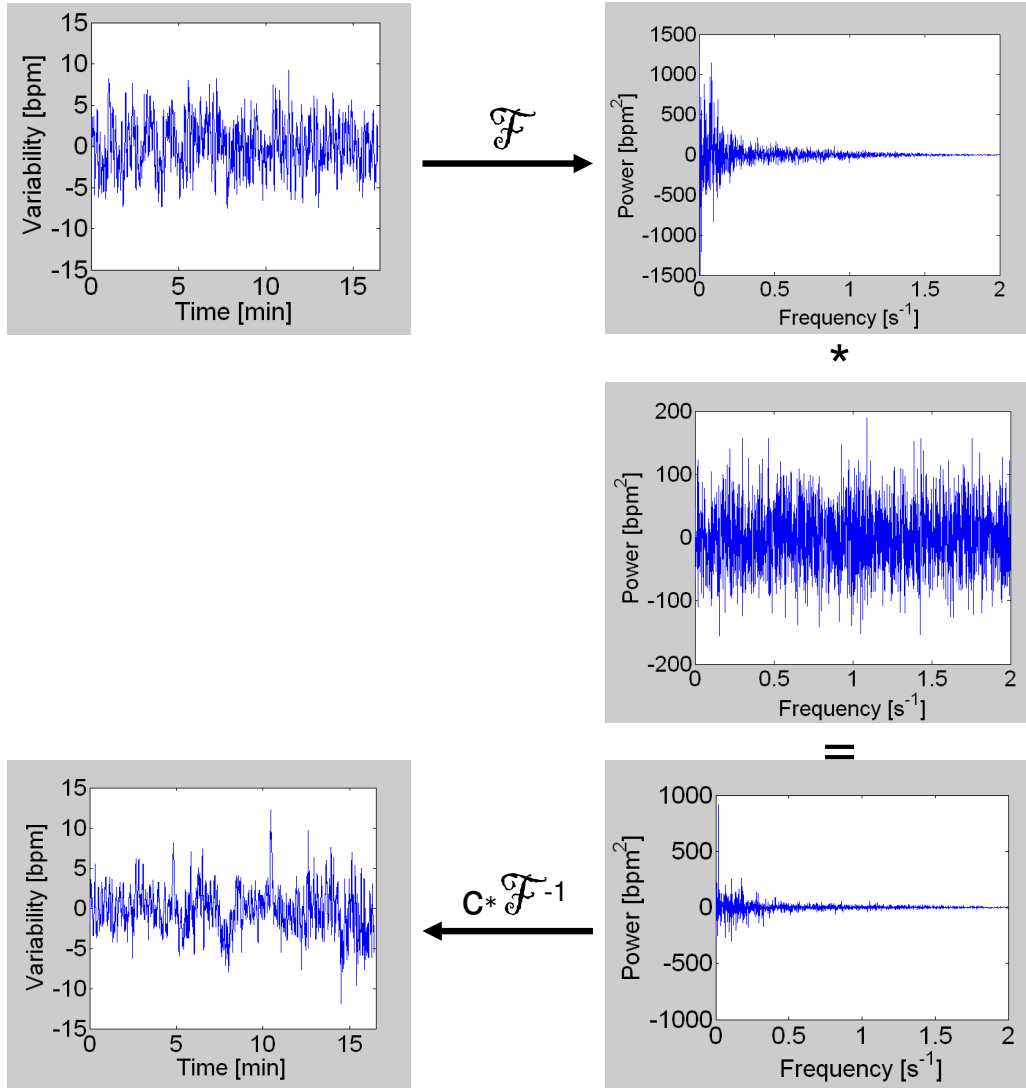


Figure C.4: Calculation of new heart rate variability. The original signal (upper left) is fourier-transformed, and serves as a filter (upper right). This filter is multiplied with a new white noise signal that is fourier-transformed (middle right), and results in a new variability signal in the Fourier domain (lower right). Back transformation leads to a variability signal, but needs to be multiplied by a factor c based on the standard deviation ratio between original and heart rate variability to obtain a realistic amplitude in the new variability signal (lower left).

D Model in Matlab

An overview of the hierarchy in m-files is given in the diagram in figure D.1. Per m-file a short description is given in the following paragraphs.

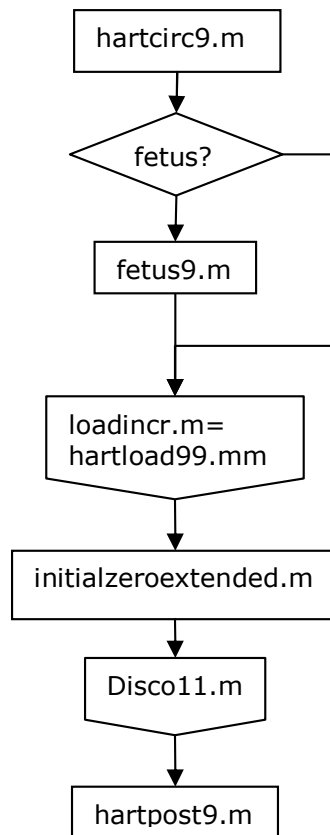


Figure D.1: Flowchart of Matlab routines. First level overview of the Matlab routines. The blocks *loadincr.m* and *disco11.m* will be elaborated in subsequent diagrams.

D.1 Initialization

Firstly the initial state has to be defined for both mother and fetus. This is done in several m-files:

hartcirc9.m

In *hartcirc9.m* the simulation set-up is worked out. Simulation parameters are initiated (pregnant or not? which simulation scenario? what simulation time? etc.) and the vascular map of the mother is made. By running *hartcirc9.m* the whole program will run.

foetus9.m

If the mother is pregnant, the fetal vascular map has also to be defined, which is done in *foetus9.m*.

loadincr.m

The file *loadincr.m* contains external (i.e. not calculated by *disco11.m*) pressure calculation, which can be used each new increment as applied external pressures in *disco11.m*. Each simulation in DiSCo uses its own *loadincr.m* to calculate external applied loads; *loadincr.m* may be empty.

updaelda.m

If the system matrix *eldaC* needs to be updated incrementally, data needs to be saved this can be defined in the general file *updaelda.m* that is used by DiSCo. If system parameters do not change in time, *updaelda.m* may be empty.

initialzeroextended.m

To prevent large unnecessary calculation times, matrices expected to become very large (i.e. time-dependent matrices) are preallocated and created as null-matrices according to their expected length based on total simulation time.

D.2 DiSCo

The incremental calculation is performed in *disco11.m*, which consists of different small routines, as explained in figure D.2. Each block with a routine is described below.

checkinput.m

Files and parameters needed for further calculation are created with this m-file. These parameters are mainly derived from the vascular map (number of nodes, etc.).

lcase.m

Based on the initial applied loads, simulation parameters used for system partitioning are defined.

initialzero.m

Flow- and pressure (derivatives) arrays are created and set at zero.

eldata1.m

The system matrix is build from the vascular system map as defined in *hartcirc9.m* and *foetus9.m*. The system matrix is saved in three forms: initial (*elda0*), current (*eldaC*) and previous (*eldaB*).

elmat1.m

In *elmat1.m* the system is divided in three different submatrices from *eldaC*, based on the three element types C, R, and L: respectively matrix *ema*, *emb* and *emc*.

loadincr.m

With this routine, the new ventricular pressure is calculated. *Loadincr.m* invokes a serie of m-files, as can be seen from the diagram in figure D.3. Segmental volumes are updated based on volume flows from the previous increment and used to calculate the new ventricular volume. It's internal invoked routines are:

lv_model.m & *mat_model1.m*

The maternal left ventricular pressure is based on the 1-fiber model as defined in *lv_model.m* and *mat_model1.m*. Ventricular volumes are used to calculate active and passive stresses that are both needed for left ventricular pressure calculation.

baro5.m

The heart frequency for the next beat is based on calculations made after each increment in *baro5.m*. After a cardiac cycle, this data is combined to calculate new heart frequency in *loadincr.m*.

flv_model.m & *fmat_model1.m*

The fetal right ventricular pressure is based on the 1-fiber model as defined in *flv_model.m* and *fmat_model1.m*. Ventricular volumes are used to calculate active and passive stresses that are both needed for left ventricular pressure calculation.

fbaro3.m

The heart frequency for the next beat is based on calculations made after each increment in *fbaro3.m*. After a fetal cardiac cycle, this data is combined to calculate the new heart frequency in *loadincr.m*.

After *loadincr.m* has been invoked, *disco11.m* continues with the following routines:

intsys.m

In *intsys.m* the differential equation is defined for all nodes. The second time *intsys.m* is invoked (after *partit.m*) pressure derivatives are calculated.

partit.m

The system is partitioned in *partit.m* for the known and unknown nodal pressures. After this routine, in *disco11.m* the system is solved and the new pressure values per node are assigned.

updaelda.m

Based on the calculated pressure values, the heart valve resistances are changed if necessary with *updaelda.m* in system matrix *eldaC*. Other resistance values that might change (due to scenarios etc.) are also changed at this point. If needed, compliances and inertias can be changed as well.

savedata.m

All nodal pressure values are saved according to *savedata.m*.

D.3 Postprocessing

After calculation of the system response for the simulated time, postprocessing is done with *oxygenss.m*, *hartpost9.m*, and *oxygenhulp.m*.

oxygenss.m

The steady state of oxygen pressures is calculated based on a steady state in blood pressure. Currently this is done after the simulation, but in closed loop simulation has to be done earlier in the simulation.

hartpost9.m

This file generates pictures of pressures and flows in all vessel segments.

oxygenhulp.m

Oxygen pressures as function of time are based on blood flow and volumes, as well as oxygen pressure derivatives. When oxygen pressures are used in closed loop simulation, this m-file has to be invoked in *loadincr.m*, so that it's values can influence cardiovascular regulation.

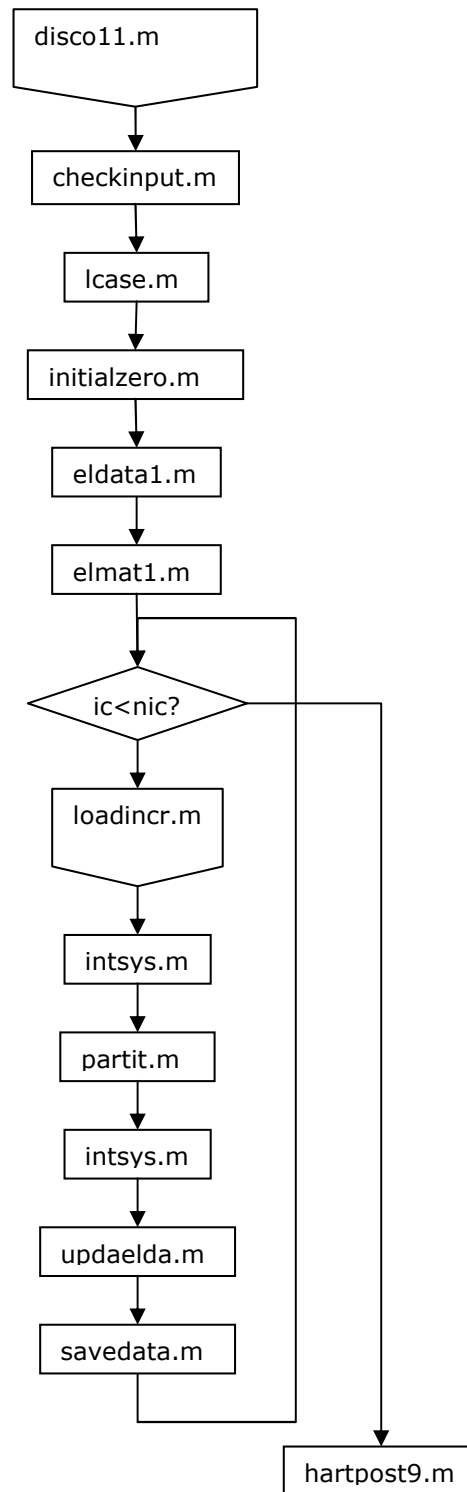


Figure D.2: Flowchart of Matlab routines: *disco11.m*. Second level overview of the Matlab routines, as used in *disco11.m*. If the current increment (*ic*) is larger than the total number of increments, *disco11.m* is ended and the program continues with *hartpost9.m* that is invoked in *hartcirc9.m*. The block *loadincr.m* will be elaborated in figure D.3.

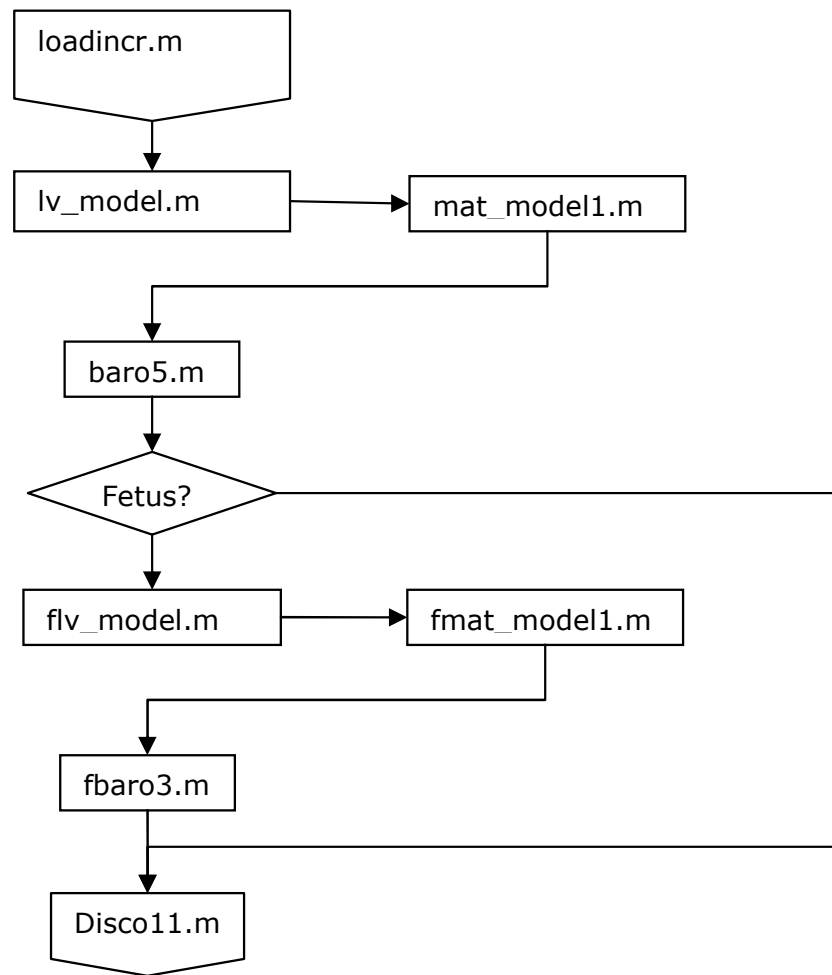


Figure D.3: Flowchart of Matlab routines: *loadincr.m*. Third level overview of the Matlab routines, as used in *loadincr.m*. At the end of *loadincr.m*, *disco11.m* is continued as can be seen in figure D.2.

E Analysis of CTG traces with early decelerations

Available CTG traces with early decelerations were analyzed to use quantitative data in the mathematical model with regard to several parameters. A summary is presented in this appendix. Investigated parameters are schematically shown in figure E.1. A total of 28 decelerations from seven different tracings were found and analyzed. Mean and standard deviation are calculated for

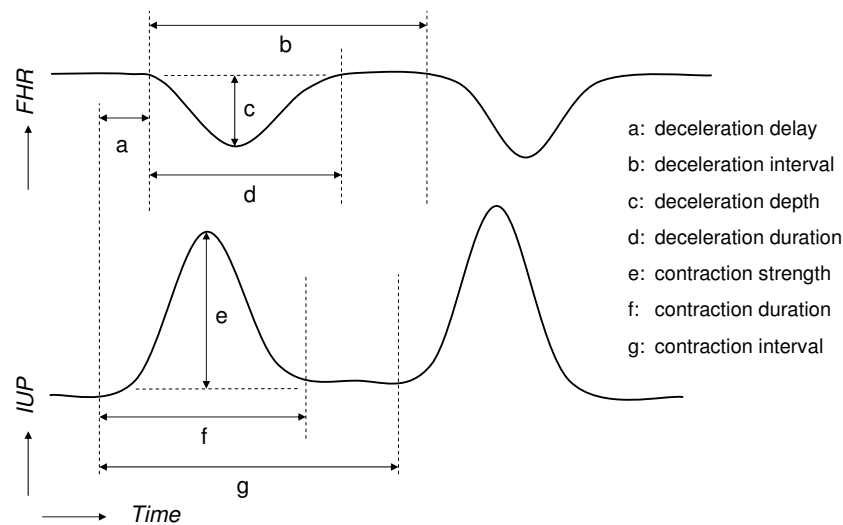


Figure E.1: Schematic representation of investigated parameters. In a total of 28 early decelerations, seven different parameters were analyzed: deceleration delay (time delay of deceleration after onset of contraction), deceleration interval (time interval between two subsequent decelerations), deceleration depth (maximum decrease in fetal heart rate in relation to baseline), deceleration duration, contraction strength (maximum pressure of contraction in relation to baseline), contraction duration and contraction interval (time interval between two subsequent decelerations).

all parameters (deceleration delay, deceleration interval, deceleration depth, deceleration duration, contraction strength, contraction duration and contraction interval), this is presented in table E.1.

Table E.1: Model segments with abbreviations

	Mean	Standard deviation	Unit
Deceleration delay	9	8	s
Deceleration interval	127	33	s
Deceleration depth	24	9	bpm
Deceleration duration	60	15	s
Contraction strength	49	29	mmHg
Contraction duration	64	20	s
Contraction interval	117	35	s

F Validation study

The validation study was performed with experts' opinion of 10 CTG tracings, of which 5 were real, and 5 were computer-generated. Each tracing had to be rated according to table F.1. Finally, an overall classification had to be given (*real*, *computer-generated* or *not distinguishable*). This clinical evaluation was performed in Dutch. On the next pages the evaluated CTG tracings can be found. The real tracings are: nrs. 1, 3, 4, 5 and 7; the computer-generated tracings are: nrs. 2, 6, 8, 9 and 10.

Table F.1: Items to be rated

FHR		realistic	fairly realistic	not realistic	evt. remarks
baseline					
variability					
early decelerations	delay				
	duration				
	depth				
	morphology				
TOCO		realistic	fairly realistic	not realistic	evt. remarks
resting tone	height				
	morphology				
contractions	amplitude				
	frequency				
	duration				
	morphology				

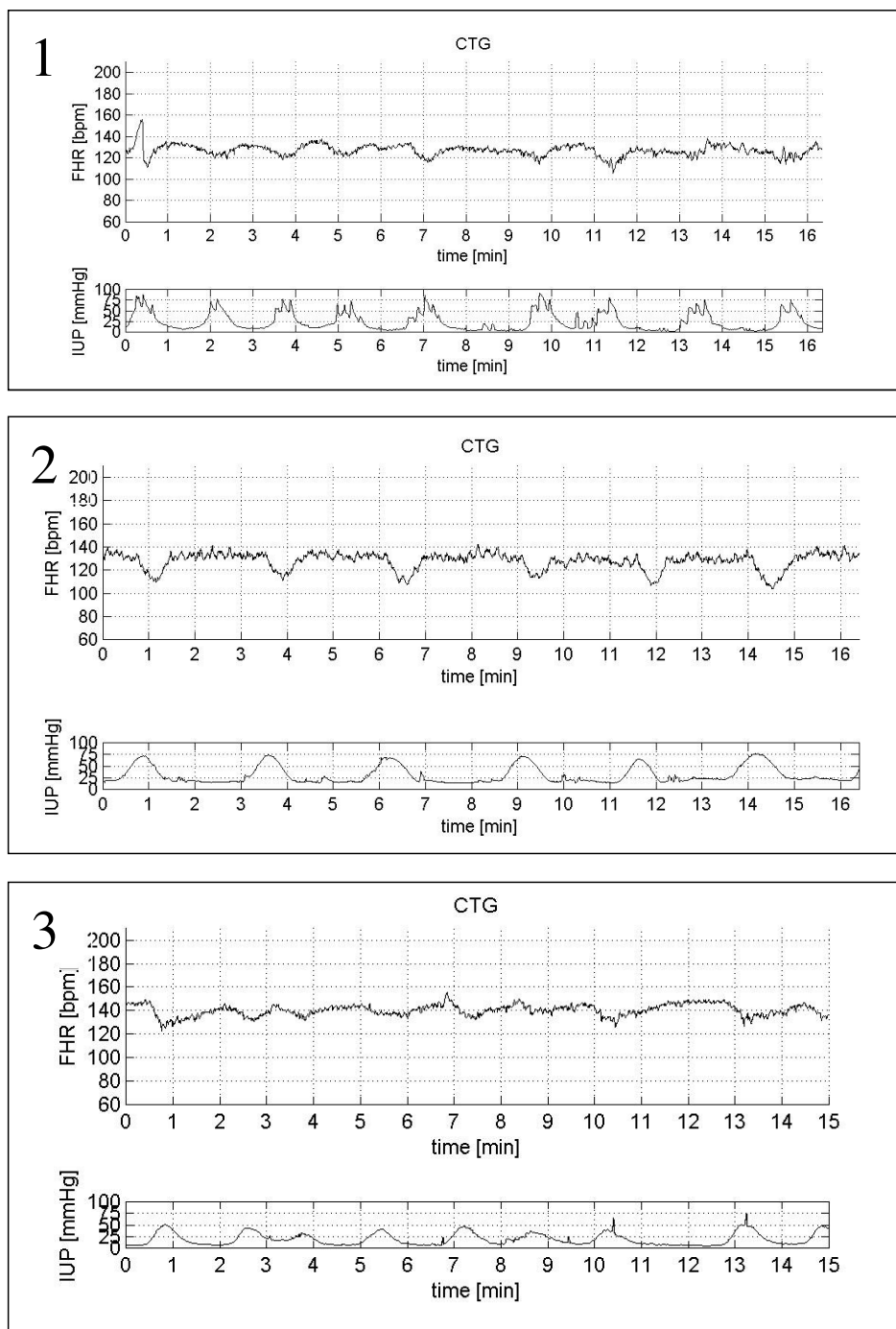


Figure F.1: CTG 1-3.

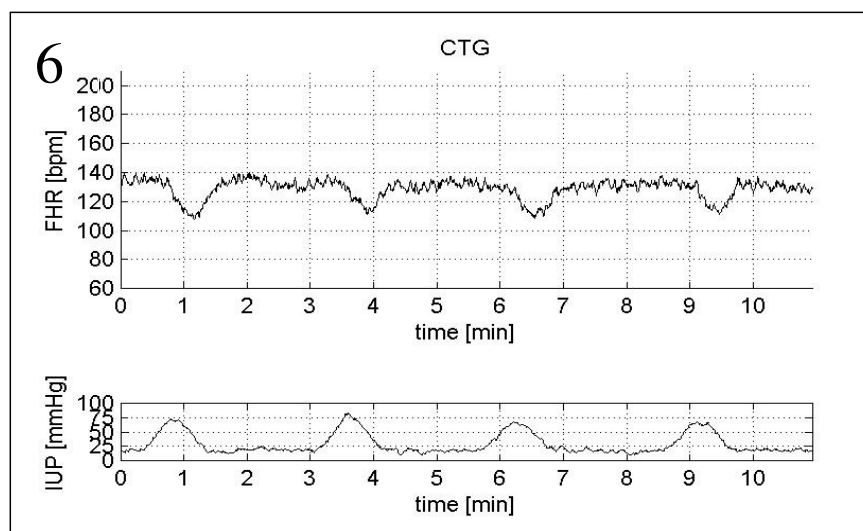
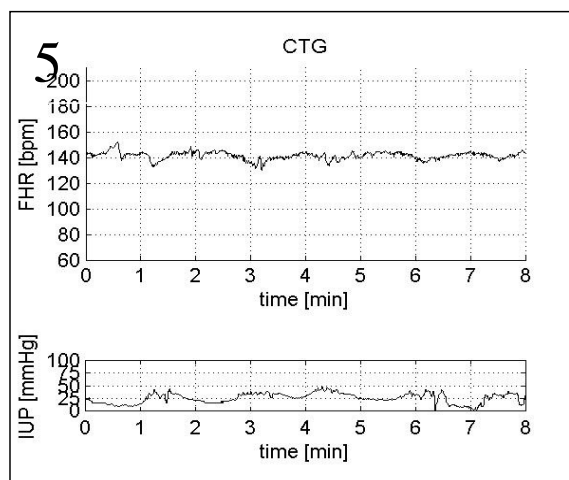
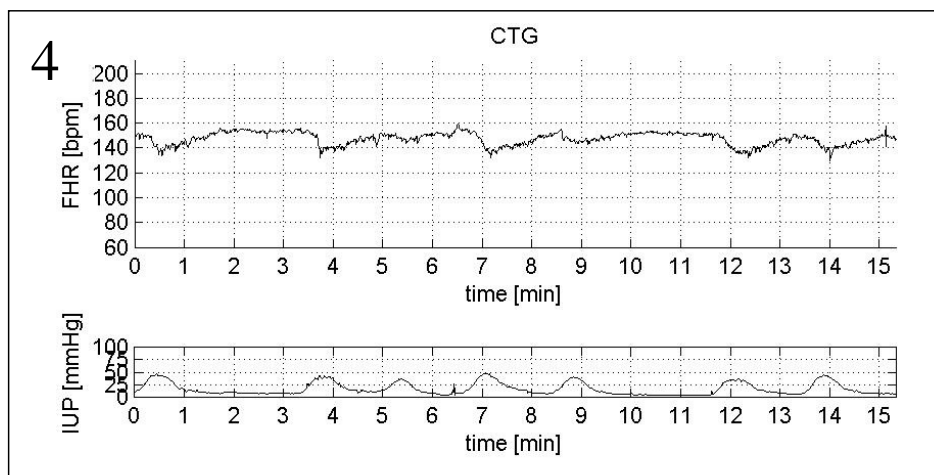


Figure F.2: CTG 4-6.

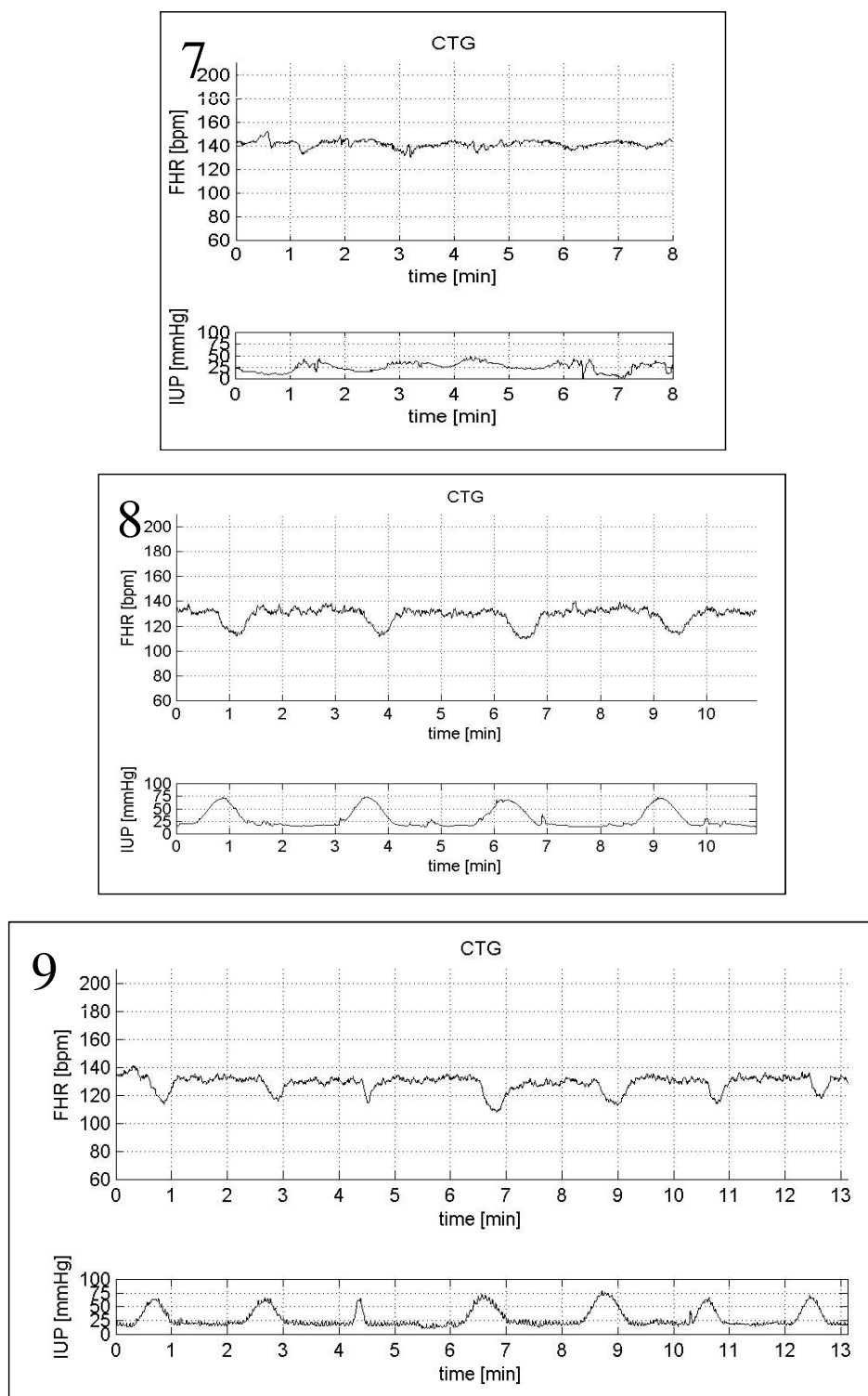


Figure F.3: CTG 7-9.

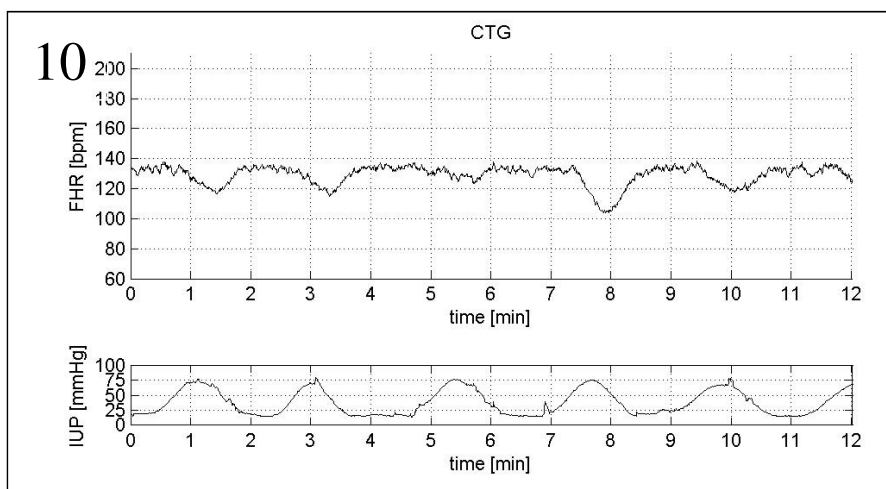


Figure F.4: CTG 10.

Bibliography

- [1] R.A. Adams. *Calculus*. Addison-Wesley Don Mills, Ontario,, 1999.
- [2] I. Ahmer-Walin, S. Arulkumaran, H. Hagberg, K. Maršál, and G.H.A. Visser. Fetal electrocardiogram: St waveform analysis in intrapartum surveillance. *Br J Obstet Gynecol*, 114:1191–1193, 2007.
- [3] C.J. Aldrich, D. D’Antona, J.A.D. Spencer, D.T. Delpy, E.O.R. Reynolds, and J.S. Wyatt. Fetal heart rate changes and cerebral oxygenation measured by near-infrared spectroscopy during the first stage of labour. *Europ J Obstet Gynecol Reprod Biol*, 64:189–195, 1996.
- [4] S.E. Andreassen, S. Rees. Mathematical models of oxygen and carbon dioxide storage and transport: interstitial fluid and tissue stores and whole-body transport. *Crit Rev Biomed Eng*, 33:265–298, 2005.
- [5] T. Arts, P. Bovendeerd, T. Delhaas, and F. Prinzen. Modeling the relation between cardiac pump function and myofiber mechanics. *J Biomechanics*, 36:731–736, 2003.
- [6] T. Arts, T. Delhaas, P. Bovendeerd, X. Verbeek, and F.W. Prinzen. Adaptation to mechanical load determines shape and properties of heart and circulation: the CircAdapt model. *Am J Physiol Heart Circ Physiol*, 288:H1943–1954, 2005.
- [7] N.S. Assali, B. Nuwayhid, and M. Zugaib. Control of the uteroplacental circulation in health and disease. *Eur J Obstet Gynecol Reprod Biol*, 8:43–55, 1978.
- [8] P.C.A.M. Bakker, G. Colenbrander, A.A. Verstraeten, and H.P. van Geijn. The quality of intrapartum fetal heart rate monitoring. *Eur J Obstet Gynecol*, 116:22–27, 2003.
- [9] M. Bellotti, G. Pennati, C. De Gaspari, F.C. Battaglia, and E. Ferrazzi. Role of ductus venosus in distribution of umbilical blood flow in human fetuses during second half of pregnancy. *Am J Physiol Heart Circ Physiol*, 279:H1256–H1263, 2000.
- [10] J.E.W. Beneken. *A mathematical approach to cardiovascular function: the uncontrolled human system*. PhD thesis, Medisch Fysisch Instituut TNO, Utrecht, 1965.
- [11] C.E. Blanco, G.S. Dawes, M.A. Hanson, and H.B. McCooke. The response to hypoxia of arterial chemoreceptors in fetal sheep and new-born lambs. *J Physiol*, 351:25–37, 1984.
- [12] P.H.M. Bovendeerd. Cardiac modeling: The heart in the circulatory system - lecture notes. Eindhoven University of Technology, 2005.
- [13] P.H.M. Bovendeerd, P. Borsje, T. Arts, and F.N. van de Vosse. Dependence of intramyocardial pressure and coronary flow on ventricular loading and contractility: a model study. *Ann Biomed Eng*, 34:1833–1845, 2006.

- [14] V.L. Brooks, R.R. Quesnell, S.R. Cumbee, and V.S. Bishop. Pregnancy attenuates activity of the baroreceptor reflex. *Clin Exp Pharmacol Physiol*, 22:152–156, 1994.
- [15] R. Caldeyro-Barcia, C. Méndez-Bauer, J.J. Poseiro, L.A. Escarena, S.V. Pose, J. Bieniarz, I. Arnt, L. Gulin, and O. Althabe. *The heart and circulation in the newborn and infant*, chapter Control of the human fetal heart rate during labor, pages 7–36. Grune & Stratton, New York, 1966.
- [16] W.L. Capper, J.G. Cowper, and L.J. Myers. A transferfunction-based mathematical model of the fetal-placental circulation. *Ultrasound Med Biol*, 28:1421–1431, 2002.
- [17] B. Carbonne, C. Cudeville, F. Maillard, and F. Goffinet. Predictive value of pulse oximetry and fetal scalp blood ph in the case of meconium-stained amniotic fluid. *Eur J Obstet Gynecol Reprod Biol*, 109:27–32, 2003.
- [18] A. Costa, M.L. Costantino, and R. Fumero. Oxygen exchange mechanisms in the human placenta: mathematical modelling and simulation. *J Biomed Eng*, 14:385–389, 1992.
- [19] D. Danilenko-Dixon, L. Tefft, R.A. Cohen, B. Haydon, and M.W. Carpenter. Positional effects on maternal cardiac output during labor with epidural analgesia. *Am J Obstet Gynecol*, 175:876–872, 1996.
- [20] M.C. de Bruijne, M. Zegers, L.H.F. Hoornhout, and C. Wagner. *Onbedoelde schade in Nederlandse ziekenhuizen: dossieronderzoek van ziekenhuisopnames in 2004*. Instituut voor extramuraal geneeskundig onderzoek, NIVEL, Amsterdam,, 2007.
- [21] T. Draycott, J.F. Crofts, Ash. J.P., L.V. Wilson, E. Yard, T. Sibanda, and A. Whitelaw. Improving neonatal outcome through practical shoulder dystocia training. *Obstet Gynecol*, 112:14–20, 2008.
- [22] E.M.K. Ekholm and R.U. Erkkola. Autonomic cardiovascular control in pregnancy. *Eur J Obstet Gynecol Reprod Biol*, 64:29–36, 1996.
- [23] T.Y. Euliano, D. Caton, W. van Meurs, and M.L. Good. Modeling obstetric cardiovascular physiology on a full-scale patient simulator. *J Clin Monit*, 13:293–297, 1997.
- [24] R.K. Freeman, T.J. Garite, and M.P. Nageotte. *Fetal heart rate monitoring*. Lippincott Williams & Wilkins, Philadelphia, 2000.
- [25] T. Geva, M.B. Mauer, L. Striker, B. Kirshon, and J.M. Pivarnik. Effects of physiologic load of pregnancy on left ventricular contractility and remodeling. *Am Heart J*, 133:53–59, 1997.
- [26] J.W. Goldkrand, D.H. Moore, S.U. Lentz, S.P. Clements, D.U. Turner, and J.L. Bryant. Volumetric flow in the umbilical artery: normative data. *J Matern Foetal Med*, 9:224–228, 2000.
- [27] A. Guettouche, J.C. Challier, Y. Ito, C. Papapanayotou, Y. Cherruault, and A. Azancot-Benisty. Mathematical modelling of the human fetal arterial blood circulation. *Int J Biomed Comput*, 31:127–129, 1992.
- [28] A. Guettouche, C. Papapanayotou, and Y. Cherruault. Optimization and resolution algorithm of the human fetal blood circulation model. *Math Comput Modelling*, 18:1–8, 1993.

- [29] C. Guiot, P.G. Piant, and T. Todros. Modeling the feto-placental circulation: I. a distributed network predicting umbilical hemodynamics throughout pregnancy. *Ultrasound Med Biol*, 18:535–544, 1992.
- [30] A.C. Guyton and J.E. Hall. *Textbook of medical physiology*. Saunders company, Philadelphia, 2000.
- [31] M.V. Hart, M.J. Morton, J.D. Hosenpud, and J. Metcalfe. Aortic function during normal human pregnancy. *Am J Obstet Gynecol*, 154:887–891, 1986.
- [32] A. Holdcroft and T.A. Thomas. *Principles and practice of obstetric anaesthesia and analgesia*. Blackwell Science Ltd., Oxford, 2000.
- [33] W. Huberts. The hemodynamical effects of arteriovenous fistula. Master's thesis, Eindhoven University of Technology, 2006.
- [34] F. Huikeshoven, T.G. Coleman, and H.W. Jongsma. Mathematical model of the fetal cardiovascular system: the uncontrolled case. *Am J Physiol*, 239:R317–R325, 1980.
- [35] G.B. Huntington and H.F. Tyrrell. Oxygen consumption by portal-drained viscera of cattle: comparison of analytical methods and relationship to whole body oxygen consumption. *J Dairy Sci*, 68:2727–2734, 1985.
- [36] A. Jensen, Y. Garnier, and R. Berger. Dynamics of fetal circulatory responses to hypoxia and asphyxia. *Reprod Biol*, 84:155–172, 1999.
- [37] R. Katz, J.S. Karliner, and R. Resnik. Effects of a natural volume overload state (pregnancy) on left ventricular performance in normal human subjects. *Circulation*, 58:434–441, 1978.
- [38] T. Kiserud. Foetal circulation. *Semin Foetal Neonatal Med*, 10:493–503, 2005.
- [39] L.T. Kohn, J.M. Corrigan, and M.S. Donaldson. *To err is human. Building a safer health care system*. National Academy Press, Washington, D.C., 2000.
- [40] J.C. Konje, E.S. Howarth, P. Kaufmann, and D.J. Taylor. Longitudinal quantification of uterine artery blood volume flow changes during gestation in pregnancies complicated by intrauterine growth restriction. *Br J Obstet Gynecol*, 110:301–305, 2003.
- [41] T. Korakianitis and Y. Shi. A concentrated parameter model for the human cardiovascular system including heart valve dynamics and atrioventricular interaction. *Med Eng Phys*, 28:613–628, 2006.
- [42] A. Kozák-Bárány, E. Jokinen, P. Kero, J. Tuominen, T. Rönnemaa, and I. Välimäki. Impaired left ventricular diastolic function in newborn infants of mothers with pregestational or gestational diabetes with good glycemic control. *Early Hum Dev*, 77:13–22, 2004.
- [43] W. Lee, R. Rokey, J. Miller, and D.B. Cotton. Maternal hemodynamic effects of uterine contractions by m-mode and pulsed-doppler echocardiography. *Am J Obstet Gynecol*, 161:974–977, 1989.
- [44] O. Linderkamp, H.T. Versmold, K. Messow-Zahn, W. Müller-Holve, K.P. Riegel, and K. Betke. The effect of intra-partum and intra-uterine asphyxia on placental transfusion in premature and full-term infants. *Eur J Pediatr*, 127:91–99, 1978.

- [45] G. Link, K.E. Clark, and U. Lang. Umbilical blood flow during pregnancy: evidence for decreasing placental perfusion. *Am J Obstet Gynecol*, 196:489e1–489e7, 2007.
- [46] Merck Manuals. <http://www.merck.com/mmhe/sec22/ch259/ch259a.html>.
- [47] C.B. Martin Jr., J. de Haan, B. van der Wildt, H.W. Jongsma, A. Dieleman, and T.H.M. Arts. Mechanism of late decelerations in the fetal heart rate. a study with autonomic blocking agents in the fetal lamb. *Europ J Obstet Gynec Reprod Biol*, 9:361–373, 1979.
- [48] E. Ménigault, M. Berson, P. Vieyres, P.B. Lepoivre, D. Pourcelot, and L. Pourcelot. Feto-maternal circulation: mathematical model and comparison with doppler measurements. *Eur J Ultrasound*, 7:129–143, 1998.
- [49] B. Messing, S.M. Cohen, D.V. Valsky, D. Rosenak, D. Hochner-Celnikier, S. Savchev, and S. Yagel. Fetal cardiac ventricle volumetry in the second half of gestation assessed by 4d ultrasound using stic combined with inversion mode. *Ultrasound Obstet Gynecol*, 30:142–151, 2007.
- [50] L.Y.L. Mo, P.A.J. BascomKnox Ritchie, and L.M.E. McCowan. A transmission line modelling approach to the interpretation of uterine doppler waveforms. *Ultrasound Med Biol*, 14:365–376, 1988.
- [51] W. Moll. Die physiologische kreislaufumstellung in der schwangerschaft - ihre bedeutung fr kardiale erkrankungen. *Z Kardiol*, 90:IV/2–IV/9, 2001.
- [52] E.G. Morgan, M.S. Mikhail, and M.J. Murray. *Clinical Anesthesiology*. McGraw-Hill Professional, New York, 2001.
- [53] M. Murray. *Antepartal and intrapartal fetal monitoring*. Springer Publishing Company, New York, 2007.
- [54] L.J. Myers and W.L. Capper. A transmission line model of the human fetal circulatory system. *Med Eng Physics*, 24:285–294, 2002.
- [55] A.C.C. van Oppen, I. van der Tweel, G.P.J. Alsbach, R.M. Heethaar, and H.W. Bruinse. A longitudinal study of maternal hemodynamics during normal pregnancy. *Obstet Gynecol*, 88:40–46, 1996.
- [56] J.T. Parer. Evaluation of the fetus during labor. *Curr Probl Pediatr*, 12:3–25, 1982.
- [57] G. Pennati, M. Bellotti, and R. Fumero. Mathematical modelling of the human fetal cardiovascular system based on doppler ultrasound data. *Med Eng Phys*, 19:327–335, 1997.
- [58] H. Prystowsky. Fetal blood studies, VII. the oxygen pressure gradient between the maternal and fetal bloods of the human in normal and abnormal pregnancy. *Bull Johns Hopkins Hosp*, 101:48–56, 1957.
- [59] E.J. Quilligan, A. Vasicka, R. Aznar, P.J. Lipsitz, T. Moore, and B.M. Bloor. Partial pressure of oxygen in the intervillous space and the umbilical vessels. *Am J Obstet Gynecol*, 79:1048–1052, 1960.
- [60] S.C. Robson, W. Dunlop, R.J. Boys, and S. Hunter. Cardiac output during labour. *Br Med J*, 295:1169–1172, 1987.

- [61] S. Rubler, P.M. Damani, and E.R. Pinto. Cardiac size and performance during pregnancy estimated with echocardiography. *Am J Cardiology*, 40:534–540, 1997.
- [62] P.M. Sá Couto, W.L. van Meurs, J.F. Bernardes, J.P. Marques de S, and J.A. Goodwin. Mathematical model for educational simulation of the oxygen delivery to the fetus. *Control Eng Prac*, 10:59–66, 2002.
- [63] Y. Saburi, A. Mori, I. Yasui, T. Makino, and M. Iwabuchi. Fetal aortic blood flow assessment from the relationship between fetal aortic diameter pulse and flow velocity waveforms during fetal development. *Early Hum Dev*, 65:57–70, 2001.
- [64] K.G. Schmidt, N.H. Silverman, and J.I.E. Hoffman. Determination of ventricular volumes in human fetal hearts by two-dimensional echocardiography. *Am J Cardiol*, 76:1313–1316, 1995.
- [65] W. Schmidt and A. Kurjak. *Color Doppler sonography in gynecology and obstetrics*. Thieme Medical Publishers, Stuttgart, 2005.
- [66] P.J.G. Schreurs. <http://www.mate.tue.nl/~piet/>.
- [67] G.B. Sherard and E.R. Newton. Is routine hemoglobin and hematocrit testing on admission to labor and delivery needed? *Obstet Gynecol*, 98:1038–1040, 2001.
- [68] H.M. Silver, M. Seebeck, and R. Carlson. Comparison of total blood volume in normal, preeclamptic, and non-proteinuric gestational hypertensive pregnancy by simultaneous measurement of red blood cell and plasma volumes. *Am J Obstet Gynecol*, 179:87–93, 1998.
- [69] P.C. Struijk. *Assessment of hemodynamic parameters in the fetal and uteroplacental circulation using Doppler ultrasound*. PhD thesis, Erasmus University Rotterdam, The Netherlands, 2006.
- [70] H. Suga, K. Sagawa, and A.A. Shoukas. Load independence of the instantaneous pressure-volume ratio of the canine left ventricle and effects of epinephrine and heart rate on the ratio. *Circ Res*, 32:314–322, 1973.
- [71] B.R. Sweet and D. Tiran. *Mayes Midwifery. A textbook for midwives*. Baillière Tindall, London, 1997.
- [72] R.S. Thompson and R.J. Stevens. Mathematical model for interpretation of doppler velocity waveform indices. *Med Biol Eng Comput*, 27:269–276, 1989.
- [73] R.S. Thompson and R.J. Stevens. Doppler waveform pulsatility index and resistance, pressure and flow in the umbilical placental circulation: an investigation using a mathematical model. *Ultrasound Med Biol*, 16:449–458, 1990.
- [74] T. Todros, C. Guiot, and P.G. Piantà. Modelling the feto-placental circulation: II. a continuous approach to explain normal and abnormal flow velocity waveforms in the umbilical arteries. *Ultrasound Med Biol*, 18:545–551, 1992.
- [75] M. Ursino. Interaction between baroregulation and the pulsating heart: a mathematical model. *Am J Physiol Heart Circ Physiol*, 275:1733–1747, 1998.

- [76] M. Ursino and E. Magosso. Acute cardiovascular response to isocapnic hypoxia. I. a mathematical model. *Am J Physiol Heart Circ Physiol*, 279:H149–H165, 2000.
- [77] F.N. van de Vosse and M.E.H. van Dongen. Cardiovascular fluid mechanics - lecture notes. Eindhoven University of Technology, 1998.
- [78] M.B. van der Hout-van der Jagt. Development of a foeto-maternal-placental circulation model. Master's thesis, Eindhoven University of Technology,, 2007.
- [79] A.M. van Roon. *Short term cardiovascular effects of mental tasks. Physiology, experiments and computer simulations*. PhD thesis, University of Groningen, 1998.
- [80] A. Vasicka, E.J. Quilligan, R. Aznar, P.J. Lipsitz, and B.M. Bloor. Oxygen tension in maternal and fetal blood, amniotic fluid, and cerebrospinal fluid of the mother and the baby. *Am J Obstet Gynecol*, 79:1041–1047, 1960.
- [81] Y. Ville, I. Sideris, K. Hecher, R.J.M. Snijders, and K.H. Nicolaides. Umbilical venous pressure in normal, growth-retarded, and anemic fetuses. *Am J Obstet Gynecol*, 170:487–494, 1994.
- [82] W. Visser. *Hemodynamic studies in preeclampsia: implications for management*. PhD thesis, Erasmus University of Rotterdam, 1995.
- [83] M. Žaček and E. Krause. Numerical simulation of the blood flow in the human cardiovascular system. *J Biomechanics*, 29:13–20, 1996.
- [84] N. Westerhof, F. Bosman, C.J. de Vries, and A. Noordergraaf. Analog studies of the human arterial tree. *J Biomechanics*, 2:121–143, 1969.
- [85] R.B. Wilkening and G. Meschia. Fetal oxygen uptake, oxygenation, and acid-base balance as a function of uterine blood flow. *Heart Circ Physiol*, 13:H749–H755, 1983.
- [86] R.A. Woodbury, W.F. Hamilton, and R. Torpin. The relationship between abdominal, uterine and arterial pressures during labor. *Am J Physiol*, 121:640–649, 1938.
- [87] A.C. Yao, M. Moinian, and J. Lind. Distribution of blood between infant and placenta after birth. *Lancet*, 294:871–873, 1969.